Structural Reliability Based Position Mooring

Per Ivar Barth Berntsen

A DISSERTATION SUBMITTED IN PARTIAL FULFILLMENT
OF THE REQUIREMENTS FOR THE DEGREE OF

PHILOSOPHIAE DOCTOR

Department of Marine Technology
Norwegian University of Science and Technology

2008

Thesis for degree of Philosophiae Doctor

NTNU
Norwegian University of Science and Technology
Faculty of Engineering, Science and Technology
Department of Marine Technology
N-7491 Trondheim
Norway

IMT Report 2008-33

ISBN 978-82-471-7197-4 (electronic ver.)
ISBN 978-82-471-7183-7 (printed ver.)
ISSN 1503-8181

PhD thesis at NTNU, 2008:62

Printed by Tapir trykk

Abstract

This thesis considers control of moored marine structures, referred to as position mooring. Moored marine structures can take on a number of different forms, and two applications are considered in this work, namely aquacultural farms and petroleum producing vessels. It is anticipated that future aquacultural farms will be significantly larger than the existing ones, and placed in much more exposed areas. Hence, there is a significant technology transfer potential between the two seemingly different fields of aquaculture and petroleum exploitation.

Today's implemented state of the art positioning controllers use predetermined safety regions and gain-scheduling for evaluating the necessary thruster force for the vessel to operate safely. This represents a suboptimal solution; the operator is given a significant number of variables to consider, and the thrusters are run more than necessary. Also, it is likely that a more conservative controller regime does not necessarily increase the overall reliability of the structure as compared with a less conservative but better designed controller.

Motivated by this, a new control methodology and strategy for position mooring is developed. Two controllers using information about the reliability of the mooring system are implemented and tested, both via numerical simulations and model scale experiments. The first controller developed uses a reliability criterion based on the tension in the mooring system as a pretuning device. A nonlinear function based on the energy contained by the system is included in the controller to ensure that the thrusters are run only when needed. The controller is an output-feedback controller, based on measurement of position and estimated values of the velocities and slowly varying environmental loads. The second controller developed contains the reliability criterion intrinsically, thus, less pretuning is needed. The backstepping technique is applied during the design process, and the controller has global asymptotical stability properties.

Acknowledgements

This thesis is based on my research from 2003 through 2007, at the Norwegian university of Science and Technology, under the guidance of Professor Bernt J. Leira, Professor Ole Morten Aamo and Professor Asgeir J. Sørensen, and funded by the Norwegian Research Council (NFR).

Writing a PhD thesis is much like sailing into unchartered waters, you know your port of origin, and if your lucky you know your destination, but the path from the origin to the destination is blurred and filled with unknown obstacles. Making such a journey without the support of family, friends and experienced supervisors would make it a very unpleasant experience.

I gratefully appreciate all the guidance from my supervisor Professor Bernt Leira, and that he gave me the opportunity to start and complete a Ph.D study. I thank my advisor Professor Asgeir Sørensen for the inspiration throughout my master studies and for convincing me to pursue a PhD. My greatest thanks goes to my advisor Professor Ole Morten Aamo, without his help, his time and his encouragement, this work would never have been completed, most likely not even started!

I am grateful for all the help, the great lunches and long coffee breaks, for the lengthy discussions and world-problem solving I've had with all my dear colleagues. I am thankful for the valuable guidance within the field of aquaculture from Professor Trygve Gjedrem; for the help with the model setup, the software and the excellent tips during my experimental tests from Eivind Ruth, Dr. Trong Dong Nguyen and Torgeir Wahl; Saverio Messineo for being the best colleague sharing office with; Dr. Øyvind Smogeli for the help on MSS; and secretary Marianne Kjølås for guidance within the administrative minefield.

Thanks to the committee, consisting of Professor Chien Ming Wang, PhD Karl-Petter W. Lindegaard and Professor Mogens Blanke, for the time and effort they have put down. Their comments regarding this manuscript ensured the quality of the thesis.

I owe my wife Katrine a thousands thanks for her continuous confidence in

me and my work, and for allowing me to work on even when the house was a mess and the car did not start. To Maren for making life less troublesome, and stability proofs less important; and to *Knøttet*, for being patient and holding on. Finally, thanks to mum and dad for their unchallenged support and believe in me through my whole life; and to both Katrine's and my family for all the help in these last hectic months.

Trondheim 29th of February, 2008

Per Ivar Barth Berntsen

Contents

Chapter 1

Introduction

This thesis considers development of new positioning strategies for marine vessels moored to the sea bed via a mooring system which allows the vessel to freely rotate, e.g. a turret based mooring system. Possible marine vessels utilizing such a mooring system spans from aquacultural farms, wave energy converters, drilling vessels and petroleum producing vessels. The possible needs for control of these structures range from automatic feeding regimes, Kaushik (2000), motion damping via connectors between modules, Joshi (1989), synchronization of motions, Ihle et al. (2006), and dynamic positioning and position mooring controllers. While dynamic positioning refers to positioning via thrusters only, position mooring refers to positioning via mooring lines combined with thrusters. The latter is the focus of this thesis, and new positioning strategies for floating vessels connected to a mooring system are developed.
The different applications considered, the development they have undergone from the early days until today, and some future aspects, are described in Section 1.1. Then, previous work on position mooring controllers is reviewed in Section 1.2, followed by the motivation for developing new types of position mooring controllers in Section 1.3. The contributions of this work are listed in Section 1.4.

1.1 Applications

Position mooring may be applied to a number of marine installations. In general, it can be said that the prerequisite is that the structure is supposed to spend a relatively long time at the same geographical location (typically 30–45 days for a drilling vessel), in order to justify the relatively high installation and deployment costs of the mooring system. This thesis considers

position mooring of two different marine structures; *aquacultural farms* and *petroleum producing vessels*. Aquaculture is facing large challenges when it comes to ensuring a sustained profitable industry. For the aquacultural field, the focus has so far mostly been on the biological side. However, new challenges, as described in this section, will enforce technological advances and new concepts. The petroleum producing vessels studied are referred to as 'floating production storage and offloading' vessels, (FPSO vessels), and are mainly refitted supertankers, Brown (2007). They produce, refine and store petroleum products, and the products are transported onshore by shuttle tankers. Apart from the Gulf of Mexico, where there currently are no FPSOs, and west of Africa where FPSOs are moored with a fixed heading, turret mooring is the favored mooring system. This configuration is advantageous since it allows the vessel to weather vane, reducing both the required size of the chain links, the individual mooring line length and the required number of mooring lines.
The rest of this section will give an outline of the development within the fields of aquaculture and oil production.

1.1.1 Aquaculture: Past, Present and Future

As defined by the United Nations Food and Agriculture Organization, FAO (2006), aquaculture is the 'farming of aquatic organisms including fish, molluscs, crustaceans and aquatic plants. Farming implies some sort of intervention in the rearing process to enhance production, such as regular stocking, feeding, protection from predators, etc. Farming also implies individual or corporate ownership of the stock being cultivated.'
The earliest reports of aquaculture originate from China, some 4000 years ago. The production methods were simple, and limited to small ponds and rivers with low water velocity. The production spread west, and reached Europe around year 0 AD. The early production was very area extensive, limiting the effectiveness of the production. In the middle ages, the main species used for aquaculture in Europe were trout and carpe, and the monks were the ones performing and enhancing the science of breeding fish. In the 19th century, driven by the great biologists and zoologists of the era, proper cultivation methods were developed, increasing the survival rate and production significantly. This happened at the same time as prefabricated feed was introduced, which further enhanced the production. In Japan around 1920, a net cage called *Bridgestone* became the first for use with salt water fish.
As being one of the countries blessed with an abundance of natural resources, Norway lacked for many years the incentive for implementing

aquaculture as an industry. In 1970, the Grøntvedts became the first Norwegians to design, construct and install an aquacultural farm. Their design still forms the basis for most net cages used in Norway today. Although it is a clever design, new designs are essential for future growth, for instance when new species, such as cod and halibut, are introduced, since their behaviour and demands are significantly different than those of the salmon.

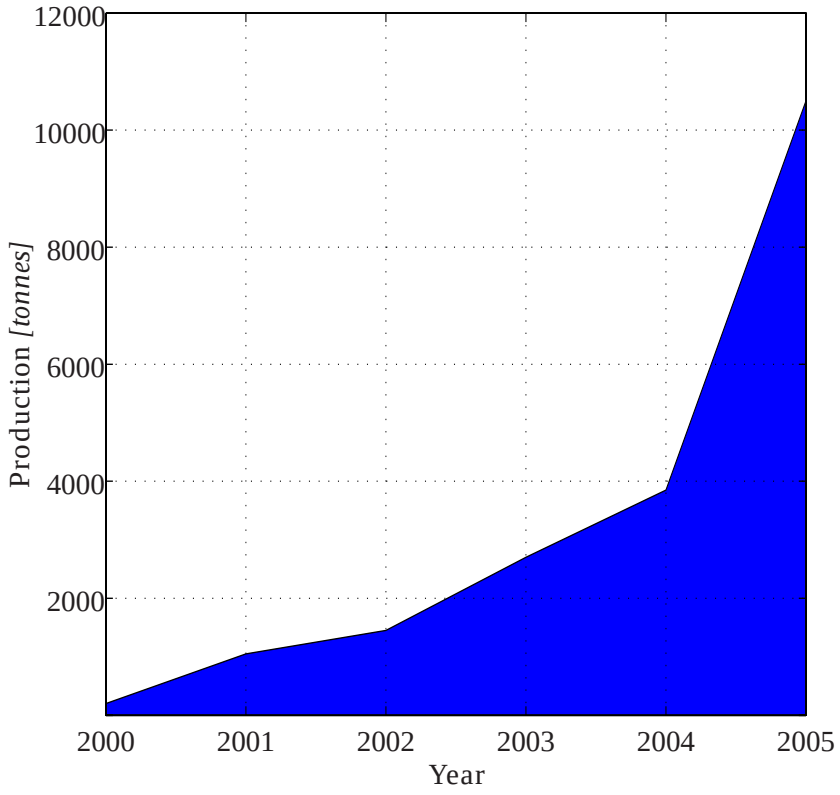

Figure 1.1: World aquacultural cod production, Alaska Seafood Marketing Institute, ASMI (2006).

Aquaculture is today the fastest growing sector of the world food economy, increasing in volume by more than 10% per year, and currently accounting for more than 35% of all fish consumed, quickly becoming the world's number one protein source. The total aquacultural production of the world in 2004 was 45.5 million tons, FAO (2006), of which small–scale

systems in China constitute some 70%. However, as happened with the 'green revolution' of agriculture in the previous century, the current 'blue revolution' of aquaculture is becoming an industrial mode of food production. As it seems like the traditional fisheries have peaked, FAO (2005) and Worm et al. (2006), new and more efficient methods for growing fish are needed. At the same time, new species are being introduced for large scale production, one of them being cod. The production of captured cod has fallen from 4.1 million metric tons in 1968 to less than 1.3 million metric tons in 2004. The worldwide aquacultural production of cod increased by some 2000% from 2000–2004, see Figure 1.1. According to Cherry (2006), McGovern (2006) and Solsletten (2006), the aquacultural production of cod will reach as much as 100,000 metric tons by 2010, escalating to between 300,000 and 500,000 metric tons by 2015. It is anticipated that the main contributors to this growth will be Norway, UK, and Canada. It is estimated that the twelve largest cod farming companies of Norway today have a total production capacity of 115,000 tons.

The increased production of cod will demand both new production methods and new locations. Cod is known for being 'smarter' than salmon, so the danger of escapes will increase if no new technical solutions are developed. By introducing large scale production of cod, the environmental impact must be taken into consideration. As with salmon, parasites and other pathogenic organisms which thrive inside the fish cage will pose a threat to the local cod stock. In addition to this, controlling the spawn process of the cod has proven to be difficult, since spawning takes places inside the net cage, in contrast to salmon, which spawns in fresh water. The possibility of gene-pollution from the bred fish to the local cod stock is thus imminent. To emphasize the danger that cod is facing, the World Conservation Union placed cod on the red list in 2006, Kålås et al. (2006), a list which defines the species that are facing a possible threat of extinction. Cod is listed due to a dramatic fall in number of individuals over a consecutive number of years. Thus, large farms for breeding cod will constitute a double-edged sword. On one hand, it will produce fish in such a quantity that the traditional fishing industry may let the local stock grow to a healthy number of individuals. On the other hand it will introduce new dangers, such as parasites and poor gene qualities. These are contradictions which must be taken into consideration when designing and placing new aquacultural farms.

In Norway the aquacultural farms are located in sheltered waters, inside the fjords, where the farms are protected from extreme weather. However, the very calmness of the water means that currents do not disperse the inevitable plume of waste. A farm of 200,000 salmons flushes nitrogen and phosphorus into the water equivalent to the sewage from 20,000 people,

Mann (2004). Recently, several projects have been started in order to investigate the possibilities of farming fish at more exposed areas. *Offshore Aquaculture Technology Platform* is a European project under the management of the Marine Institute of Ireland. This project has as a goal to map interests, possibilities, challenges and limitations for aquaculture at more exposed areas. Already, there are commercial concepts available; one is named *Storm merd* and is shown in Figure 1.2. The farm has all the necessary auxiliaries integrated, such as feed storage, office and control room, and all components are substantially more robust than the standard of today, in order to withstand a more severe excitation by the environment. Another project, called *Intellistruct*, proposed by Sintef Fisheries and Aquaculture, is shown in Figure 1.3. The innovative concept involves a huge farm where the individual net cages have the possibility of being lowered deeper into the water to avoid the impact from waves or algae attacks. However, there are many problems to solve before the project can be realized, among others how to feed the fish effectively when the farm is totally submerged.

Figure 1.2: 'Storm merd'. Shown with courtesy of Marine Construction AS.

In order to ensure a sustained growth of the aquacultural sector, new species will be introduced. These new species will demand new designs of aquacultural farms if the production shall be successful. New and more exposed areas will be utilized. Thus, future designs must be significantly more robust than the present designs, which frequently experience escape of fish. From an engineering perspective, the main focus will be to design a system which has an overall acceptable reliability. Any component which is critical

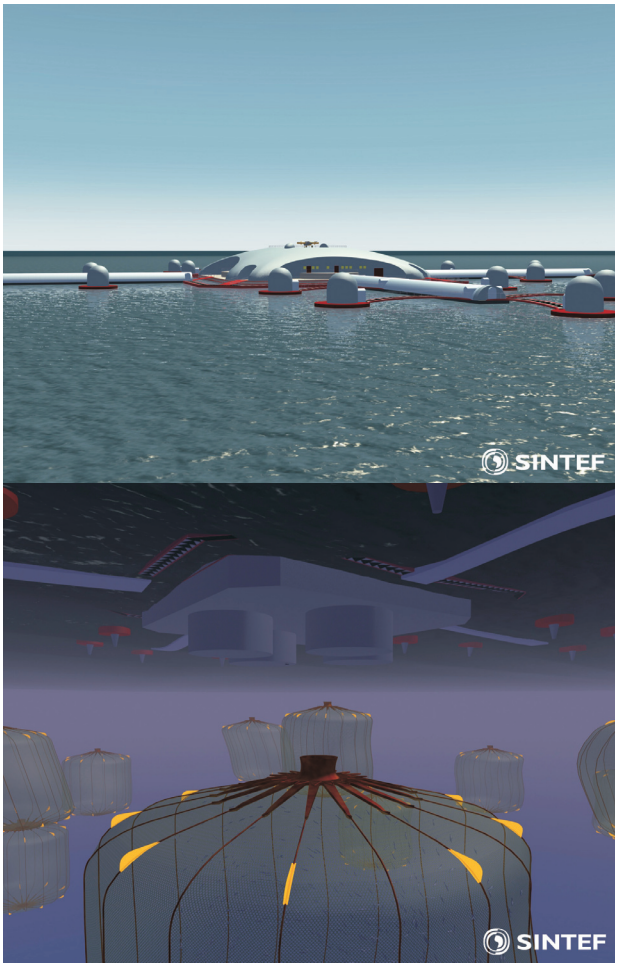

Figure 1.3: Illustration of *Intellistruct*. Shown with courtesy of Sintef Fisheries and Aquaculture.

for the sustained operation must be supervised so that any harmful situation can be avoided or stopped from developing further. For both existing and future farms, the integrity of the mooring system will be one of the key factors in order to withstand the environmental forces.

1.1.2 Offshore Oil Exploration and Production: Past, Present and Future

The history of the development of petroleum products and the offshore industry is brilliantly told by Yergin (1991) and Pratt et al. (1997). This section aims to give the reader a short introduction to the history of oil exploration and exploitation, and give a glimpse into the future of offshore production.

Some of the first to put oil into use was the Native Americans, who used it as a medicine. The oil was located on the surface of the earth, bubbling up or seeping into salt wells, e.g. in the area around Oil Creek, Pennsylvania. In 1854, Benjamin Silliman Jr., a professor of chemistry at Yale University, was given the task of investigating whether the oil could be used as an illuminant. His findings were very promising: It worked better than the existing illuminants, and could be produced both cheaper and faster. Although lucrative, the illumination industry only worked as a door opener. The really big market for crude oil and its derivatives came with the invention of the petroleum engine, first introduced for marine vessels, later for automobile and airplane engines. Until 1900, all exploration and production were land based. Then, at the same time in both USSR and the US, piers which stretched out into the open ocean were built. These piers, an illustration shown in Figure 1.4, had relatively little resistance against the environmental forces. Quite often they were destroyed by storms, partially because they were overloaded with equipment at the time when the storm hit.

In the 1940's the first real offshore installations were built. In the USSR, the oil platform Oil Rocks (Neft Dashlari) was constructed near Baku in Azerbaijan. It was located some 25 nautical miles offshore in the Caspian Sea and housed more than 5000 workers. In the US, the Creole field became the first to be exploited by proper offshore constructions. In the early years, the legislators had their hands full controlling the very powerful oil industry, making sure that the delicate environment of the sea, as well as the safety of the crew, were taken care of. Long dismissed by many as a potential source of oil or gas, the North Sea has, during the last four decades, become the centre of one of the most productive energy industries of the world. Gas was first found in quantity in the Groningen area of The Netherlands in 1959, followed by the first British discovery of gas in the West Sole field, off the coast of East Anglia, late in 1965. In 1969 Philips Petroleum discovered a reservoir on the field *Ekofisk* in the Norwegian sector, which proved to contain more than 2 billion barrels of oil. For more background on the history of the petroleum offshore industry, the interested reader is encouraged

Figure 1.4: Early oil production, Summerland, California, 1902.

to read Yergin (1991), Glenne (1997) and Solberg (2007).
Accidents involving offshore petroleum installations are dramatic and extremely costly. The necessity of increasing the safety of offshore installations has been proven time and again through accidents such as Piper Alpha, Alexander Kielland and, more recently, Petrobras P-36, shown in Figures 1.5–1.7. These accidents have revealed weaknesses in the construction, operation and maintenance of offshore vessels. New laws and regulations have consequently appeared after such major accidents.
When a vessel conducts a dynamic positioning (frequently referred to as *DP*) or position mooring operation, an error typically results in loss of position. This is referred to as drift-off if it is caused by failure in the power or propulsion systems, and drive-off if the sensor system fails. The possible result can be a collision between two vessels, or damage or loss of the drilling or production riser. Costs associated with these accidents are in the multi-million class, with possible huge consequences for the company, the workers and the local environment. Knowing that human error is the major contributor to marine accidents, Baker and McCafferty (2005), designing supervisory monitoring and control systems which ensure that the human

Figure 1.5: Piper Alpha.

operator is not overloaded with tasks, will improve the overall safety of marine vessels. Also, when the industry moves into harsher waters, for instance when initiating arctic exploration, impacts from floating objects and effects of ice on the structures will enforce new designs, both for the hardware and the software. The complexity of these structures will vouch for a widespread use of safety monitoring systems and different accident avoidance systems in order to operate safely, realizing that the capacity of the human operator is limited.

1.2 Previous Work on Position Mooring Controllers

A dynamic positioning system may be defined as 'a unit or a vessel which automatically maintains its position (fixed location or predetermined track) exclusively by means of thruster force', IMO (1994), while a position mooring system uses thrusters mainly for heading control, motion damping and for reducing the load acting on the mooring system when necessary.
When the offshore industry came about some 50–60 years ago, new technology was developed at a staggering pace. Already during the early years,

Figure 1.6: Alexander Kielland.

the offshore installations could match the complexity of any other man-made structure. Today, the systems involved are becoming more and more complex, with a huge number of subsystems critical for successful operation. Motivated by increasing operability and reducing number of incidents due to human error, a consortium consisting of the oil companies Continental, Union, Superior and Shell Oil started to develop CUSS 1 in 1956, see Figure 1.8. CUSS 1 was a sophisticated drilling vessel for the rapidly developing oil industry, and utilized four azimuthing thrusters mounted over the side of the vessel, directly driven by the engine and manually controlled (i.e. the dynamic positioning system was manual), to solve the positioning task. The performance of this system was not very convincing, the vessel could stay on station within a radius of about 180 meters. However, due to the depth of the water (approximately 3500 meters), the drilling stem had enough flexibility to allow such a large operating radius. The position of the vessel was determined by the first version of a hydro acoustic reference system. The first task for CUSS 1 was to take part in the project Mohole, a project which aimed for drilling through the Earth's crust into the Mohorovicic discontinuity (the boundary between the Earth's crust

Figure 1.7: Petrobras P-36.

and the mantle, see Taggart (1962)). However, the oil industry saw the potential for using dynamically positioned vessels both for drilling operations and production. Shell Oil Company developed the positioning system further, and in 1961 the first vessel with a computer based positioning system, Eureka, was built. These early dynamic positioning systems were not very scientific; trial-and-error and ad-hoc controllers were the chosen strategies. Crucial for the performance of dynamic positioning and position mooring systems is the position measurement system. Today, the Global Positioning System (GPS), extended with a series of known ground based reference stations (referred to as *differential* GPS, DGPS), is the preferred position measuring device. However, due to the necessity of redundancy, a number of other systems may also provide the controller with position measurements, such as Hydro-acoustic position reference (HPR), riser angle monitoring, Artemis and taut wire. The accuracy of these systems vary, from DGPS which can achieve a measurement error of less than 1 meter, to the other systems which can have errors in the order of 5 – 10 meter. When using these measurement devices, it is important to realize that their performance strongly depends on the location of the vessel, and the water depth

Figure 1.8: CUSS 1.

in which the operation takes place. Because of this, redundancy as well as voting algorithms for detecting false measurements are necessary for a safe operation.

The popularity of dynamic positioning systems increased as the exploration and production moved into deeper waters, as application of only mooring became insufficient. In 1980 there were 65 vessels classified for dynamic positioning operations, while in 1985 this number had increased to 150. In 2002 there were more than 2000 designated dynamic positioning vessels. At the same time, the theory and software used for these systems have developed, making the entire operation more automated, but at the same time, more complex. Optimal control theory and Kalman-filtering were proposed in Balchen et al. (1976), and extended in Balchen et al. (1980), Balchen et al. (1981), Grimble et al. (1980), Grimble et al. (1983), Fung and Grimble (1983), Sælid et al. (1983) and Sørensen et al. (1996). The motivation for introducing a filter is to separate the low frequency and wave frequency components, such that only the low frequency part of the measurements are considered in the controller. This is motivated by the fact that the thrusters cannot counteract excitations caused by first order wave

effects. More options have been added to the dynamic positioning control system, such that they can perform tasks related to e.g. pipelaying, operation of remotely operated vehicles, and optimal setpoint chasing, Sørensen et al. (2001). Also, the control systems have been extended from the normal surge, sway and yaw control problem, to include using the thrusters to reduce the roll and pitch motion, see Sørensen and Strand (1998) and Sørensen and Strand (2000). Koditschek (1987), Sonntag and Sussmann (1988), Tsinas (1989) and Byrnes and Isidori (1989) proposed, almost simultaneously, a new design approach referred to as *integrator backstepping*. Integrator backstepping may be considered as a special case of stabilization through a *strictly positive real* transfer function Kokotović (1991). Inspired by this, nonlinear controllers for dynamic positioning systems based on integrator backstepping have been developed, see Fossen and Grøvlen (1998), Robertsson and Johansson (1998), Strand and Fossen (1999), Strand (1999) and Aarset et al. (1998). Fossen and Strand (2001) proposed a nonlinear passive weather optimal positioning control system for ships and rigs in order to reduce the environmental impact. A method referred to as acceleration feedback was developed for marine DP systems by Lindegaard (2003), which improved the positioning accuracy without using more thrust than a standard PID controller.

The majority of industrial control systems are based on linear theory and gain-scheduling. Gain-scheduling refers to change of controller parameters based on different modes of operation and state conditions. For position mooring, the different modes of operation can be defined according to which type of operation the vessel is conducting, e.g. drilling, interaction with supply vessel etc., while the state condition typically is the heading or deviation from some operation point. The kinematic equation is assumed constant over a certain span of degrees. This is illustrated in Figure 1.9, where the controller parameters are gain-scheduled both with respect to the pre-chosen number of headings, and the deviation from an operation point in the horizontal plane, with a more aggressive controller the further the vessel is from the origin. The complexity of such a control system is clear, and chances of misinterpretation or confusion is obvious. In addition, it poses a nontrivial programming task, with an imminent danger of logical errors. The controller objective is for most cases to drive the system states to zero, or some preset desired position and heading. It is common to use the measured position and filtered or estimated velocities to determine the controller output. Using estimated states is referred to as output feedback, while using only measured states is referred to as state feedback. The introduction of nonlinear observers based on the backstepping technique by Fossen and Grøvlen (1998) and Strand and Fossen (1999) removed the

necessity of lengthy pretuning and gain-scheduling procedures. It also allowed for using the system properties more directly in the controller design.

Most of these controllers aim to drive the system states to zero (or some other preset value) by the use of thrusters, and it is left to the operator to switch between heading control, motion damping or complete control. Thus, these controllers are still based on the assumption that the operator will have the capability of foreseeing whether the vessel will reach a state where thruster assistance is necessary, or if the mooring system can handle the loads without any assistance, or limited assistance only. If the controller itself can make this decision, for instance by using the energy level of the vessel as an argument, the controller can relieve the operator of tasks, which again lets him focus on other work tasks. In this work, such an energy consideration is discussed, see Paper I. Also, a solution where the part of the controller which is based on the reliability criterion is active only when the mooring lines are critically loaded is considered, while heading control and motion damping is continuously active, see Papers II-III.

For vessels which are supposed to operate at one location for a significant amount of time, adding a mooring system will reduce the fuel consumption of the thrusters significantly, since the mooring system will position the vessel and counteract the slowly varying environmental loads, such as current and second order wind and wave loads. Most of the proposed controllers for position mooring are based on the ones used for dynamic positioning, with some modifications to include the mooring line term in the controller, see for instance Strand et al. (1997), Sørensen et al. (1999), Aamo and Fossen (1999) and Ryu and Kim (2005). In order to expand the operational weather window for moored vessels, Nguyen et al. (2007) proposed a hybrid position mooring system which automatically switches between different controllers based on the actual weather condition. Nguyen and Sørensen (2007) implemented a setpoint chasing algorithm in order to reduce the possibility of mooring line breakage in extreme conditions.

An illustration of the overall vessel–mooring–riser–thruster system is shown in Figure 1.10, illustrating the Alvheim FPSO located off the coast of Bergen, Norway, in 120 meter water depth. As can be seen, the system is very complex, consisting of several mooring lines and risers, as well as several rotatable thrusters. For the Dalia FPSO off the coast of Angola, almost 70 subsea wells are tied in. Off-take and delivery of oil is accomplished using shuttle tankers, typically using tandem stern loading on weathervaning units and transfer via a buoy with spread moored units, with tandem loading usually provided as backup. With their huge displacement (the storage capacity of the world's FPSO vessels ranges from 10000 [m^3] for FPSO San

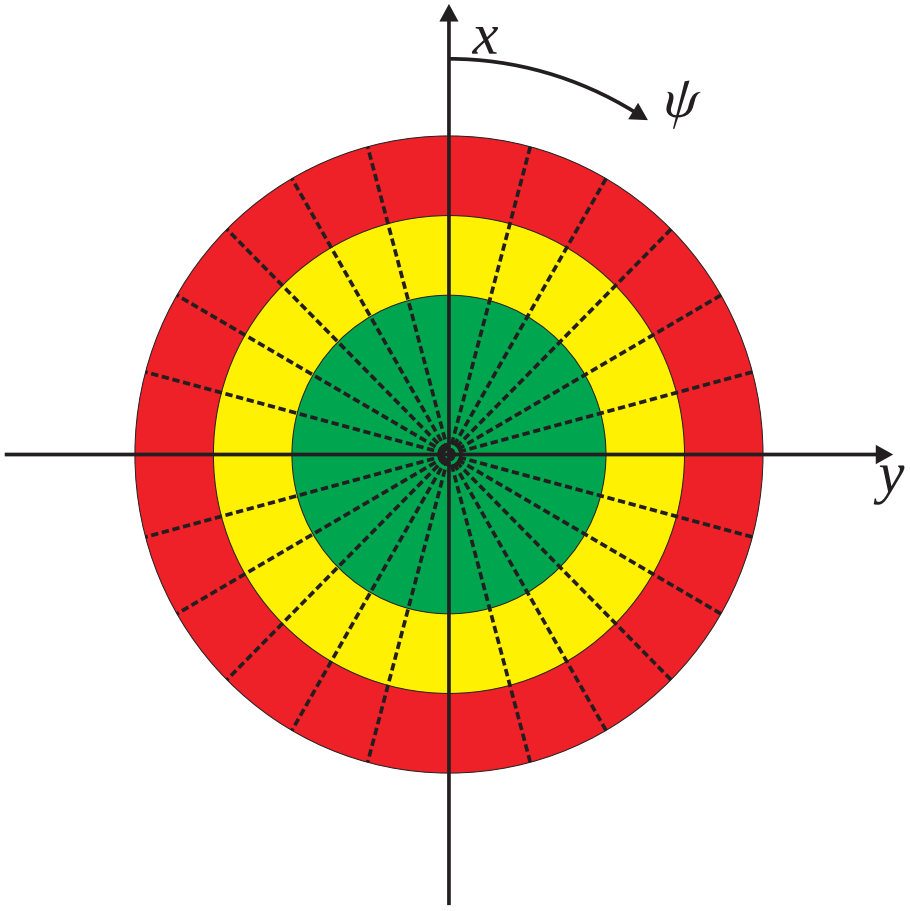

Figure 1.9: Illustration of gain-scheduling in the horizontal plane for linear controllers.

Jacinto, to 350000 [m^3] for Girassol FPSO), and their very rectangular cross-sectional shape, FPSO vessels make a perfect target for the environmental loads. Thus, the mooring system, as well as the thrusters and control system, will need to be carefully designed according to the different tasks it will perform, along with its location.

The primary risk for offshore petroleum installations is hydrocarbon release, constituting nearly 50% of the total number of incidents in the period 1996–2002, see Muncer (2003). The second largest incident group is unwanted vessel motion (causing loss of position and objects dropped and damaged), which constitutes some 12% in the same period. In the pe-

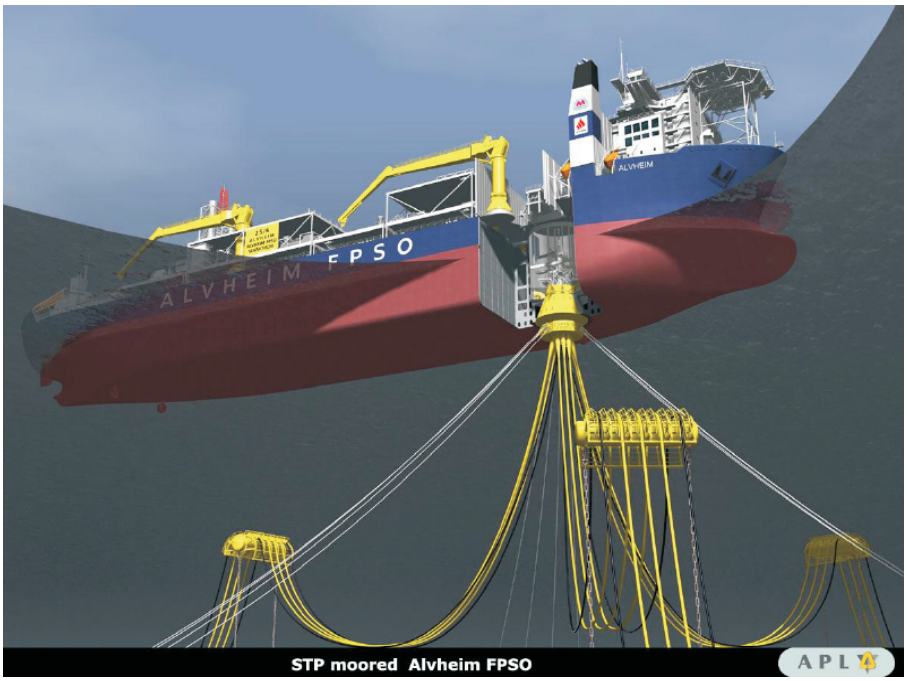

Figure 1.10: Illustration of a turret anchored FPSO. Courtesy of APL / Axis.

riod 2000–2001, there is a clear increase of the relative number of incidents caused by vessel motion, now constituting more than 25% of the total number of incidents. Loss of position may also cause damage to connected systems such as the mooring system and risers, and may also cause a collision between two vessels. For DP and position mooring operations, the operator typically has in the order of 10–20 seconds from the time the position measurement systems fail, until the situation becomes critical. Decreasing the number of tasks for the operator, and designing a useful supervisory system may decrease the reaction time of the operator.

1.3 Motivation

At a first glimpse, it may seem like the two applications aquaculture and petroleum offshore installations have very little in common. However, when introducing large aquacultural farms, the necessity of a more complex and complete automation scheme than existing solutions is obvious. Then, the technology transfer potential from the mature offshore petroleum

industry, in the sense of automation in general, and dynamic positioning and position mooring in particular, is evident. By investigating these technology transfer possibilities, and at the same time identifying new needs, improved (in the sense of safety and cost-effectiveness) controller schemes can be designed.

The previous sections have described the state-of-the-art for the aquacultural and petroleum industries, as well as for DP and position mooring controllers. However, both industries are facing new challenges; for the aquacultural industry it is the necessity of industrialization that drives the changes. 'The bigger, the better' seems to be the overall agreement within the industry. With the lack of suitable locations inshore, large offshore facilities will inevitably emerge. As for the petroleum industry, the persistently high oil prices motivates for developing new fields, fields that previously have been disregarded due to too high investment costs or a too high risk of failing engineering wise. Many of these fields require 'a first', i.e. new technology development.

The scope of this work is *to develop new position control schemes for moored marine vessels, which increase the safety of the structure at the same time as being a cost-effective alternative*. Section 1.1 gave a background on the different challenges that the two industries are faced with. It is likely that both future aquacultural farms and offshore oil installations will utilize mooring systems to some extent, therefore there is a clear possibility that the two industries can benefit from each other concerning mooring system design, installation, supervision and control. It is emphasized in Section 1.1.1 that the aquacultural industry in particular is in need of a technological leap, both on the biological side when introducing new species, and on the engineering side. It is the engineering perspective that is adopted in this thesis; the challenges concerning the biological part of the problem are described in order to give the reader the complete picture of the complex problem of implementing full scale offshore aquacultural plants. This thesis aims to identify and solve a given positioning problem, under the assumption that the structure utilizes a mooring system and have thrusters available for aiding the mooring system.

1.4 Contributions

This thesis contains development of a new approach for control of complex marine structures, applicable for both aquacultural farms and moored oil producing vessels. Most of the state of the art position mooring controllers use geometrical boundaries and gain-scheduling for determining the de-

sired thruster force. By including the state of the limiting systems directly in positioning task, it is possible to develop less conservative controllers, saving both fuel and increasing the overall reliability of the system. The methodology developed in this thesis uses a measure of the reliability of the mooring system for determining the desired thruster force. The methodology allows for different approaches when designing the controller. Either, the reliability measure can be used intrinsically in the controller, or it can be used as a pretuning mechanism in order to determine the parameters of a given controller. A third option is to use the reliability measure for monitoring an operation, aiding the operator in making the right decisions. The first two options are studied in detail in the work presented in the aft of this thesis, identified by Paper I – Paper III. The upsides of the proposed controllers are first and foremost i) reliability against mooring line failure, ii) a more intelligent thruster usage, resulting in a presumably less consumption of fuel, and iii) a reduced necessity of lengthy pretuning procedures.
The methodology is not limited to offshore structures, but can be implemented on other structures where monitoring of structural components is crucial for the safety of the operation, and where means of control are available. Three journal papers constitute the main contributions of the thesis. These are added chronologically at the end of the thesis, and the specific contributions of each of these three papers are:

Paper I Published in *Control Engineering Practice*. A model of an interconnected marine structure, consisting of three semi-submersible types of modules, is developed. The controller which is developed takes the energy of the system into consideration when determining the magnitude of the necessary actuator force. A methodology using a reliability criterion, referred to as the δ-index, is introduced to evaluate the integrity of the mooring system.

Paper II Accepted for publication in *International Journal of Control*. The concept of a controller acting on the reliability of a connected subsystem, the mooring line system, is developed further. The δ-index is included directly in the controller to ensure the integrity of the system. The part of the controller which depends on the δ-index is only active when the loading becomes critical.

Paper III Provisionally accepted for publication in *Automatica*. A controller which depends on the δ-index is implemented on CyberShip III, and experimental tests are performed in the Marine Cybernetics Laboratory. The results show that the controller performs well in calm to moderate seas.

1.4.1 List of Publications

This list contains both accepted and submitted papers by the author, 2003–2007.

Journal Papers

- Leira, B.J., Barth Berntsen, P.I., Aamo, O.M. (2005). Structural Reliability Criteria and Dynamic Positioning of Marine Vessels, *Advances in safety and reliability.* London: Taylor & Francis.

- Leira, B.J., Sørensen A., Barth Berntsen, P.I., Aamo, O.M. (2006). Structural Reliability Criteria and Dynamic Positioning of Marine Vessels, *International Journal of Materials & Structural Reliability.* **4(2)**: 161–174.

- Barth Berntsen, P.I., Aamo, O.M., Leira B.J., Sørensen A. J. (2007). Structural Reliability–based Control of Moored Interconnected Structures, *Control Engineering Practice.* **16(4)**: 495–504.

- Barth Berntsen, P.I., Aamo, O.M., Leira B.J.(2008). Thruster Assisted Position Mooring Based on Structural Reliability, *International Journal of Control.* **In Press.**

- Leira B.J., Barth Berntsen, P.I., Aamo, O.M. (2008). Station–keeping of Moored Vessels by Reliability-based Optimization , *Probabilistic Engineering Mechanics.* **Accepted for Publication.**

- Barth Berntsen, P.I., Aamo, O.M., Leira B.J.(2008). Ensuring Mooring Line Integrity by Dynamic Positioning: Experimental Tests, *Automatica,* **Provisionally accepted .**

Conference Papers

- Barth Berntsen, P.I., Aamo, O.M., Sørensen, A.J. (2003). Modelling and Control of Single Point Moored Interconnected Structures, *Proceedings of the 6th Conference on Manoeuvring and Control of Marine Crafts, 16–19 September, Girona, Spain.*

- Barth Berntsen, P.I., Leira, B.J., Aamo, O.M., Sørensen, A.J. (2004). Structural Reliability Criteria for Control of Large–Scale Interconnected Marine Structures, *Proceedings of the 23rd International Conference on Offshore Mechanics and Arctic Engineering, 20–25 June, Vancouver, Canada.*

- Leira, B.J., Barth Berntsen, P.I., Aamo, O.M., Sørensen, A.J. (2004). Positioning and Motion Control of Multiple Interconnected Marine Structures Based on Structural Design Criteria, *Proceedings of the 9th International Symposium on Practical Design of Ships and other Floating Structures, 12–17 September Lübeck-Travemünde, Germany.*

- Leira, B.J., Barth Berntsen, P.I., Thomassen, P. (2004). Aspects of Design and Operation of Fish–farming Plants for Harsh Environments, *Proceedings of the Seventh International Conference on Marine Science and Technology 07–09 October, Varna, Bulgaria.*

- Leira, B.J., Sørensen, A.J., Barth Berntsen, P.I., Aamo, O.M. (2005). Integration of Structural Reliability Criteria with On–line Control Schemes, *Proceedings of the Ninth International Conference on Structural Safety and Reliability of Engineering Systems and Structures, 19–23 June, Rome, Italy.*

- Leira, B.J., Barth Berntsen, P.I., Aamo, O.M. (2006). Reliability–based structural optimization for positioning of marine vessels, *Proceedings of the 25th International Conference on Offshore Mechanics and Arctic Engineering, 4–9 June, Hamburg, Germany.*

- Barth Berntsen, P.I., Aamo, O.M., Leira, B.J. (2006). Position Mooring Based on Structural Reliability, *Proceeding of the 7th IFAC Conference on Manoeuvering and Control of Marine Craft, 20–22 September, Lisbon, Portugal.*

- Barth Berntsen, P.I., Aamo, O.M., Leira, B.J. (2006). Dynamic Positioning of Moored Vessels Based on Structural Reliability, *Proceeding of the 45th IEEE Conference on Decision and Control, 13–15 December, San Diego, CA, US.* 5906–5911

- Barth Berntsen, P.I., Aamo, O.M., Leira, B.J. (2007). Structural Reliability–Based Control for Moored Vessels: Experimental Results, *Proceeding of the 26th International Conference on Offshore Mechanics and Arctic Engineering, 10–15 June, San Diego, CA, US.*

1.5 Thesis Layout

This thesis is a collection of papers produced throughout the work with my PhD. The three most significant ones are presented in the second part of the thesis, identified as Papers I–III. The papers included are identical to those submitted, with only minor changes to the layout, so that the style of the thesis is contained throughout the text.

In Chapter 2 the mathematical modelling of marine vessels is discussed, and a description of the experimental setup in MCLab in January 2007 is given. This Chapter also includes the statistical tools used for obtaining the main results. In Chapter 3 the conclusions and suggestions for future work are presented. In Paper I a model of an interconnected marine structure and a control strategy for evaluating the reliability of the mooring system are developed. The paper is accepted for publication in *Control Engineering Practice*. In Paper II the reliability index, called the δ-index, is included directly in the controller to ensure the integrity of the mooring line system. The paper is accepted for publication in *International Journal of Control*. In Paper III the controller is developed further and experimental tests are carried out with the vessel CyberShip III, in the Marine Cybernetics Laboratory. The paper is provisionally accepted for publication in *Automatica*.
Please note that the bibliography lists following Chapter 3 contains all references appearing in the thesis, i.e. those from Chapters 1–3, as well as those in Papers I-III.

Chapter 2

Mathematical Modelling and Experimental setup

The controllers proposed have been evaluated both by means of a numerical simulator, the Marine Systems Simulator (MSS), and in the Marine Cybernetics Laboratory (MCLab), which is a test basin at the Department of Marine Technology. The mathematical modelling of marine vessels for use with MSS is described in Section 2.1, while the test setup is described in Section 2.2. The concept of structural reliability, along with some basic statistical tools needed, are presented in Section 2.3.

2.1 Mathematical Modelling of Marine Vessels

The modelling of marine vessels is usually divided into two regimes, referred to as modelling for *manoeuvering* and modelling for *seakeeping*. The two models have different validity properties, thus it is important to choose a model based upon the type of operation the vessel will conduct. Manoeuvring refers to the study of ship motion in the absence of wave excitation, i.e. a calm water assumption, whereas seakeeping refers to the study of vessels in waves while the vessel keeps its course and speed constant. The separation between the two models allows for making different assumptions that simplify the study in each case. In this thesis, position mooring is considered. Hence the most correct choice of model is the *seakeeping model*. In recent years the focus has been on describing a unified model, see Bailey et al. (1997), Fossen and Smogeli (2004), Fossen (2005) and Smogeli et al. (2005). However, this will not be reviewed here.

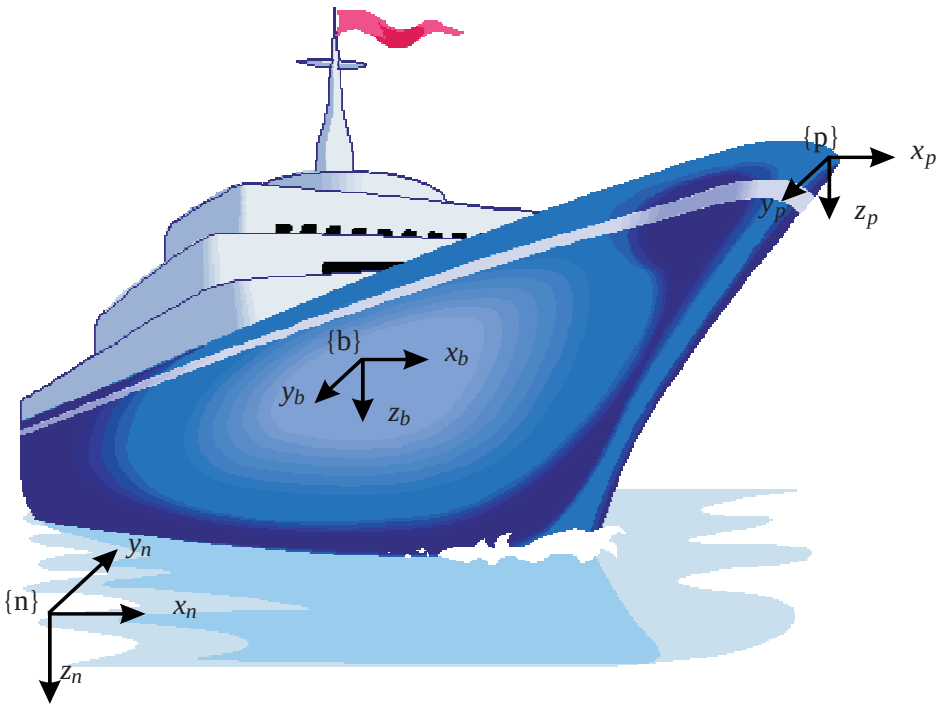

Figure 2.1: Illustration the different reference frames.

2.1.1 Reference Frames

Three different reference frames are utilized in this thesis in order to describe the motion of the vessels adequately, based on Fossen (2002). The different frames are described in the following and illustrated in Figure 2.1.

NED–frame The *North–East–Down* reference system, {n}-frame, is fixed to the surface of the earth, and the curvature of the earth is neglected. It is common to assume that the frame is inertial, so that Newton's laws apply. The reference system is described by (x_n, y_n, z_n), where x_n is positive towards the North, y_n is positive towards the East, and z_n is positive downwards. The position and orientation of the vessel is usually described in this frame.

BODY–frame The *Body–fixed–frame*, {b}–frame, is fixed to the vessel, usually at the center of gravity. The translational and rotational velocities relative to the *NED*–frame are usually described in the b–frame. The reference system is chosen to coincide with the principal axes of inertia, and is described by (x_b, y_b, z_b), where x_b is directed from the stern to the bow, y_b is directed to the starboard, and z_b is directed towards the keel.

p–frame The *p–fixed frame*, {p}–frame, describes an arbitrary point on the vessel, under the assumption that the vessel behaves as a rigid body. The point is described relative to the body-fixed reference system by (x_p, y_p, z_p), where x_p, y_p and z_p describe the distance from the b–frame to the p–frame along the x_b, y_b and z_b axes, respectively.

The position and orientation of a marine vessel are, in the {n}-frame, given in vector format as

$$\boldsymbol{\eta} = [\boldsymbol{\eta}_1, \boldsymbol{\eta}_2]^T = [n, e, d, \phi, \theta, \psi]^T \in \mathbb{R}^3 \times \mathcal{S}^3, \tag{2.1}$$

where n, e and d are the x, y and z position, respectively. The quantities ϕ, θ, and ψ are the rotations (Euler angles) around the n, e and d axes respectively, defined positive clockwise in a *right–handed–system*. The vector is commonly divided into two terms, $\boldsymbol{\eta}_1$ and $\boldsymbol{\eta}_2$, which contain the positions and rotations, respectively.
The velocity vector of the vessel in the {b}–frame is given as

$$\boldsymbol{\nu} = [\boldsymbol{\nu}_1, \boldsymbol{\nu}_2]^T = [u, v, w, p, q, r]^T \in \mathbb{R}^6, \tag{2.2}$$

where $\boldsymbol{\nu}_1 = [u, v, w]^T$ are the translational velocities, and $\boldsymbol{\nu}_2 = [p, q, r]^T$ are the rotational velocities.

Transformation Between Reference Frames

Having positions and velocities defined in different reference frames motivate for establishing a connection between the two frames {n} and {b}. Also, it is convenient to introduce the connection between {b} and {p}. This is referred to as Kinematics, and treats the geometrical aspects of motion only. These relationships are described in detail in the following.

Transformation Between {n} and {b}
Using Euler angles, the translational velocities are transformed from the {b}–frame to the {n}–frame according to

$$\dot{\boldsymbol{\eta}}_1 = \mathbf{R}(\boldsymbol{\eta}_2)\,\boldsymbol{\nu}_1, \tag{2.3}$$

where $\mathbf{R}(\boldsymbol{\eta}_2)$ is referred to as a *rotation matrix*, given by

$$\mathbf{R}(\boldsymbol{\eta}_2) = \begin{bmatrix} c\psi c\theta & -s\psi c\phi + c\psi s\theta s\phi & s\psi s\phi + c\psi c\phi s\theta \\ s\psi c\theta & c\psi c\phi + s\phi s\theta s\psi & -c\psi s\phi + s\theta s\psi c\phi \\ -s\theta & c\theta s\phi & c\theta c\phi \end{bmatrix} \in \mathcal{SO}(3), \tag{2.4}$$

where s and c denotes *sine* and *cosine*, respectively. Since $\mathbf{R}(\boldsymbol{\eta}_2)$ is an element in the *special orthogonal group of order 3*, the following holds

$$\mathbf{R}(\boldsymbol{\eta_2})\,\mathbf{R}^T(\boldsymbol{\eta}_2) = \mathbf{R}^T(\boldsymbol{\eta}_2)\,\mathbf{R}(\boldsymbol{\eta}_2) = \mathbf{I}, \tag{2.5}$$

$$\det \mathbf{R}(\boldsymbol{\eta}_2) = 1 \quad , \tag{2.6}$$

$$\mathbf{R}^{-1}(\boldsymbol{\eta}_2) = \mathbf{R}^T(\boldsymbol{\eta}_2). \tag{2.7}$$

The rotational velocities are transformed from the {b}–frame to the {n}–frame according to

$$\dot{\boldsymbol{\eta}}_2 = \mathbf{T}(\boldsymbol{\eta}_2)\,\boldsymbol{\nu}_2, \tag{2.8}$$

where

$$\mathbf{T}(\boldsymbol{\eta}_2) = \begin{bmatrix} 1 & s\phi t\theta & c\phi t\theta \\ 0 & c\phi & -s\phi \\ 0 & s\phi/c\theta & c\phi/c\theta \end{bmatrix} \quad \theta \neq \pm\pi/2, \tag{2.9}$$

$$\mathbf{T}^{-1}(\boldsymbol{\eta}_2) = \begin{bmatrix} 1 & 0 & -s\theta \\ 0 & c\phi & c\theta s\phi \\ 0 & -s\phi & c\theta c\phi \end{bmatrix}, \tag{2.10}$$

where t denotes *tangent*.
Now, the 6 degrees of freedom kinematic equations may be expressed in compact form as

$$\dot{\boldsymbol{\eta}} = \mathbf{J}(\boldsymbol{\eta}_2)\,\boldsymbol{\nu}, \tag{2.11}$$

where

$$\mathbf{J}(\boldsymbol{\eta}_2) = \begin{bmatrix} \mathbf{R}(\boldsymbol{\eta}_2) & \mathbf{0} \\ \mathbf{0} & \mathbf{T}(\boldsymbol{\eta}_2) \end{bmatrix}.$$

Transformation Between {n} and {p}

The position of the {p}–frame in the {n}–frame is given as

$$\mathbf{p}_p^n = \boldsymbol{\eta}_1 + \mathbf{R}(\boldsymbol{\eta}_2)\,\mathbf{p}_p, \tag{2.12}$$

where $\mathbf{p}_p^n$ denotes the location of the {p}–frame in the {n}–frame, $\boldsymbol{\eta}_1$ is the position of the {b}–frame in the {n}–frame, and $\mathbf{p}_p = \left[x_p, y_p, z_p\right]^T$ is the vector describing the location of the {p}–frame in the {b}–frame (by assuming that the vessel is a rigid body, this vector is constant). The translational velocities of the {p}–frame in the {n}–frame are

$$\begin{aligned} \dot{\mathbf{p}}_p^n &= \dot{\boldsymbol{\eta}}_1 + \dot{\mathbf{R}}(\boldsymbol{\eta}_2)\,\mathbf{p}_p && (2.13)\\ &= \mathbf{R}(\boldsymbol{\eta}_2)\,\boldsymbol{\nu}_1 + \mathbf{R}(\boldsymbol{\eta}_2)\,\mathbf{S}(\boldsymbol{\nu}_2)\,\mathbf{p}_p && (2.14)\\ &= \mathbf{R}(\boldsymbol{\eta}_2)\,\boldsymbol{\nu}_1 - \mathbf{R}(\boldsymbol{\eta}_2)\,\mathbf{S}\left(\mathbf{p}_p\right)\boldsymbol{\nu}_2, && (2.15) \end{aligned}$$

where the skew-symmetric cross-product operator $\mathbf{S}\left(\mathbf{p}_p\right) : \mathbb{R}^3 \rightarrow \mathbb{R}^3$ is given as

$$\mathbf{S}\left(\mathbf{p}_p\right) = \begin{bmatrix} 0 & -z_p & y_p \\ z_p & 0 & -x_p \\ -y_p & x_p & 0 \end{bmatrix}, \; \mathbf{S}\left(\mathbf{p}_p\right) = -\mathbf{S}^T\left(\mathbf{p}_p\right). \tag{2.16}$$

The velocities of the {p}–frame in the {n}–frame can be written in compact form as

$$\dot{\boldsymbol{\eta}}_p = \mathbf{J}(\boldsymbol{\eta}_2)\,\mathbf{H}\left(\mathbf{p}_p\right)\boldsymbol{\nu}, \tag{2.17}$$

where

$$\mathbf{H}\left(\mathbf{p}_p\right) = \begin{bmatrix} \mathbf{I} & \mathbf{S}^T\left(\mathbf{p}_p\right) \\ \mathbf{0} & \mathbf{I} \end{bmatrix}. \tag{2.18}$$

Transformation Between {b} and {p}

From (2.17) it can be seen that the velocities in the {p}–frame can be expressed as

$$\boldsymbol{\nu}_p = \mathbf{H}\left(\mathbf{p}_p\right)\boldsymbol{\nu}. \tag{2.19}$$

Similarly, forces and moments in the {p}–frame may written

$$\boldsymbol{\tau}_p = \mathbf{H}\left(\mathbf{p}_p\right)\boldsymbol{\tau}. \tag{2.20}$$

The latter transformation is particularly useful, since hydrodynamic software can have a coordinate system different from that associated with the center of gravity. Thus, the calculated forces may be transformed to any given reference system through (2.20).

2.1.2 Dynamics

The hydrodynamic modelling described in the following is based on Faltinsen (1990), Fossen (2002) and Sørensen (2005). When modelling for control purposes, it is common to separate the model in a low frequency part and a wave frequency part. It is assumed that the two parts can be superimposed in order to determine the total motion of the vessel. Also, it is common to assume that the body does not deform, i.e. it behaves like a rigid body.

Rigid body dynamics

Newton's second law of motion states that

Definition 2.1 *The relationship between an object's mass m, its acceleration a, and the applied force F is*

$$F = ma. \tag{2.21}$$

This applies in an inertial frame, such as the {n}–frame. For a marine vessel, (2.21) can be written in the {n}–frame as

$$\mathbf{M}(\boldsymbol{\eta})\ddot{\boldsymbol{\eta}} = \boldsymbol{\tau}^{\{n\}}, \tag{2.22}$$

where $\mathbf{M}(\boldsymbol{\eta}) \in \mathbb{R}^{6\times6}$ is the rigid body mass matrix in the {n}–frame, and $\boldsymbol{\tau}^{\{n\}} \in \mathbb{R}^6$ denotes the vector containing the external forces and moments. In the {b}–frame, (2.22) can be written

$$\mathbf{M}_{RB}\dot{\boldsymbol{\nu}} + \mathbf{C}_{RB}(\boldsymbol{\nu})\boldsymbol{\nu} = \boldsymbol{\tau}, \tag{2.23}$$

where the term $\mathbf{C}_{RB} \in \mathbb{R}^{6\times6}$ denotes the rigid body Coriolis–centripetal matrix, and must be added since the {b}–frame is not inertial. The system matrices $\mathbf{M}_{RB}$ and $\mathbf{C}_{RB}$ have some inherent properties which are frequently exploited in control system design:

$$\mathbf{M}_{RB} = \mathbf{M}_{RB}^T > 0, \quad \dot{\mathbf{M}}_{RB} = \mathbf{0}, \tag{2.24}$$

$$\mathbf{C}_{RB}(\boldsymbol{\nu}) = -\mathbf{C}_{RB}^T(\boldsymbol{\nu}), \quad \forall \boldsymbol{\nu} \in \mathbb{R}^6. \tag{2.25}$$

The rigid–body Coriolis–centripetal matrix can be computed from $\mathbf{M}_{RB}$. The final rigid–body dynamic equation, neglecting the surrounding environment, may be written

$$\mathbf{M}_{RB}\dot{\boldsymbol{\nu}} + \mathbf{C}_{RB}(\boldsymbol{\nu})\boldsymbol{\nu} = \boldsymbol{\tau}_{RB}, \tag{2.26}$$

$$\dot{\boldsymbol{\eta}} = \mathbf{J}(\boldsymbol{\eta}_2)\boldsymbol{\nu}. \tag{2.27}$$

The environmental effects acting on a vessel are numerous. The importance of the different effects depend strongly on the weather condition, the hull and topside design and the velocity and heading of the vessel. Generally speaking, wind will for offshore vessels be the dominating second order effect, at least for heavy weather conditions. However, waves and current will also have significant second order effects. Waves will in addition constitute the main first order effects. The different environmental effects and hydrodynamic phenomena acting on marine vessels are described in Faltinsen (1990).
The nonlinear, low-frequency, 6 degrees of freedom mathematical model of a marine vessel including environmental effects can be written

$$(\mathbf{M}_{RB} + \mathbf{M}_A)\,\dot{\boldsymbol{\nu}} + \mathbf{C}_{RB}(\boldsymbol{\nu})\,\boldsymbol{\nu} + \mathbf{C}_A(\boldsymbol{\nu}_r)\,\boldsymbol{\nu}_r + \mathbf{D}(\boldsymbol{\nu}_r)\,\boldsymbol{\nu}_r + \mathbf{g}(\boldsymbol{\eta}) = \boldsymbol{\tau}_{env} + \boldsymbol{\tau}_m + \boldsymbol{\tau}, \quad (2.28)$$

where $\mathbf{M}_A \in \mathbb{R}^{6\times6}$ denotes the asymptotic added mass matrix for $\omega \to 0$, $\mathbf{C}_A(\boldsymbol{\nu}_r) \in \mathbb{R}^{6\times6}$ denotes the Coriolis–centripetal matrix originating from $\mathbf{M}_A$, $\mathbf{D}(\boldsymbol{\nu}_r) \in \mathbb{R}^{6\times6}$ denotes the damping matrix, including effects from wave drift damping, skin friction and vortex shedding, $\mathbf{g}(\boldsymbol{\eta}) \in \mathbb{R}^6$ denotes the vector containing the buoyancy effects, $\boldsymbol{\tau}_{env} \in \mathbb{R}^6$ denotes the vector containing the environmental loads, $\boldsymbol{\tau} \in \mathbb{R}^6$ is the propulsion vector, and $\boldsymbol{\tau}_m \in \mathbb{R}^6$ denotes the vector containing the generalized mooring forces. Based upon the desired accuracy, the hydrodynamic properties identified by $\mathbf{M}_A$, $\mathbf{C}_A(\boldsymbol{\nu}_r)$, $\mathbf{D}(\boldsymbol{\nu}_r)$ and $\mathbf{g}(\boldsymbol{\eta})$ in (2.28) can be determined through: i) comparison with existing structures; ii) numerical software such as HydroD and ShipX; iii) model tests, and iv) full scale tests. It is commonly recognized that the chronology of the list represents an increased accuracy in the results. Determining the desired propulsion vector is the aim of this work. In general, there are loss terms and rate saturations between the desired thrust and the actual output. However, in this work, these loss terms are neglected. For a thorough description of the loss terms associated with propellers and machinery, and their importance, see Smogeli (2006). The mooring system was implemented in the MSS for this specific work, based on the finite element model developed by Aamo and Fossen (2001). The number of necessary finite elements for each mooring line depends strongly on the water depth, and have a strong influence on the simulation time. Therefore, in order for the MSS to be an efficient simulation tool, the water depth considered in this work is limited to 200 meters. Four mooring lines consisting of traditional stud-chain links make up the mooring system, spread evenly around the turret center. Each line is divided into 30 finite elements. The terms $\mathbf{M}_A$

and $\mathbf{C}_A(\boldsymbol{\nu}_r)$ have the following properties

$$\mathbf{M}_A = \mathbf{M}_A^T, \tag{2.29}$$

$$\mathbf{C}_A(\boldsymbol{\nu}_r) = -\mathbf{C}_A^T(\boldsymbol{\nu}_r). \tag{2.30}$$

The relative velocity vector,$\boldsymbol{\nu}_r \in \mathbb{R}^6$, is given as

$$\boldsymbol{\nu}_r = \boldsymbol{\nu} - \boldsymbol{\nu}_c, \tag{2.31}$$

where $\boldsymbol{\nu}_c \in \mathbb{R}^6$ is the vector containing the current velocities. It is assumed that $\dot{\boldsymbol{\nu}}_c = \mathbf{0}$. Note that the rigid–body terms are only depended on $\boldsymbol{\nu}$.
The wave frequency model is based on a linear theory, i.e. it is assumed that the waves and motions are relatively small and are given in the hydrodynamic frame. For station keeping operations, the hydrodynamic frame is given by the parameters $\bar{\boldsymbol{\eta}} = [\bar{\boldsymbol{\eta}_1}, \bar{\boldsymbol{\eta}_2}]^T = [x_d, y_d, 0, 0, 0, \psi_d]^T$, i.e. the desired operating location. As long as the vessel oscillates with small amplitudes about this frame, the linear assumption holds. The wave frequency motions in the hydrodynamic frame can, according to Sørensen (2005), be described as

$$\mathbf{M}(\omega)\ddot{\boldsymbol{\eta}}_{Rw} + \mathbf{D}_p(\omega)\dot{\boldsymbol{\eta}}_{Rw} + \mathbf{G}\boldsymbol{\eta}_{Rw} = \boldsymbol{\tau}_{wave1}, \tag{2.32}$$

$$\dot{\boldsymbol{\eta}}_w = \mathbf{J}(\bar{\boldsymbol{\eta}}_2)\dot{\boldsymbol{\eta}}_{Rw,} \tag{2.33}$$

where $\boldsymbol{\eta}_{Rw} \in \mathbb{R}^6$ is the vector describing the wave frequency motions in the hydrodynamic frame, $\boldsymbol{\eta}_w \in \mathbb{R}^6$ is the wave frequency motion vector in the earth fixed frame, $\boldsymbol{\tau}_{wave1} \in \mathbb{R}^6$ is the vector containing the first-order generalized wave excitation forces, $\mathbf{M}(\omega) \in \mathbb{R}^{6\times6}$ is the frequency dependent mass matrix, containing both the rigid body and the added mass effects, $\mathbf{D}_p(\omega) \in \mathbb{R}^{6\times6}$ is the frequency dependent potential damping matrix and $\mathbf{G} \in \mathbb{R}^{6\times6}$ is the linear restoring matrix due to gravity and buoyancy. It is common to assume that the mooring lines do not affect the wave frequency motions, Triantafyllou (1994).
The frequency dependent terms $\mathbf{M}(\omega)$ and $\mathbf{D}_p(\omega)$ have memory effects which in general are important to consider. Kristiansen and Egeland (2003) have proposed a state space representation of these effects, which improves the effectiveness in numerical simulations. Again, the determination of the hydrodynamic effects constituting (2.32) can be determined with a different degree of accuracy.

2.2 Experimental Setup

The experimental tests were carried out in January 2007, in MCLab. The motivation of the model tests was to verify the performance of the controller demonstrated in numerical tests, as well as to verify the numerical

vessel model. The latter objective will prove wether or not MSS will be useful for testing the controller numerically, or if further model tests are necessary. The basin is 6.45 by 40 meters, and approximately 1.5 meters deep. The laboratory is equipped with a wave generator, which can produce both regular and irregular waves. It also has a position measurement system based upon four cameras, detecting five light bulbs located at the vessel, flashing with a frequency of 50 [*Hz*]. *At least* two cameras must detect *at least the same three* light bulbs in order for the positioning system to work. Loss of measurements usually leads to severe loss of position and termination of the experiment. The laboratory is also equipped with a moveable carriage, and a control room, where the operator can supervise the experiment. The vessel used in the experiments is called CyberShip III, and is shown in Figure 2.2. The main properties, along with those of the full-size vessel, are presented in Table 2.1. The vessel is equipped with four thrusters, three fully rotatable and one bow thruster. However, the heading of the thrusters is fixed during the experiments in order to reduce the number of error sources. As can be seen from Table 2.1, the scaling of the thrusters are not consistent. The bow thruster is over–dimensioned for the model vessel as compared with the other thrusters. (However, the actual output force from the bow thruster is negligible, indicating considerable losses for this specific thruster). For the experiments presented in this work, the vessel is equipped with a mooring line, composed of a spring, a wire and a gauge ring. The mooring line is attached to the bow of the vessel. The measurement of the tension in the mooring line enters the vessel's computer and is, along with a number of other measurements, transmitted via a wireless link to a computer located in the control room. The controller parameters are set in the control room, while the controller algorithm itself is implemented on the onboard computer, making it possible for the operator to change the controller parameters while the system is running. In order to simulate water current, a string running over a series of pulleys and connected to weights is attached to the stern of the vessel. Preferably, this load should be applied at the point where the hydrodynamic forces act, however, the layout of the light bulbs used for the position measurements does not allow this. Due to the fact that the external load is acting at the stern of the vessel, a yawing moment arises when the vessel turns relative to the string. This yawing moment would not appear if the forces were acting at the center of hydrodynamic forces. However, if this out-of-position setup is taken into consideration when designing the controller, and the thrusters are able to counteract this yawing moment, this poses no real problem. For the tests performed, the incorrectness in setup was counteracted by estimating the external loads in the frame that the appeared,

i.e. at the stern of the vessel. The string used is a very light weight line (monofilament), making the net weight of the line itself very small. However, when the line comes in contact with water (which inevitably happens from time to time) the weight is somewhat increased. Also, the pulleys used have a significant friction in their ball-bearings.

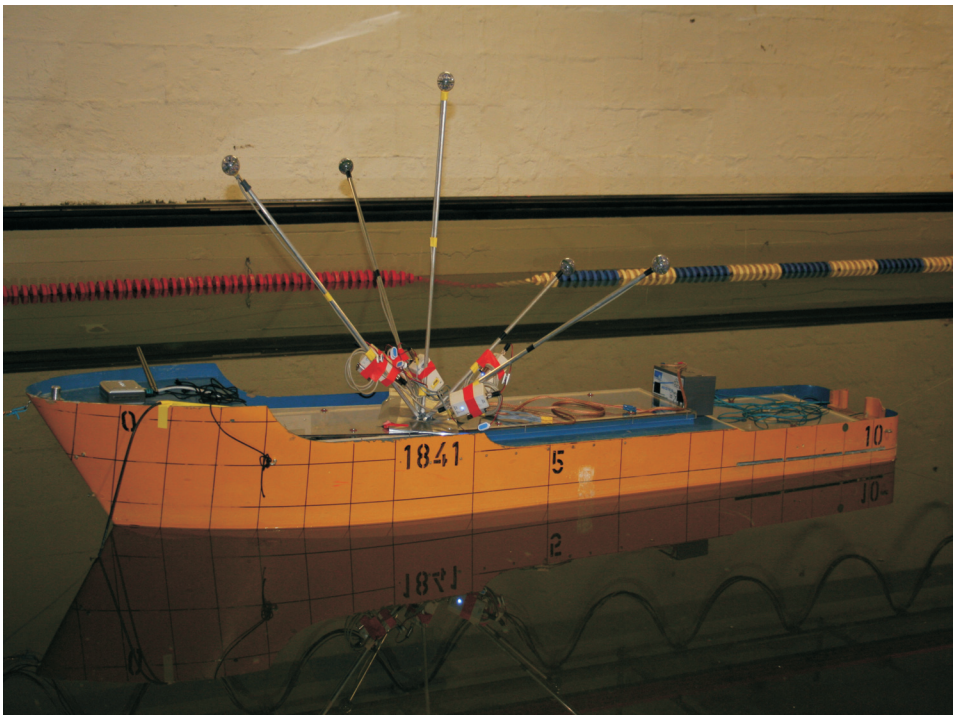

Figure 2.2: CyberShip III.

2.3 Structural Reliability

As stated in Section 1.3 the scope of this work is to develop a position mooring controller which ensures the integrity of the mooring system, at the same time as being a cost-effective alternative. Integrity in this context should be understood as reliability, or trustworthiness, during an operation, or during the entire lifetime of the structure. As mentioned in the introduction, marine structures may be very complex, often comprising several major components, such as mooring systems and risers, all critical for a safe and successful operation. The focus of this work is the safety

Table 2.1: Main characteristics of CyberShip III.

	Model	Full Scale
Length over all	2.275 $[m]$	68.28 $[m]$
Length between particulars	1.971 $[m]$	59.13 $[m]$
Breadth	0.437 $[m]$	13.11 $[m]$
Draught	0.153 $[m]$	4.59 $[m]$
Weight	74.2 $[kg]$	$2.3 * 10^6$ $[kg]$
Azimuth thrusters(3)	27 $[W]$	1200 $[kW]$
Tunnel thruster	27 $[W]$	410 $[kW]$

of the mooring system, with the possible failure mode corresponding to a single mooring line breakage. Due to manufacturing errors and deviations, wear and tear and possible previous unnoticed damages, the mooring lines may break under different loading conditions. In this work, it is assumed that these problems are taken care of by proper inspection routines. During the design of the mooring system, a safety factor is added to the diameter of the different mooring line sections in order to account for corrosion. By doing this, less strict inspection routines are needed. Also, the different classification societies, such as Det Norske Veritas (DNV) and The American Bureau of Shipping (ABS), along with governmental institutions such as The Norwegian Maritime Directorate (NMD), demand that each mooring line is over-dimensioned with a factor typically equal to 1.65 according to the expected maximum loading in a 100 year storm. Although these precautions are taken, there still exists a probability of failure. By deciding on the allowable failure probability, it is possible, from statistical data provided by the manufacturer of the mooring lines, to compute the maximum allowable static loading of the mooring lines. This section will give a short introduction to statistical methods used in this thesis, based on Madsen et al. (1986) and Melchers (1999), and describe the concept of structural reliability.

When concerned with waves and the linear responses of marine structures, it is common to assume that the statistical parameters are constant over a time period with a duration of (at least) 1 hour. This is frequently referred to as *short term statistics*. A second assumption is that the wave process (i.e. the surface elevation) is of a Gauss distribution (named after Carl Friedrich Gauss, 1777–1855). In Figure 2.3, an illustration of the probability density function (PDF) for a Normal distribution is shown in the upper half.

The corresponding cumulative distribution function (CDF) is shown in the lower half. The PDF is a real-valued function whose integral over any set gives the probability that a random variable has a value within this set. The PDF for the Normal distribution is given as

$$f(x) = \frac{1}{\sqrt{2\pi}} e^{\frac{-x^2}{2}}, \tag{2.34}$$

while the corresponding CDF is given as

$$F(x) = \int_{-\infty}^{x} f(t)\, dt. \tag{2.35}$$

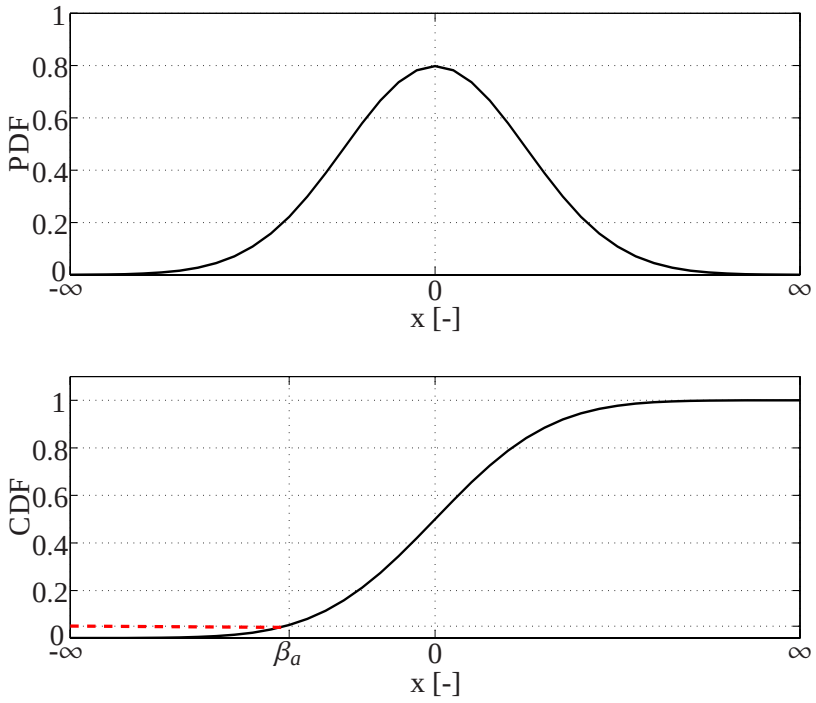

Figure 2.3: Illustration of the probability density function and the cumulative distribution function for a Normal distribution.

In order to be able to estimate the failure probability, it is necessary to know the difference between the maximum load a structure is able to withstand, R (often referred to as *resistance*), and the loads Q that it will be exposed to,

with the corresponding load effects S found from conventional structural analysis methods. The loads on marine structures are caused by wave-, wind- and current, and will fluctuate with time. The resistance will also in general be a function of time. A typical situation is that the extreme load effects increase with time, while the resistance decreases, as illustrated in Figure 2.4. Here t denotes the time, t_1 is the start time, t_2 is some arbitrary chosen time, while $f_S(s|t = t_1)$ and $f_S(s|t = t_2)$ are the probability density functions for the load effects at time t_1 and t_2 respectively. Similarly, $f_R(r|t = t_1)$ and $f_R(r|t = t_2)$ are the probability density functions for the resistance at time t_1 and t_2 respectively. The two dotted lines in Figure 2.4 are the mean values of R and S.

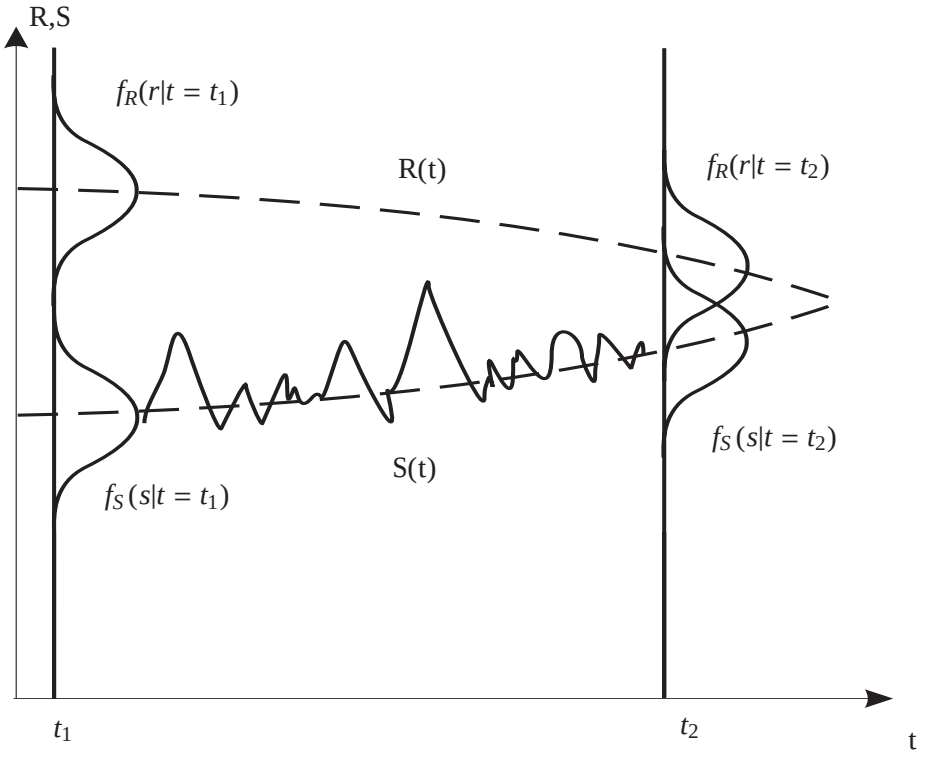

Figure 2.4: Illustration of the time-varying resistance, R(t), and the time-varying load S(t).

From the figure it is seen that the structure will fail if

$$Z = R(t) - S(t) < 0, \tag{2.36}$$

where Z is referred to as the safety margin. The probability that the event described by (2.36) will take place can be evaluated from the amount of overlap by the two probability density functions f_R and f_S, shown in Figure 2.4. At $t = t_1$, these two functions barely touch each other, while at $t = t_2$, they have a significant amount of overlap. The latter case represents a corresponding increase in the failure probability.
If it is chosen to use time-independent values of either R or S (or both), the minimum value of (2.36) on the interval [0,T], where T denotes the design life time or the time which a specific operation is expected to last, must be used. When concerned with maximum (minimum) value theory, an extreme value distribution, such as the Gumbel distribution, (also referred to as the type I asymptotic form), must be used, see Gumbel (1958) and Sødahl (1991). The Gumbel distribution may be applied in cases where the initial distribution has an exponentially decaying tail (which is the case for the Gauss distribution).
The probability of failure may be expressed as

$$p_f = P(Z = R - S \leq 0) = \int_{-\infty}^{\infty} \int_{-\infty}^{s \geq r} f_R(r)\, f_S(s)\, dr ds, \tag{2.37}$$

where it is assumed that R and S are independent. This can also be expressed as

$$p_f = P(Z \leq 0) = \int_{-\infty}^{\infty} F_R(x)\, f_S(x)\, dx, \tag{2.38}$$

where

$$F_R(x) = P(R \leq x) = \int_{-\infty}^{x} f_R(y)\, dy. \tag{2.39}$$

The integral in (2.38) is known as a convolution integral, where F_R denotes the CDF of R. Closed-form expressions of this integral can be obtained for certain distributions, such as the Gauss distribution. The first term of (2.37), $f_R(r)$, is frequently represented as a Gaussian variable, while the second term, $f_S(s)$, will for extreme sea states correspond to a Gumbel distribution.

2.3.1 δ-index

Assuming that R and S are independent and Gaussian random variables, with mean values μ_R and μ_S and variances σ_R^2 and σ_S^2, the quantity Z has a mean and variance given by

$$\mu_Z = \mu_R - \mu_S, \tag{2.40}$$
$$\sigma_Z^2 = \sigma_R^2 + \sigma_S^2. \tag{2.41}$$

The probability of failure may then be written as

$$p_f = P(R - S \leq 0) = P(Z \leq 0) = \Phi\left(\frac{0 - \mu_Z}{\sigma_Z}\right), \tag{2.42}$$

where $\Phi()$ is the standard normal distribution function (corresponding to $\mu = 0$ and $\sigma^2 = 1$). By inserting (2.40)–(2.41) into (2.42), we get

$$p_f = \Phi\left[\frac{-(\mu_R - \mu_s)}{\sqrt{\sigma_R^2 + \sigma_S^2}}\right] = \Phi(-\beta), \tag{2.43}$$

where

$$\beta = \frac{\mu_Z}{\sigma_Z} = \frac{(\mu_R - \mu_S)}{\sqrt{\sigma_R^2 + \sigma_S^2}}, \tag{2.44}$$

is defined as the safety index, see Cornell (1969). By defining an acceptable failure probability, $p_f = p_A$, one can find the corresponding value of β, i.e. β_A, that represents an acceptable lower bound on β (since decreasing β results in a higher failure probability). This lower value can be used to determine whether the resistance R is within the acceptable range as compared to the load effect, S. This is illustrated in Figure 2.3, where the red dotted line in the lower half represents a failure probability of 5%, with the corresponding β_A found along the horizontal axis.

As previously stated, the integrity of the mooring system is the concern of this work, with the failure mode corresponding to breakage of a single mooring line. The load results in a time-varying line tension, T_k, where the subscript k denotes mooring line k. The signal is filtered through a low-pass filter, so T_k may be written

$$T_k(t) \leq T_{k,lf}(t) + \varkappa\sigma_k, \tag{2.45}$$

where t denotes the time and $T_{k,lf}$ denotes the filtered, low frequency signal. The scalar $\varkappa$ is a scaling factor based on the tail behaviour of the chosen type of distribution which is applied to represent the extreme load effect (Gauss, Gumbel, etc.). The scaling factor measures the expected extreme value in terms of the standard deviation of the basic process. For a Gaussian dynamic response process with a corresponding Gumbel extreme value distribution, it can be shown that (Myrhaug (2005), Sødahl (1991))

$$\varkappa = \sqrt{2\ln(n)} + \frac{0.57722}{\sqrt{2\ln(n)}}, \tag{2.46}$$

where n is the number of individual maxima which occur during the considered time period. Finally, σ_k in (2.45) is the standard deviation of T_k, defined as

$$\sigma_k = \sqrt{\frac{1}{N}\sum_{i=1}^{N}\left(T_{k,i} - \bar{T}_k\right)^2}, \tag{2.47}$$

where N is the total number of samples used (i.e. N samples backwards in time), and $\bar{T}_k$ is the mean tension given as

$$\bar{T}_k = \frac{1}{N}\sum_{i=1}^{N} T_{k,i}. \tag{2.48}$$

The factor $\varkappa$ in (2.46), along with σ_k in (2.47), will compensate for the missing first order variations in the filtered measurement of the mooring line tension. From a thruster's point of view this is advantageous, since 1. order variations in the control signal are known to introduce unnecessary wear and tear of marine machinery.
For this application, the safety index β, (2.44), is reformulated (and renamed) according to

$$\delta_k(t) = \frac{T_{b,k} - \left(T_{k,lf}(t) + \varkappa\sigma_k\right)}{\sigma_{b,k}}, \tag{2.49}$$

where $T_{b,k}$ is the mean breaking strength of mooring line k, and $\sigma_{b,k}$ is the standard deviation of the mean breaking strength. As long as $\sigma_{b,k} \gg \sigma_k$ is fulfilled, we have that $\beta \approx \delta$. This condition is in general fulfilled, however there are two exceptions: i) for extreme sea states, and ii) when a large number of samples are used for calculating σ_k. In the case of extreme sea states, σ_k may become significant as compared to $\sigma_{b,k}$. Then $\sigma_{b,k}$ in the denominator of (2.49) is replaced by $\sqrt{\sigma_{b,k}^2 + \sigma_k^2}$. As for exception ii), this is best explained by an illustration. In Figure 2.5, an example of a particular load, T_k, is given in the upper part of the figure, with the corresponding $\sigma_{k,i}$ being plotted below, using different number of samples N for its estimation (see (2.47)). (Note that the load is not affected by the changing number of samples). The load is acquired from open loop simulations, i.e. no controller forces are active, and the sea state is kept constant. The number of samples used for the different $\sigma_{k,i}$ are $N_1 = 25$, $N_2 = 50$, $N_3 = 150$, and $N_4 = 300$ (where N_i corresponds to $\sigma_{k,i}$), with a sampling frequency of 5 [Hz]. The figure illustrates how, when using a relatively low number of samples ($\sigma_{k,1}$),

the first order variations dominate $\sigma_{k,i}$. However, as the number of samples is increased, the second order variations become more dominant. This is observed from the graphs of $\sigma_{k,2}$–$\sigma_{k,4}$, while $\sigma_{k,1}$ mainly reflects the high frequency energy in the signal. This is an important feature of σ_k that needs to be assessed thoroughly when choosing the sampling interval. By selecting a relatively large number of samples, significant second order changes in the tension will be captured by σ_k, thus increasing the right-hand term of (2.45), without actually representing a change in the sea state. For the cases where σ_k becomes significant, it should be included in the denominator of (2.49). However, it is important that the number of samples, N, is chosen such that changes of σ_k actually represent changes in the magnitude of the first order variations. It is also important that when the tests are initiated, the measurements are allowed to run for some time prior to turning the controller on, so that σ_k has a value based on the relevant environmental conditions.

The assumption that the tension in the mooring line is available for measurement needs some justification. Such measurement devices, exposed to a very harsh climate (salt water, possibly icy conditions, mechanical impacts, etc), are known to suffer from significant drift. Redundancy of measurement devices will somewhat reduce the drift, or at least help to detect it, however it will not alone solve the problem. When discussing drift of measurements, it is the second order tension variations that are of concern: The relative magnitude of the first order variations will not be affected by the drift. For mooring lines that are stock products, one will have good data for the relationship between force and extension, by knowing the anchor point, water depth and amount of chain laying on the sea floor. Thus, a possible solution is an observer checking the measurements from time to time for drift, in order to recalibrate the measurement devices when needed. Tests have shown, see Paper I, that a second order equation may represent the tension in a mooring line adequately for control purposes. The estimate of the mooring force based on the second order equation may be used for detecting and correcting drift of the measurements.

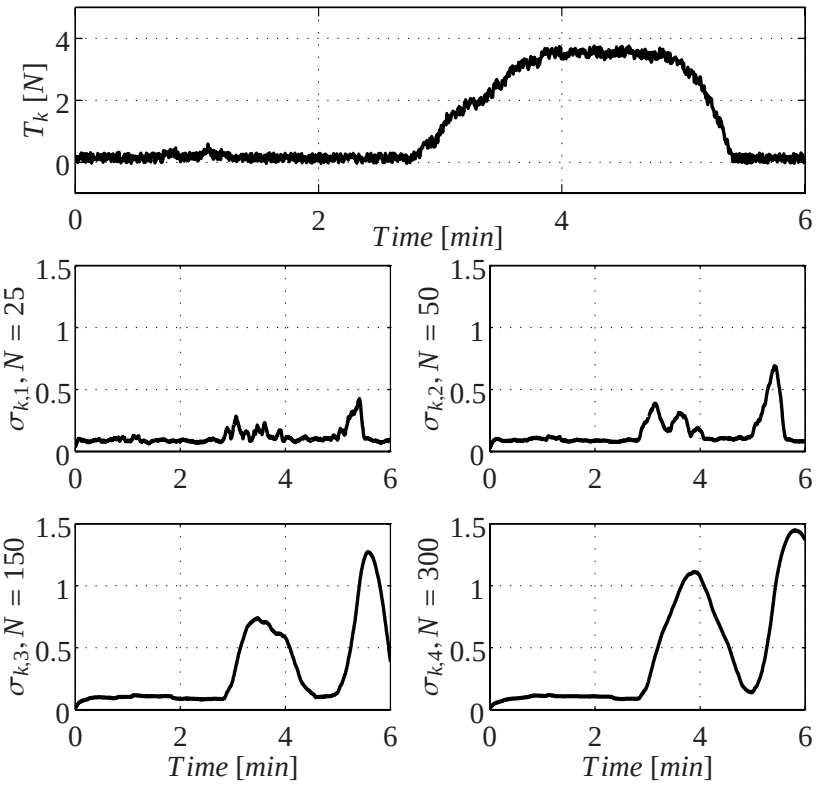

Figure 2.5: Variation of σ for different choices of N.

Chapter 3

Conclusions and Suggestions for Future Work

This thesis has considered control of surface vessels moored to the sea bed. A new approach for design of position mooring controllers have been developed, implemented and tested both numerically and experimentally. In Section 3.1 the results from the different papers are summarized and the conclusions are presented, while suggestions for future work are given in Section 3.2.

3.1 Conclusions

Control of marine systems in a harsh environment is an important issue. Presently, there is a strong research focus on this topic, ranging from supervisory control to local thruster control. By identifying critical components, and including their condition intrinsically in the controller, the load on the operator, and thus the possibility of false handling of an emergency situation may be reduced. As the aquacultural industry develops, with larger structures which are exposed to a harsher climate, the structures will become more complicated and more advanced. Thus, supervision and control of the structure will become necessary. A new controller methodology has been developed in order to include the condition of the mooring system directly in the controller. The methodology has been introduced for different controller schemes, both using the reliability index as a pre-tuning criterion (Paper I), and using it intrinsically in the controller (Papers II-III). The different controllers have been tested on different vessel models and since both the models and controllers vary, comparison of quantities in the form of thruster levels and vessel response presented in the different papers have

little meaning. Also the time used for tuning varies strongly. However, the properties, in the form of tuning ability, and behaviour of the closed-loop system, may be compared.

In Paper I a model of a futuristic aquacultural farm was developed. It consisted of three semi-submersible like modules, illustrated in Figure P1.2, a mooring system, and finally, control actuators in the form of a thruster and a foil. A reliability index, given by (P1.45), was applied to determine the maximum allowed deviation from the origin, which again determined the maximum energy that the vessel should have at any time. By introducing a nonlinear function using the energy of the system as an argument, described by (P1.47)–(P1.49), the closed loop system described by (P1.51)–(P1.52) ensured a smooth control and reduced loading of the thrusters. This again reduced the fuel consumption. The numerical simulations showed that the controller performed satisfactory. The controller ensured that the maximum allowed energy level was not violated, at the same time the thrusters were not run unnecessarily, see Figure P1.12. Also, the results showed that it is possible to utilize a foil to place the structure transversely to the incoming water current. This ensures the fish contained in the aft part of the structure supply of fresh water, see Figure P1.14. The ingenuity of the design was the nonlinear function, which ensured the reliability of the mooring system, and at the same time limited the fuel consumption to a minimum when the mooring system was able to sustain the environmental forces.

In Paper II the application was changed to an FPSO, moored to the seabed via a single point spread mooring system. However, the more important change was that the paper aimed at including the reliability criterion intrinsically in the controller. This was achieved by employing the backstepping technique for the controller design. The main result was summarized in a theorem, see Theorem P2.1. This time, it was not necessary to include a nonlinear function like the one introduced in Paper I, since the controller inherently had both motion damping capabilities and the ability of reducing the thrust when possible. The performance of the controller, when the vessel was exposed to a time varying current that eventually will make the tension in the mooring lines reach a critical level, is shown in Figure P2.6. The figure shows the time variation of δ and ψ. This proved that the controller behaved perfectly in this context. In Figure P2.8, the output of the thrusters is shown, with some leaps in the thrust as $\delta = \delta_s$. In addition to the above, the paper illustrated how a rather simple adaptive mechanism can detect changes in the environmental load. This estimate can be used in the controller, assuming that the loads are not available for measurement, see Figure P2.9. The paper also discusses the importance of the variable

σ_k, a variable that captures the effect of the first order loads, and how an increase in the sea state will affect this variable, as shown in Figure P2.10.
In Paper III the controller developed in Paper II was implemented on a model vessel named *CyberShip III*, a 1:30 model of an offshore supply vessel. The objective was to show that the controller performed well under realistic conditions. Three sea states were used, namely $H_s = 0$, 0.03 and 0.06 meters, which corresponds to $H_s = 0$, 0.9 and 1.8 meters for the full scale vessel. The results, see Figures P3.3 and P3.6, show that the controller was implementable for the given conditions, and that it worked the way it was supposed to; aiding the mooring system when necessary, otherwise it carried out motion damping and heading control. The thruster force was relatively smooth, and with no big leaps in the thruster usage for either of the sea states, shown in Figures P3.4 and P3.6. Since the laboratory time was limited, and a number of anticipated, and unanticipated, problems were encountered, more tests are needed in order to verify the results. Also, some modifications to the test setup would improve the validity of the results. New tests would make it possible to designate more time for tuning of the controller, thereby further improving its performance.
In order to be able to verify the numerical simulator, numerical simulations were run after the experiments to see if the main behaviour could be recreated. Numerical simulations are very useful in order to tune the controller prior to running experiments in order to save time in the laboratory. It is important to estimate the consistency of the numerical model as compared to the real world, and to understand the area of application of the numerical model. The vessel data used in the numerical model were obtained from various reports regarding CyberShip III, see Marintek (1988) and Nilsen (2003), while the mooring force was approximated by a second order polynomial. The artificial water current was introduced over a time span of two seconds, in order to simulate the friction introduced by the line running over three pulleys. Engine and propeller dynamics were excluded in the mathematical model. For the numerical tests, the load was applied at $Time = 2$ [min] and removed at $Time = 4$ [min], while the experimental load / unload times deviate slightly from this. The results for a significant waveheight $H_s = 0$ [m], are shown in Figure 3.1. In the left half, the δ-index, the heading ψ and the thrust τ from the experimental tests are plotted. The corresponding numerical results are plotted in the right half. The reference values, δ_s and ψ_s are plotted as dashed blue lines. The overall behaviour of the numerical results are much smoother than those obtained from the experiments. There are a number of possible reasons for this, for instance disturbances in the form of repercussive waves from previous experiments, in addition to unmodelled engine and thruster dynamics which

are not included in the numerical model. For the δ-index, both the level and the rate of convergence is in good accordance, while the convergence time for ψ is significantly longer for the numerical simulation, as compared to the experimental result. This may be caused by an overestimation of the damping in yaw used in the simulator. The coupling effects between the different degrees-of-freedom are obvious, with a small dip in the δ-index as ψ converges to ψ_s. The peaks in the thrust are in general lower and fewer for the numerical simulation, and the converged level in the period $3-4$ minutes is approximately 10% higher for the numerical simulations than in the experiments. Similar results have been obtained for an increase in the sea state.

It is clear that the numerical and experimental results are in relatively good agreement, at least for low velocities, which is the case for the translational degrees of freedom. For increasing velocities (the yaw rate is high compared to the translational velocity), it may seem that the numerical model does not match the experiments completely. More extensive model testing is therefore needed in order to verify whether or not the numerical model is adequate for moderate and higher velocities. Also, a more complete numerical model should be introduced, describing engine and propeller dynamics. However, it is concluded that the numerical simulator is adequate for testing the controller algorithms.

From a tuning perspective, and also from an implementability perspective, the controller proposed in Paper I is the preferred one. Determining the different parameters is a straight forward procedure, and the time used for tuning after implementation was short. The controller presented in Papers II and III is much more complicated and requires significantly more time for both implementation and tuning. However, for this controller, the reliability criterion is included directly in the controller. This avoids spending time to determine the controller limits prior to the initiation of the operation, saving vessel time, which constitutes an important economical aspect. Also, from the experience gained in the laboratory, the latter controller seems very robust when it comes to erroneous measurements and unmodelled effects.

3.2 Future Work

There are a number of possibilities for future work. On the theoretical side, an identification algorithm for the system matrices could be developed, so that the controller allows for changing system properties. This is relevant both for aquacultural farms and FPSOs, since both will load and offload

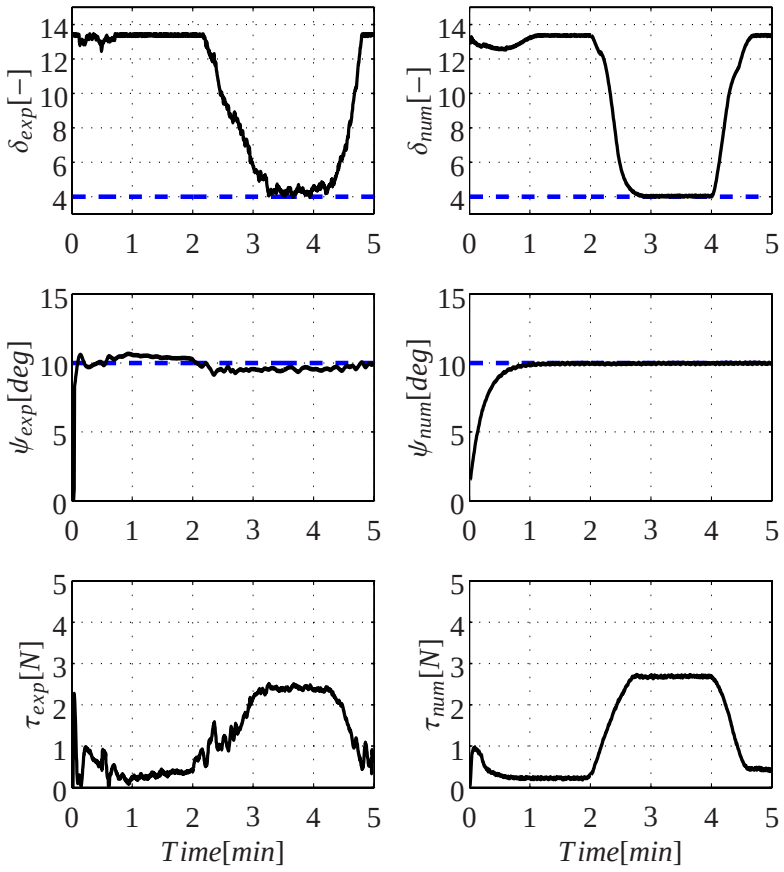

Figure 3.1: Comparison of experimental results, left half, and numerical results, right half.

a significant amount of mass from time to time, significantly changing the system properties. In order to be able to perform more realistic numerical simulations and experimental tests of aquacultural farms, a more elaborate model must be developed in order to determine the effects from the net itself and the fish contained by it.

There are also a number of fields which may benefit from introducing reliability based control. The only prerequisite is that it is possible to establish a reliability criterion and that the means of control are available or imple-

mentable. Possible applications for reliability based control are

- Production and drilling risers: Similar to the mooring application discussed in this text, with the riser angle as input argument for the reliability index, instead of the line tension.
- Pipe laying operations: Control of strain in order to avoid buckling and ovalization.
- Towing operations: Control of tension in towing cables.
- Couplings between two bodies: Control of clamping forces via active connectors.
- Lifting operations: Control of tension in the lifting cable, and supervision of environmental changes which may affect the operation.
- Road friction control: Active control of the ground pressure from foils in order to avoid skidding.

Also, it is possible to establish the reliability criterion as a monitoring criterion only, without any active control. This is in order to evaluate wether an operation can continue, or if it should be stopped due to a too high probability of failure.

Bibliography

Aamo, O. M. and Fossen, T. I. (1999). Controlling line tension in thruster assisted mooring systems, *Proceedings of the IEEE International Conference on Control Applications, Hawai'i, US* **2**: 1104–1109.

Aamo, O. M. and Fossen, T. I. (2001). Finite element modelling of moored vessels, *Mathematical and Computer Modelling of Dynamical Systems* **7(1)**: 47–75.

Aarset, M. F., Strand, J. P. and Fossen, T. I. (1998). Nonlinear vectorial backstepping with integral action and wave filtering for ships, *Proceedings of the IFAC Conference on Control Applications in Marine Systems, Fukuoka, Japan* pp. 83–89.

ASMI (2006). Marketplace competition: Farmed cod, *Seafood Market Bulletin, Juneau, Alaska, US* .

Bailey, P., Price, W. and Temarel, P. A. (1997). A unified mathematical model describing the manoeuvring of a ship in seaway, *Transactions The Royal Institution of Naval Architects, RINA* **140**: 131–149.

Baker, C. C. and McCafferty, D. B. (2005). Accident database review of human–element concerns: What do the results mean for classification?, *ABS Technical Papers* .

Balchen, J. G., Jenssen, N. A., and Sælid, S. (1981). Dynamic positioning of floating vessels based on Kalman filtering and optimal control, *Proceedings of the 19th IEEE Conference on Decision and Control, Albuquerque, New Mexico, US*, pp. 1–13.

Balchen, J. G., Jenssen, N. A., Mathisen, E. and Sælid, S. (1980). A dynamic positioning system based on Kalman filtering and optimal control, *Modeling, Identification and Control* **1(3)**: 135–163.

Balchen, J. G., Jenssen, N. A. and Sælid, S. (1976). Dynamic positioning using Kalman filtering and optimal control theory, *Proceedings of the IFAC/IFIP Symposium, Amsterdam, The Netherlands* pp. 183–186.

Berntsen, P. I. B., Aamo, O. M. and Leira, B. J. (2006). Position mooring based on structural reliability, *Proceedings of the 7th Conference on Manoeuvring and Control of Marine Craft Lisbon, Portugal* .

Berntsen, P. I. B., Aamo, O. M. and Leira, B. J. (2008). Structural reliability–based control of moored interconnected structures, *Control Engineering Practice* **16(4)**: 495–504.

Berntsen, P. I. B., Aamo, O. M. and Sørensen, A. J. (2003). Modelling and control of single point moored interconnected structures, *Proceedings of the 6th Conference on Manoeuvring and Control of Marine Crafts, Girona, Spain* .

Berntsen, P. I. B., Leira, B. J., Aamo, O. M. and Sørensen, A. J. (2004). Structural reliability criteria for control of large–scale interconnected marine structures, *Proceedings of the 23rd International Conference on Offshore Mechanics and Arctic Engineering, Vancouver, Canada* .

Brown, D. (2007). Recent advances in floating production systems and their seabed connections, *Proceedings of the 26th International Conference on Offshore Mechanics and Arctic Engineering, San Diego, California, US* .

Byrnes, C. I. and Isidori, A. (1989). New results and examples in nonlinear feedback stabilization, *Systems and Control Letters* **12**: 437–442.

Cherry, D. (2006). Farmed cod where is it?, *The Wave, Seattle, Washington, US* .

Cornell, C. A. (1969). A probability-based structural code, *Journal of the American Concrete Institute* **60(12)**: 974–985.

Faltinsen, O. M. (1990). *Sea Loads on Ships and Offshore Structures*, Cambridge University Press, Cambridge, UK.

FAO (2005). The state of world fisheries and aquaculture, *Rome, Italy* .

FAO (2006). The state of world fisheries and aquaculture, *Rome, Italy* .

Fossen, T. (2005). A nonlinear unified state–space model for ship maneuvreing and control in a seaway, *International Journal of Bifurcation and Chaos* **15**: 2717–2746.

Fossen, T. I. (2002). *Marine Control Systems*, Marine Cybernetics, Trondheim, Norway.

Fossen, T. I. and Grøvlen, Å. (1998). Nonlinear output feedback control of dynamically positioned ships using vectorial observer backstepping, *IEEE Transactions on Control Systems Technology* **6(1)**: 121–128.

Fossen, T. I. and Smogeli, Ø. N. (2004). Nonlinear time–domain strip theory formulation for low–speed manoeuvring and station–keeping, *Modeling, Identification and Control* **24(4)**: 201–221.

Fossen, T. I. and Strand, J. P. (2001). Nonlinear passive weather optimal positioning control (wopc) system for ships and rigs: Experimental results, *Automatica* **37(5)**: 701–715.

Fung, P. T. and Grimble, M. J. (1983). Dynamic ship positioning using self–tuning Kalman filter, *IEEE Transactions on Automatic Control* **28(3)**: 339–350.

Glenne, B. (1997). *The Saga of Saga*, Saga Petroleum, Oslo, Norway.

Grimble, M. J., Patton, R. J. and Wise, D. A. (1980). The design of dynamic ship positioning control systems using stochastic optimal theory, *Optimal Control Applications and Methods*, **1**: 167–202.

Grimble, M. J., Patton, R. J. and Wise, D. A. (1983). Use of Kalman filtering techniques in dynamic ship positioning systems, *IEEE Transactions on Automatic Control* **28(3)**: 331–339.

Gumbel, E. J. (1958). *Statistics of Extremes*, Columbia University Press, New York, US.

Ihle, I. A. F., Jouffroy, J. and Fossen, T. I. (2006). Formation control of marine surface craft: A lagrangian approach, *IEEE Journal of Oceanic Engineering* **31(4)**: 922–934.

IMO (1994). Guidelines for vessels with dynamic positioning systems, *IMO MSC Circular Resolution 645* .

Joshi, S. M. (1989). *Control of Large Flexible Space Structures*, Springer-Verlag New York Inc., New York, US.

Kaushik, S. J. (2000). Feed allowance and feeding practices, *Recent advances in Mediterranean aquaculture finfish species diversification* **47**: 53–59.

Khalil, H. K. (2002). *Nonlinear Systems, 3rd ed.*, Prentice Hall, New Jersey, US.

Koditschek, D. E. (1987). Adaptive techniques for mechanical systems, *Proceedings of the 5th Yale Workshop on Adaptive Systems, Connecticut, New Haven, US* pp. 259–265.

Kokotović, P. V. (1991). The joy of feedback, *IEEE Control Systems Magazine* **12**: 7–17.

Kålås, J. A., Å. Viken and Bakken, T. (2006). 2006 Norwegian red list, *Norwegian Biodiversity Information Centre, Trondheim, Norway* .

Kristiansen, E. and Egeland, O. (2003). Frequency–dependent added mass in models for controller design for wave motion damping, *Proceedings of the 6th Conference on Manoeuvring and Control of Marine Crafts, Girona, Spain* pp. 2195–2216.

Krstić, M., Kanellakopoulos, I. and Kokotović, P. V. (1995). *Nonlinear and Adaptive Control Design*, John Wiley and Sons, Inc, New York, US.

Lin, J.-S. and Kanellakopoulus, I. (1997). Nonlinear design of active suspensions, *IEEE Control Systems Magazine* **17(3)**: 45–59.

Lindegaard, K. P. W. (2003). *Acceleration Feedback in Dynamic Positioning Systems*, PhD thesis, Norwegian University of Science and Technology, Trondheim, Norway.

Madsen, H., Krenk, S. and Lind, N. C. (1986). *Methods of Structural Safety*, Prentice–Hall, Inc., Englewood Cliffs, New Jersey, US.

Mann, C. C. (2004). The blue revolution, *Wired* **12(5)**.

Marintek (1988). Seakeeping tests on T–Agos 1–main report, *Trondheim, Norway* .

McGovern, D. (2006). Cooke harvest first farmed cod, *The Wave, Seattle, Washington, US* .

Melchers, R. E. (1999). *Structural Reliability Analysis and Prediction, 2.ed.*, John Wiley & Sons, Chichester, UK.

Muncer, M. (2003). *Analysis of Accident Statistics for Floating Monohull and Fixed Installations*, HSE Books, Suffolk, UK.

Myrhaug, D. (2005). *Statistics of Narrow Band Processes and Equivalent Linearizing*, Lecture notes, UK-2005-74, Department of Marine Technology, NTNU, Trondheim, Norway.

Newman, J. N. (1977). *Marine Hydrodynamics*, MIT Press, Cambridge, MA, US.

Nguyen, T. D. and Sørensen, A. J. (2007). Setpoint chasing for thruster-assisted position mooring, *Proceedings of the 26th International Conference on Offshore Mechanics and Arctic Engineering, San Diego, California, US* .

Nguyen, T. D., Sørensen, A. J. and Quek, S. T. (2007). Design of hybrid controller for dynamic positioning from calm to extreme sea conditions, *Automatica* **43**: 768–785.

Nilsen, T. (2003). *Development of CyberShip 3*, Master thesis, Norwegian University of Science and Technology, Dept. of Marine Technology, Trondheim, Norway.

NS9415 (August, 2003). Marine fish farms. requirements for design, dimensioning, production, installation and operation, *ICS 65.150; 67.260. 1. Edition, Oslo, Norway* .

Perez, T., Smogeli, Ø. N., Fossen, T. I. and Sørensen, A. J. (2006). An overview of marine systems simulator (MSS): A Simulink toolbox for marine control systems, *Modeling, Identification and Control* **27(4)**: 259–275.

Pratt, J. A., Priest, T. and Castaneda, C. J. (1997). *Offshore Pioneers: Brown & Root and the History of Offshore Oil and Gas*, Gulf Publishing Company, Houston, Texas, US.

Robertsson, A. and Johansson, R. (1998). Comments on nonlinear output feedback control of dynamically positioned ships using vectorial observer backstepping, *IEEE Transactions on Control Systems Technology* **6(3)**: 439–441.

Ryu, S. and Kim, M. H. (2005). Coupled dynamic analysis of thruster–assisted turret-moored fpso, *Proceedings of OCEANS'03, San Diego, CA, US* .

Sælid, S., Jenssen, N. A. and Balchen, J. G. (1983). Design and analysis of a dynamic positioning system based on Kalman filtering and optimal control, *IEEE Transactions on Automatic Control* **28(3)**: 331–339.

Smogeli, Ø. (2006). *Control of Marine Propellers – From Normal to Extreme Conditions*, PhD thesis, Norwegian University of Science and Technology, Trondheim, Norway.

Smogeli, Ø., Perez, T., Fossen, T. and Sørensen, A. J. (2005). The marine systems simulator state–space model representation for dynamically positioned surface vessels, *International Maritime Association of the Mediterranean IMAM Conference, Lisbon, Portugal* .

Sødahl, N. R. (1991). *Methods for Design and Analysis of Flexible Risers*, PhD thesis, Norwegian University of Science and Technology, Trondheim, Norway.

Solberg, H. (2007). *North Sea Saga*, Horn Forlag AS, Oslo, Norway.

Solsletten, V. (2006). Cod farmers top norwegian producers ranking, *The Wave, Seattle, Washington, US* .

Sonntag, E. D. and Sussmann, H. J. (1988). Further comments on the stabilization of the angular velocity of a rigid body, *Systems and Control Letters* **12**: 213–217.

Sørensen, A. J. (2004). *Marine Cybernetics–Modelling and Control*, Lecture notes, UK-2004-76, Department of Marine Technology, NTNU, Trondheim, Norway.

Sørensen, A. J. (2005). Structural issues in the design and operation of marine control systems, *Annual Reviews in Control* **29**: 125–149.

Sørensen, A. J., Leira, B. J., Strand, J. P. and Larsen, C. M. (2001). Optimal setpoint chasing in dynamic positioning of deep–water drilling and intervention vessels, *International Journal of Robust and Nonlinear Control* **11**: 1187–1205.

Sørensen, A. J., Lindegaard, K. P. and Hansen, E. D. D. (2002). Locally multiobjective H_2 and H_∞ control of large-scale interconnected marine structures, *Proceedings of the 41st IEEE Conference on Decision and Control, Las Vegas, NV, US* **2**: 1705–1710.

Sørensen, A. J., Sagatun, S. I. and Fossen, T. I. (1996). Design of a dynamic positioning system using model–based control, *Control Engineering Practice* **4(3)**: 359–368.

Sørensen, A. J. and Strand, J. P. (1998). Positioning of semi–submersible with roll and pitch damping, *Proceedings of the IFAC Conference on Control Applications in Marine Systems, Fukuoka, Japan* pp. 67–73.

Sørensen, A. J. and Strand, J. P. (2000). Positioning of small–waterplane–area marine constructions with roll and pitch damping, *Journal of Control Engineering in Practice* **8(2)**: 205–213.

Sørensen, A. J., Strand, J. P. and Fossen, T. I. (1999). Thruster assisted position mooring system for turret–anchored fpsos, *Proceedings of the IEEE International Conference on Control Applications, Hawai'i, US* **2**: 1110–1117.

Spong, M. W. (1990). The control of flexible joint robots: A survey, *New Trends and Applications of Distributed Parameter Control Systems, Lecture notes*, Marcel Dekker Publishers, New York, US.

Strand, J. P. (1999). *Nonlinear Position Control Systems Design for Marine Vessels*, PhD thesis, Norwegian University of Science and Technology, Trondheim, Norway.

Strand, J. P. and Fossen, T. I. (1999). Passive nonlinear observer design for ships using lyapunov methods: Full–scale experiments with a supply vessel, *Automatica* **35(1)**: 3–16.

Strand, J. P., Sørensen, A. J. and Fossen, T. I. (1997). Modelling and control of thruster assisted position mooring systems for ships, *Proceedings of the 4th Conference on Manouvering and Control of Marine Craft, Brijuni, Croatia*, pp. 160–165.

Taggart, R. (1962). Dynamic positioning of the mohole experimental drilling ship, *Proceedings of the IRE* **50(11)**: 2255–2262.

Teel, A. R. (2002). *Notes on Nonlinear Control and Analysis*, Lecture notes, UCSB, Santa Barbara, California, US.

Triantafyllou, M. S. (1994). Cable mechanics for moored floating systems, *Proceedings of the 7th International Conference on the Behaviour of Offshore Structures, Massachusetts Institute of Technology, US* **2**: 67–77.

Tsinas, J. (1989). Sufficient Lyapunov–like conditions for stabilization, *Mathematics of Control, Signal and Systems* **2**: 343–357.

Worm, B., Barbier, E. B., Beaumont, N., Duffy, J. E., Folke, C., Halpern, B. S., Jackson, J. B. C., Lotze, H. K., Micheli, F., Palumbi, S. R., Sala, E., Selkoe,

K. A., Stachowicz, J. J. and Watson, R. (2006). Impacts of biodiversity loss on ocean ecosystem services, *Science* **314(5800)**: 787–790.

Yergin, D. (1991). *The Prize: The Epic Quest for Oil, Money, and Power*, Simon & Scuster, New York, US.

Paper I

Structural reliability-based control of moored interconnected structures

Per Ivar Barth Berntsen[a], Ole Morten Aamo[b], Bernt J. Leira[a], Asgeir J. Sørensen[a]

[a]*Department of Marine Technology, Norwegian University of Science and Technology, N-7491 Trondheim, Norway*
[b]*Department of Engineering Cybernetics, Norwegian University of Science and Technology, N-7491 Trondheim, Norway*

Abstract

In this paper, a model of a futuristic fish farming structure is developed and problems related to interconnected marine structures and strategies for configuration control are studied. A control system is designed that: 1) Ensures limited loading of the mooring system; 2) Keeps the chain of surface modules aligned transversely to the incoming current, and; 3) Ensures positive strain in the connectors between the modules. Control actuation is by means of a thruster mounted on the first module, and a hydrofoil mounted on the last module. The performance of the control system is demonstrated by simulations, and evaluated by a structural reliability criterion referred to as the delta index.

Keywords: Marine Systems, Large-scale systems, Interconnected systems, Configuration control, Structural reliability.

Figure P1.1: Example of interconnected marine structure: floating airport. The illustration is shown by courtesy of Moss Maritime a.s.

P1.1 Introduction

Large-scale interconnected marine structures are being considered for a number of applications, such as platforms for offshore oil and gas exploitation, sea-farming and floating airports (see Figures P1.1 and P1.2). These structures may consist of a large number of modules (floating modules, mooring systems, risers, etc.), connected to each other via rigid or flexible connectors. Challenges associated with these systems include modelling of hydrodynamic loads and the development of automatic control laws for configuration control and motion damping. The control problems are related to the ones encountered in positioning and tracking of ships, Fossen (2002), but are also similar to the ones encountered in the fields of flexible joint robotics, Spong (1990), active suspensions, Lin and Kanellakopoulus (1997), and control of large flexible space structures, Joshi (1989). This paper is an extension of the work presented in Berntsen et al. (2003).
In a 20-25 year perspective, aquacultural production and harvesting of natural bio-resources in the ocean are envisaged as increasing ten-fold. Locations exposed to harsh weather are expected to be used for fish farming, creating the need for more durable structures, possibly including automatic configuration control and motion damping. It is also foreseen that mobile structures will be used making it possible to change location temporarily,

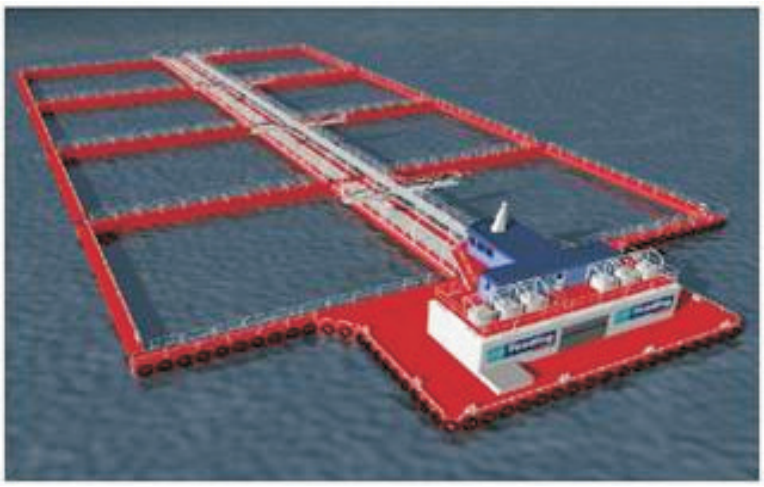

Figure P1.2: Sketch of fish farm.

for instance during algae attacks. It may then be attractive to move into more weather-exposed open water areas. By using automatic control for vibration and motion damping, marginal structures may be able to sustain higher sea states coping with fatigue and large responses.
In this paper, we develop a numerical model of a futuristic fish farming structure. Today, most fish farms are placed in locations where environmental loads from wind, waves and currents, are favorable. Typically, they are placed in fjords, or downstream of islands, where the current is smaller than 0.3 $\left[\frac{m}{s}\right]$, and the significant wave height is less than 1 $[m]$.
The paper is organized as follows. The case study is presented in Section P1.2. The process plant model is presented in Section P1.3. In Section P1.4 the controller is developed, followed by the results from the simulations in Section P1.5. Conclusions and suggestions for future work are given in Section P1.6.

P1.2 Case study

The example studied is sketched in Figures P1.2 and P1.3. The structure consists of five surface modules interconnected in a chain, with the first module moored to the seabed via four mooring cables. The four cables are connected to the same point on the first module, allowing the surface structure to rotate freely. This configuration is motivated by several con-

siderations. A single point mooring system, as opposed to multiple point mooring systems, is preferable from the point of view of: 1) Cost effectiveness; 2) Applicability in terms of the size and configuration of the attached surface structure; 3) Ease of operations like attachment and detachment of surface structure; 4) Modularity in terms of adding or removing individual modules, and; 5) Rotational mobility of the structure, which enables continuous supply of clean water to the fish by ensuring that fish contained in one part of the structure do not spend long periods of time in the wake of other parts of the structure. Control actuation is by means of a thruster mounted on the first module, and a hydrofoil mounted on the last module. The focus in this application is on problems related to tidal currents of high eccentricity. The surface current is assumed to be given by

$$\mathbf{V}_c = \begin{bmatrix} v_x \\ v_y \end{bmatrix} = \begin{bmatrix} A_x \sin\left(2\pi \cdot \frac{t}{T}\right) \\ A_y \cos\left(2\pi \cdot \frac{t}{T}\right) \end{bmatrix}, \tag{P1.1}$$

where $T = 12 \times 3600$ (tidal cycle of 12 hours), and $A_x = 0.3$ and $A_y = 0.01$ are the amplitudes of the current in the Earth-fixed x- and y- directions, respectively. Notice that $A_x \gg A_y$, giving a tidal ellipse with large eccentricity, which is typical for tidal currents found in fjords.
A steady seastate is considered which is characterized by significant wave height $H_s = 2$ $[m]$, peak period $T_P = 8.7$ $[s]$ and mean direction 60 degrees. This represents an extreme seastate for a fjord (NS9415 (August, 2003)).

P1.3 Process plant model

In the following section the process plant model of the moored interconnected fish farm structure is developed. The process plant will serve as the real world in the simulations, thus the controller performance will be judged on the basis of this mathematical model. An accurate description is therefore essential for the credibility of the work, and facilitates reproducability of the results.

Modules

Module kinematics

The following reference frames are used, see Figure P1.4:

- The Earth-fixed frame, denoted $X_E Y_E Z_E$, is placed so that the $X_E Y_E$ plane coincides with the water surface, and the Z_E axis is positive downwards.

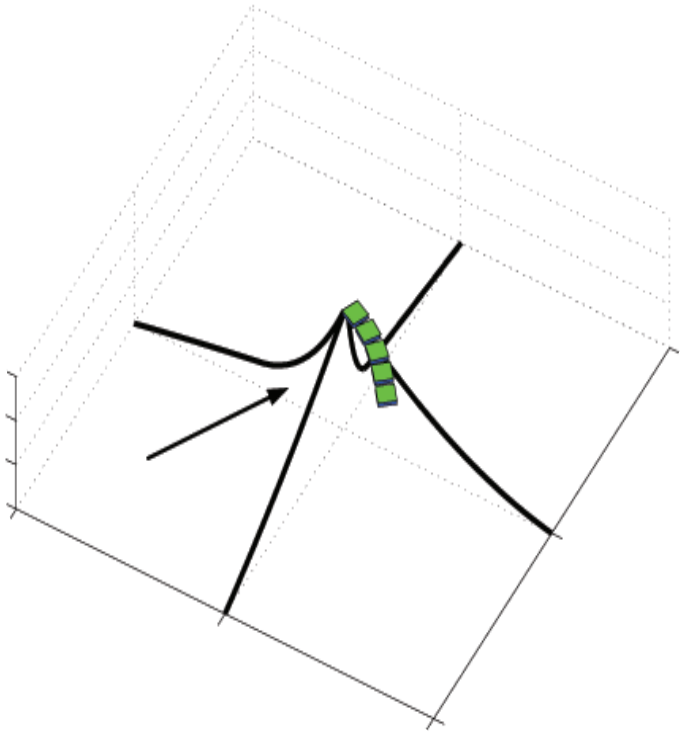

Figure P1.3: Configuration of the marine structure consisting of five surface vessels and four mooring cables.

- The body-fixed frame, denoted XYZ_i for module number i, is fixed to the module body, in such a way that the origin coincides with the center of gravity, with the X axis directed from aft to fore along the longitudinal axis of the module, and the Y axis directed to the starboard.

The position and orientation of module number i in the Earth-fixed frame are defined by $\boldsymbol{\eta}_i \triangleq [x_i\ y_i\ z_i\ \phi_i\ \theta_i\ \psi_i]^T$, where the first three variables describe the position, while the last three describe the Euler angles. The translational and rotational body-fixed velocities are defined by the vector $\boldsymbol{\nu}_i \triangleq [u_i\ v_i\ w_i\ p_i\ q_i\ r_i]^T$. The body-fixed general velocities are transformed to the Earth-fixed frame by

$$\dot{\boldsymbol{\eta}}_i = \mathbf{J}(\boldsymbol{\eta}_i)\boldsymbol{\nu}_i, \tag{P1.2}$$

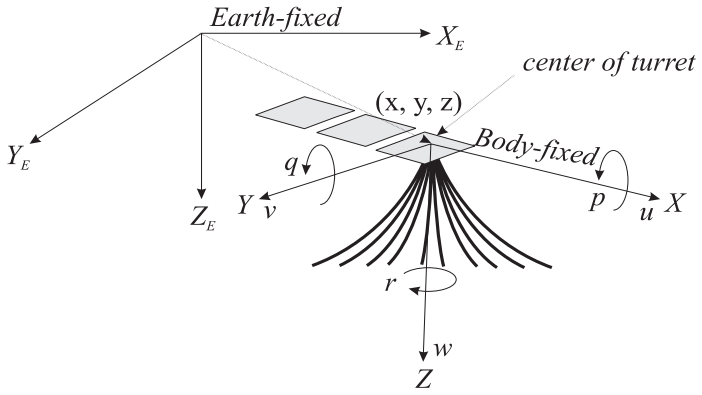

Figure P1.4: Earth-fixed ($X_E Y_E Z_E$) and body-fixed (XYZ) reference frames.

where

$$\mathbf{J}(\boldsymbol{\eta}_i) = \begin{bmatrix} \mathbf{J}_1(\boldsymbol{\eta}_i) & \mathbf{0} \\ \mathbf{0} & \mathbf{J}_2(\boldsymbol{\eta}_i) \end{bmatrix}, \tag{P1.3}$$

$$\mathbf{J}_1(\boldsymbol{\eta}_i) = \begin{bmatrix} c\psi c\theta & -s\psi c\phi + c\psi s\theta s\phi & s\psi s\phi + c\psi c\phi s\theta \\ s\psi c\theta & c\psi c\phi + s\phi s\theta s\psi & -c\psi s\phi + s\theta s\psi c\phi \\ -s\theta & c\theta s\phi & c\theta c\phi \end{bmatrix}, \tag{P1.4}$$

$$\mathbf{J}_2(\boldsymbol{\eta}_i) = \begin{bmatrix} 1 & s\phi t\theta & c\phi t\theta \\ 0 & c\phi & -s\phi \\ 0 & s\phi/c\theta & c\phi/c\theta \end{bmatrix}, \tag{P1.5}$$

where s, c, t is compact notation of sin, cos and tan respectively.

Module kinetics

Based on Sørensen et al. (2002) the equations of motion of module i in 6 degrees of freedom are described by

$$\mathbf{M}_i\dot{\boldsymbol{\nu}}_i + \mathbf{C}_i(\boldsymbol{\nu}_i)\boldsymbol{\nu}_i + \mathbf{D}_i(\boldsymbol{\nu}_i)\boldsymbol{\nu}_i + \mathbf{g}_i(\boldsymbol{\eta}_i) = \boldsymbol{\tau}_{i,M} + \boldsymbol{\tau}_{i,C} + \boldsymbol{\tau}_{i,E} + \boldsymbol{\tau}_{i,T} + \boldsymbol{\tau}_{i,F}, \tag{P1.6}$$

$$\dot{\boldsymbol{\eta}}_i = \mathbf{J}(\boldsymbol{\eta}_i)\boldsymbol{\nu}_i, \quad i = 1, 2, \ldots, n, \tag{P1.7}$$

where n is the number of modules. $\mathbf{M}_i$ is the inertia matrix, including hydrodynamic added inertia, $\mathbf{C}_i(\boldsymbol{\nu}_i)$ is the Coriolis and centripetal matrix, $\mathbf{D}_i(\boldsymbol{\nu}_i)$ is the damping matrix, and $\mathbf{g}_i(\boldsymbol{\eta}_i)$ contains the restoring forces and torques. $\boldsymbol{\tau}_{i,E}$ constitutes the environmental forces and torques, inflicted from winds, currents and waves, $\boldsymbol{\tau}_{i,M}$ is the mooring forces and torques, $\boldsymbol{\tau}_{i,C}$ is the connector forces and torques, $\boldsymbol{\tau}_{i,T}$ is the propulsion forces and torques and $\boldsymbol{\tau}_{i,F}$ the forces and torques from the hydrofoils.

Connectors

Let the connector k be connecting modules i and j, as shown in Figure P1.5, and denote by $\mathbf{f}^n_{i,k}$ the force, decomposed in the Earth-fixed frame, acting on module i from connector k. Clearly, the force acting on module j from connector k is $\mathbf{f}^n_{j,k} = -\mathbf{f}^n_{i,k}$. Vectors that are given with respect to the Earth-fixed reference frame are identified by the superscript n. In general, this force may be considered a control input, facilitating design of feedback control laws that can give the interconnected structure desirable properties. We introduce $\boldsymbol{\eta}_{i,1} = [x_i\ y_i\ z_i]^T$, $\boldsymbol{\eta}_{i,2} = [\phi_i\ \theta_i\ \psi_i]^T$, $\boldsymbol{\nu}_{i,1} = [u_i\ v_i\ w_i]^T$, $\boldsymbol{\nu}_{i,2} = [p_i\ q_i\ r_i]^T$ to simplify the notation.

Connector kinematics

Consider two modules i and j, coupled via connector k, as shown in Figures P1.5 and P1.6. The connector acts at the points $\mathbf{p}_{i,k}$ and $\mathbf{p}_{j,k}$, which are given with respect to the body-fixed reference frames and consequently are constants. In the Earth-fixed frame, the connection points are given by

$$\mathbf{p}^n_{i,k} = \boldsymbol{\eta}_{i,1} + \mathbf{J}_1(\boldsymbol{\eta}_i)\,\mathbf{p}_{i,k}, \tag{P1.8}$$

$$\mathbf{p}^n_{j,k} = \boldsymbol{\eta}_{j,1} + \mathbf{J}_1(\boldsymbol{\eta}_j)\mathbf{p}_{j,k}. \tag{P1.9}$$

The vector describing the relative position of two coupled connection points is given as

$$\mathbf{l}_{i,k} = \mathbf{p}^n_{j,k} - \mathbf{p}^n_{i,k}, \tag{P1.10}$$

while the distance between the connection points is given by

$$l_{i,k} = \left\| \mathbf{p}^n_{j,k} - \mathbf{p}^n_{i,k} \right\|. \tag{P1.11}$$

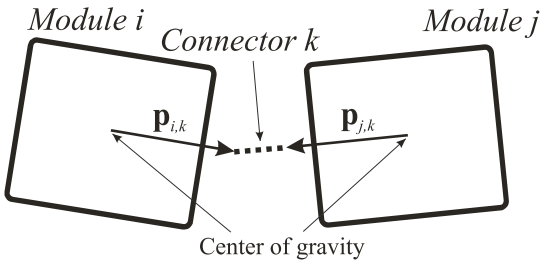

Figure P1.5: Kinematics of two interconnected surface vessels.

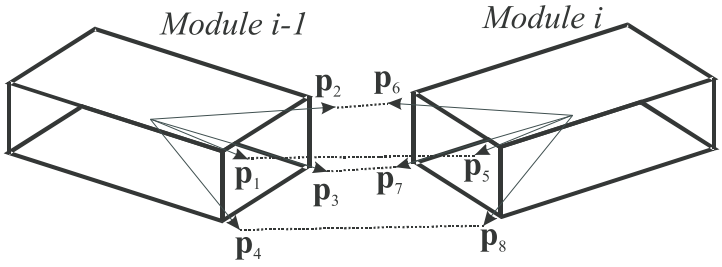

Figure P1.6: Four connectors interconnecting the two vessels.

Connector forces

The connector will impose forces on the modules, acting at $\mathbf{p}_{i,k}$ and $\mathbf{p}_{j,k}$, as well as their accompanying induced torques. The forces will consist of a restoring part and a viscous damping part, the former depending on the relative distance between the two modules, the latter depending on the relative velocities between them. The time derivative of the rotation matrix $\mathbf{J}_1$ will be needed for expressing these forces, and is given by

$$\frac{d}{dt}\left(\mathbf{J}_1\left(\boldsymbol{\eta}_i\right)\right) = \mathbf{J}_1\left(\boldsymbol{\eta}_i\right)\mathbf{S}\left(\boldsymbol{\nu}_i\right), \tag{P1.12}$$

where the cross-product operator $\mathbf{S}:\mathbb{R}^3 \to \mathbb{R}^3$ is defined as

$$\mathbf{S}\left(\mathbf{v}\right)\left(\cdot\right) = \mathbf{v}\times\left(\cdot\right) = \begin{bmatrix} 0 & -v_3 & v_2 \\ v_3 & 0 & -v_1 \\ -v_2 & v_1 & 0 \end{bmatrix}\left(\cdot\right),\ \mathbf{v} = \begin{bmatrix} v_1 \\ v_2 \\ v_3 \end{bmatrix}. \tag{P1.13}$$

Translational forces The translational restoring forces and damping forces along the connectors are derived from (P1.11) and its time derivative in the following manner

$$\mathbf{f}^n_{i,k} = \left(k_k\left(l_{i,k} - L_k\right) + d_k\frac{d}{dt}\left(l_{i,k}\right)\right)\frac{\mathbf{l}_{i,k}}{l_{i,k}}, \tag{P1.14}$$

where k_k and d_k are the spring and damping coefficients of connector k, and L_k is a positive constant constituting the nominal distance giving zero spring force. In general, k_k and d_k may not be constant, giving rise to forces that depend on the motion of the modules in a nonlinear manner. The time derivative of (P1.11) is given as

$$\frac{d}{dt}\left(l_{i,k}\right) = \frac{\mathbf{l}^T_{i,k}}{l_{i,k}}\left(\mathbf{J}_1(\boldsymbol{\eta}_j)\left(\boldsymbol{\nu}_{j,1} - \mathbf{S}(\mathbf{p}_{j,k})\boldsymbol{\nu}_{j,2}\right) - \mathbf{J}_1\left(\boldsymbol{\eta}_i\right)\left(\boldsymbol{\nu}_{i,1} - \mathbf{S}(\mathbf{p}_{i,k})\boldsymbol{\nu}_{i,2}\right)\right). \tag{P1.15}$$

In the body-fixed reference frame of module i, the connector force is given by

$$\mathbf{f}_{i,k} = \mathbf{J}_1^T(\boldsymbol{\eta}_i)\,\mathbf{f}_{i,k}^n. \tag{P1.16}$$

Notice that (P1.16) can be interpreted as a local control law feeding back from the states $\boldsymbol{\eta}_i, \boldsymbol{\eta}_j, \boldsymbol{\nu}_i, \boldsymbol{\nu}_j$.

Induced torques The forces acting on the module will induce torques about the modules center of gravity (provided $\mathbf{p}_{i,k} \neq 0$). When transformed into the modules body-fixed reference frame, the torque vector is given by

$$\mathbf{m}_{i,k} = \mathbf{p}_{i,k} \times \mathbf{f}_{i,k} = \mathbf{S}(\mathbf{p}_{i,k})\mathbf{f}_{i,k}. \tag{P1.17}$$

Interconnection forces

It is assumed that all connectors have the same spring and damping coefficients k_c and d_c, that is,

$$k_k = k_c,\, d_k = d_c, \text{ for } k = 1, ..., 4(n-1), \tag{P1.18}$$

and that the connectors are located in the same coordinates on all modules given by the points $\mathbf{p}_p$, $p = 1, ..., 8$, as indicated in Figure P1.6. Defining $\mathbf{f}_{0,k}^n = \mathbf{0}$ and $\mathbf{f}_{n,k}^n = \mathbf{0}$ for $k = 1, ..., 4$, gives

$$\boldsymbol{\tau}_{i,C} = \sum_{k=1}^{4} \begin{bmatrix} \mathbf{J}_1^T(\boldsymbol{\eta}_i)\left(\mathbf{f}_{i,k}^n - \mathbf{f}_{i-1,k}^n\right) \\ \mathbf{S}(\mathbf{p}_k)\,\mathbf{J}_1^T(\boldsymbol{\eta}_i)\,\mathbf{f}_{i,k}^n - \mathbf{S}(\mathbf{p}_{k+4})\,\mathbf{J}_1^T(\boldsymbol{\eta}_i)\,\mathbf{f}_{i-1,k}^n \end{bmatrix},\ i = 1, ..., n. \tag{P1.19}$$

Mooring system

We will employ the finite element model of a mooring system developed by Aamo and Fossen (2001). For completeness, we review the equations below. Let the mooring system consist of m cables, each of which is uniformly partitioned into n segments of length $l^j = L^j/n$, where the superscript j identifies the cable. The nodal points are enumerated from 0 to n, see Figure P1.7. Thus, the endpoints of element k are the nodes $k-1$ and k. The position of the k^{th} node in Earth-fixed coordinates is denoted by $\mathbf{r}_k^j(t)$. On this grid, the following set of m times $n-1$ coupled ordinary differential equations for the motion of the nodes is obtained

$$\frac{\rho_0^j l^j}{6}(\ddot{\mathbf{r}}_{k-1}^j + 4\ddot{\mathbf{r}}_k^j + \ddot{\mathbf{r}}_{k+1}^j) = \mathbf{f}_{k_{(hg)}}^j + \mathbf{f}_{k_{(dt)}}^j + \mathbf{f}_{k_{(dn)}}^j + \mathbf{f}_{k_{(r)}}^j, \tag{P1.20}$$
$$j = 1, ..., m,\ k = 1, ..., n-1,$$

where

$$\mathbf{f}^j_{k_{(r)}} = EA_0\left[\frac{e^j_{k+1}}{\varepsilon^j_{k+1}}\mathbf{l}^j_{k+1} - \frac{e^j_k}{\varepsilon^j_k}\mathbf{l}^j_k\right], \tag{P1.21}$$

$$\mathbf{f}^j_{k_{(hg)}} = l^j\rho^j_0\frac{\rho^j_c - \rho_w}{\rho^j_c}\begin{bmatrix} 0 & 0 & g \end{bmatrix}^T, \tag{P1.22}$$

$$\mathbf{f}^j_{k_{(dt)}} = -\frac{C^j_1}{2}\left[\left|\dot{\mathbf{r}}^j_k\cdot\mathbf{l}^j_k\right|\mathbf{P}^j_k + \left|\dot{\mathbf{r}}^j_k\cdot\mathbf{l}^j_{k+1}\right|\mathbf{P}^j_{k+1}\right]\dot{\mathbf{r}}^j_k, \tag{P1.23}$$

$$\mathbf{f}^j_{k_{(dn)}} = -\frac{C^j_2}{2}\left[\varepsilon^j_k\left|\left(\mathbf{I}_{3\times3} - \mathbf{P}^j_k\right)\dot{\mathbf{r}}^j_k\right|\left(\mathbf{I}_{3\times3} - \mathbf{P}^j_k\right)\right. \tag{P1.24}$$

$$\left.+\varepsilon^j_{k+1}\left|\left(\mathbf{I}_{3\times3} - \mathbf{P}^j_{k+1}\right)\dot{\mathbf{r}}_k\right|\left(\mathbf{I}_{3\times3} - \mathbf{P}^j_{k+1}\right)\right]\dot{\mathbf{r}}^j_k, \tag{P1.25}$$

$$\mathbf{l}^j_k = \mathbf{r}^j_k - \mathbf{r}^j_{k-1},\ e^j_k = \frac{\left|\mathbf{l}^j_k\right|}{l^j} - 1, \tag{P1.26}$$

$$\varepsilon^j_k = |\mathbf{l}_k|,\ \mathbf{P}^j_k = \frac{\mathbf{l}^j_k\mathbf{l}^{j^T}_k}{\varepsilon^{j^2}_k}, \tag{P1.27}$$

$$C^j_1 = \frac{1}{2}C_{DT}\pi d^j\rho_w,\ \ C^j_2 = \frac{1}{2}C_{DN}d^j\rho_w. \tag{P1.28}$$

ρ_0 is mass per unit length of unstreched cable, $\mathbf{f}_{(hg)}$ constitutes the buoyancy (gravity and hydrostatic) force per unit length of unstretched cable, $\mathbf{f}_{(r)}$ contains the internal reaction forces, $\mathbf{f}_{(dt)}$ and $\mathbf{f}_{(dn)}$ are tangential and normal hydrodynamic drag, respectively, per unit length of unstretched cable, E is *Young's modulus*, A_0 is the cross-sectional area of the unstreched cable, C_{DT} and C_{DN} are the tangential and normal drag coefficients for the cable, respectively, d is the diameter of the streched cable, treated as constant and equal to the diameter of the pretensioned cable; and ρ_w is the density of the ambient water.

Mooring line forces

The connection between the module and the mooring system is implemented by simply equating $\boldsymbol{\eta}_{1,1}$ and $\mathbf{r}^j_n$ for $j = 1, ..., m$. Only the foremost module is connected to the mooring system, hence $\boldsymbol{\tau}_{i,M} = \mathbf{0}$, for $i \neq 1$. The generalized mooring line forces, to be included in (P1.6), are then given by

$$\boldsymbol{\tau}_{1,M} = \begin{bmatrix} \mathbf{I} \\ \mathbf{S}(\mathbf{p}^{b_1}_M) \end{bmatrix}\mathbf{f}^{b_1}_M, \tag{P1.29}$$

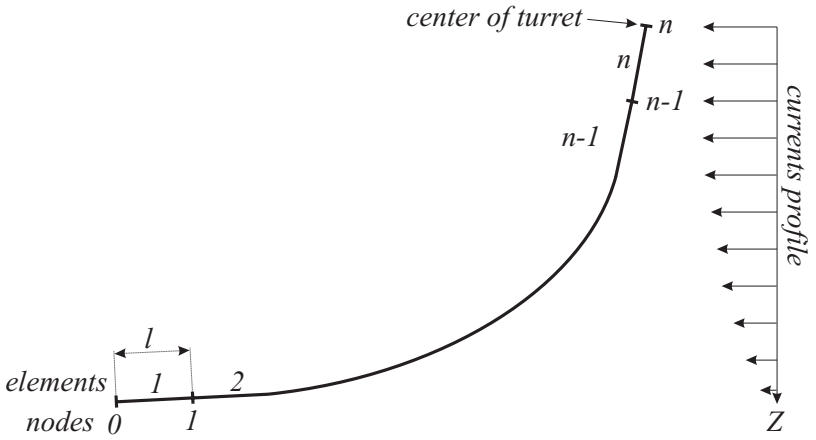

Figure P1.7: Grid for finite element discretization.

where

$$\mathbf{f}_M^{b_1} = \mathbf{J}_1(\boldsymbol{\eta}_1)^T \sum_{j=1}^{m} \left\{ \begin{array}{c} \frac{EA_0}{l}\frac{\varepsilon_n^j - l}{\varepsilon_n^j} \cdot \\ \left(\mathbf{r}_{n-1}^j - \boldsymbol{\eta}_{1,1} - \mathbf{J}_1(\boldsymbol{\eta}_1)\mathbf{p}_M^{b_1}\right) \end{array} \right\}. \tag{P1.30}$$

Hydrofoils

The lift force generated by hydrofoils is related to the circulation Γ around the hydrofoil, defined as $\Gamma = \oint_c \mathbf{v} \cdot d\mathbf{s}$, where $\mathbf{v}$ is the fluid velocity and c is the closed curve enclosing the hydrofoil. The circulation implies higher velocities on the suction side than on the pressure side of the hydrofoil, and is a consequence of the flow leaving tangentially from the trailing edge of the hydrofoil, referred to as the Kutta condition, see Newman (1977). The lift- and drag-forces can be written

$$F_L = \frac{1}{2}\rho_w A \mathbf{v}_r |\mathbf{v}_r| C_L(\alpha), \tag{P1.31}$$

$$F_D = \frac{1}{2}\rho_w A \mathbf{v}_r |\mathbf{v}_r| C_D(\alpha), \tag{P1.32}$$

where $C_L(\alpha)$ and $C_D(\alpha)$ are the lift and drag coefficients respectively. A is the projected area for $\alpha = 0$, and $\mathbf{v}_r = \left[v_{r,x}\ v_{r,y}\right]^T$ is the relative velocity between the hydrofoil and the water, where the $x-$ and $y-$subscripts denote the $x-$ and $y-$direction respectively. The lift and drag coefficients are func-

tions of α which is the angle of attack between the hydrofoil and the relative velocity.

Hydrofoil forces

The generalized force resulting from the hydrofoil connected to the last module in the chain, to be included in (P1.6), is assumed to act at the point $\mathbf{p}_F^{b_q}$ and is given by

$$\boldsymbol{\tau}_{q,F} = \begin{bmatrix} \mathbf{I} \\ \mathbf{S}(\mathbf{p}_F^{b_q}) \end{bmatrix} \mathbf{f}_F^{b_q}, \tag{P1.33}$$

where

$$\mathbf{f}_F^{b_q} = \begin{bmatrix} \frac{1}{2}\rho C_D(\alpha) A v_{r,x} |v_{r,x}| \\ \frac{1}{2}\rho C_L(\alpha) A v_{r,y} |v_{r,y}| \\ 0 \end{bmatrix}. \tag{P1.34}$$

First order wave induced motions

A common assumption for station keeping operation, see Sørensen (2004), is that the first order wave induced motions are linear and can be superimposed on the low-frequency motions. The total displacement is written

$$\boldsymbol{\eta}_{i,tot} = \boldsymbol{\eta}_i + \boldsymbol{\eta}_{i,WF}, \tag{P1.35}$$

where $\boldsymbol{\eta}_i \in \mathbb{R}^6$ is the displacement due to low frequency motion as derived in the previous section, and $\boldsymbol{\eta}_{i,WF} \in \mathbb{R}^6$ is the displacement due to wave frequency motion. For this application scaled transfer function results are used to describe the wave frequency motion. Thus, effects of waves on the interconnected structure and on controller performance can be studied.

P1.4 Control system design

Control objective

The objectives of the controller will be to 1) Ensure limited loading of the mooring system in order to avoid cable breakage; 2) Keep the chain of surface modules aligned transversely to the incoming current in order to ensure continuous supply of clean water to the fish, and; 3) Ensure positive strain in the connectors between the modules in order to avoid buckling effects due to variations in the current. It must be emphasized that the mooring system should be dimensioned such that thruster assistance is not needed under normal conditions. Thruster assistance will kick in under

harsh weather conditions with extreme loads on the mooring system, and will aim at compensating for slowly varying environmental loads, only. In positioning applications such as the one studied here, it is common to apply wave-filtering to avoid excessive energy consumption, and wear and tear of thrusters and their accompanying mechanical parts.
Traditionally, position mooring systems have been designed to restrict the movement of the surface vessel within a region in the (x, y) plane, usually given by some defined safety distance away from the origin of the mooring system. Thruster assistance is applied when the vessel moves outside this region, leading to a rather aggressive thruster use. Usually, this is compensated for by adding motion damping, which limits the speed of the vessel at the expense of higher fuel consumption.
Here, an alternative method for obtaining smoother control action is suggested. Rather than restricting position, the objective is to limit the total energy of the system, which is denoted E and defined as the kinetic energy of the surface structure plus the potential energy stored in the mooring system. In principle, the controller will slow down the vessel whenever the vessel has a kinetic energy that is larger than the maximum additional potential energy that can safely be stored in the mooring line. In this way, motion damping is only applied when the speed of the vessel threatens the capabilities of the mooring system. The maximum potential energy that the mooring system can store is given by structural reliability properties in a way that is described below. The controller design will take place in several steps. First, a simplified model for the low-frequency motion is presented. Then a state feedback control law is designed as if the objective were to drive the surface structure to the origin of the mooring system. The resulting state feedback control law is then altered to take into account the energy considerations just described. Finally, an observer is designed to provide low-frequency estimates of the vessel velocity and environmental loads, which are used in the feedback law, but are usually not measured.

Control plant model

The *process plant model* was established above, and is a detailed description of the dynamics of the system. It serves the purpose of a "real world" simulation tool for testing the performance of control systems. A simplified model, called *the control plant model*, will be used for the development of a controller. The goal of the controller is to reduce the translational motions in the $x - y-$plane. By assuming low speed and no coupling between the translational and rotational degrees of freedom, the *control plant model* is

given by

$$m\begin{bmatrix} \ddot{x}_{lf} \\ \ddot{y}_{lf} \end{bmatrix} + (k_0 + k(r))\begin{bmatrix} x_{lf} \\ y_{lf} \end{bmatrix} = \begin{bmatrix} l_x \\ l_y \end{bmatrix} + \begin{bmatrix} \tau_x \\ \tau_y \end{bmatrix}, \tag{P1.36}$$

where m is the rigid body mass, k_0 is a positive constant that constitutes the pretension of the mooring system, while $k(r)$, where $r = \sqrt{x_{lf}^2 + y_{lf}^2}$, $k(0) = 0$ and $k_0 + k(r) > 0$, is the nonlinear part of the spring coefficient introduced by the mooring system. l_x and l_y are the slowly varying environmental loads (for instance from currents and winds), whose estimates will be available through the observer developed in Section P1.4, and τ_x, τ_y are the control inputs. The subscript lf on x and y emphasizes that the model contains low-frequency components of the motion, only. Position measurements are available, that is, x and y are measured and filtered through a low pass filter to obtain x_{lf} and y_{lf}, while $\dot{x}$ and $\dot{y}$ are not measured. In Berntsen et al. (2003) it was assumed that the spring coefficient was constant for all displacements relative to the origin. In the present paper the nonlinearity of the spring coefficient is also studied. Describing the spring coefficient more precisely is assumed to result in more accurate estimates of the unmeasured states, hence reducing the required actuator force. This is confirmed by simulations presented in Section P1.5.

State feedback control law

Defining the state vector as

$$\mathbf{x} = \left[\bar{\mathbf{x}}^T \; l_x \; l_y\right]^T = \left[x_{lf} \; \dot{x}_{lf} \; y_{lf} \; \dot{y}_{lf} \; l_x \; l_y\right]^T, \tag{P1.37}$$

modelling the slowly varying environmental loads as constant, and applying the nonlinear static output feedback

$$\boldsymbol{\tau} = \begin{bmatrix} \tau_x \\ \tau_y \end{bmatrix} = k(r)\begin{bmatrix} x_{lf} \\ y_{lf} \end{bmatrix} + \mathbf{u}, \tag{P1.38}$$

(P1.36) can be written in the form

$$\dot{\mathbf{x}} = \mathbf{A}\mathbf{x} + \mathbf{B}\mathbf{u} = \left[\begin{array}{c|c} \bar{\mathbf{A}} & \bar{\mathbf{B}} \\ \hline \mathbf{0} & \mathbf{0} \end{array}\right]\begin{bmatrix} \bar{\mathbf{x}} \\ l_x \\ l_y \end{bmatrix} + \left[\begin{array}{c} \bar{\mathbf{B}} \\ \hline \mathbf{0} \end{array}\right]\mathbf{u}, \tag{P1.39}$$

$$\mathbf{y} = \mathbf{C}\mathbf{x} = \begin{bmatrix} \bar{\mathbf{C}} & \mathbf{0} \end{bmatrix}\begin{bmatrix} \bar{\mathbf{x}} \\ l_x \\ l_y \end{bmatrix}, \tag{P1.40}$$

where

$$\bar{\mathbf{A}} = \begin{bmatrix} 0 & 1 & 0 & 0 \\ -\frac{k_0}{m} & 0 & 0 & 0 \\ 0 & 0 & 0 & 1 \\ 0 & 0 & -\frac{k_0}{m} & 0 \end{bmatrix}, \bar{\mathbf{B}} = \begin{bmatrix} 0 & 0 \\ 1 & 0 \\ 0 & 0 \\ 0 & 1 \end{bmatrix}, \bar{\mathbf{C}} = \begin{bmatrix} 1 & 0 & 0 & 0 \\ 0 & 0 & 1 & 0 \end{bmatrix}. \tag{P1.41}$$

Having applied a linearizing feedback, the separation principle of linear systems can be used. Towards solving the state feedback problem, the environmental loads are canceled by setting

$$\mathbf{u} = -\begin{bmatrix} l_x \\ l_y \end{bmatrix} + \mathbf{v}, \tag{P1.42}$$

to obtain

$$\dot{\bar{\mathbf{x}}} = \bar{\mathbf{A}}\bar{\mathbf{x}} + \bar{\mathbf{B}}\mathbf{v}. \tag{P1.43}$$

It can be verified that $(\bar{\mathbf{A}}, \bar{\mathbf{B}})$ is a controllable pair, so a state feedback control law can be designed,

$$\mathbf{v} = \bar{\mathbf{K}}\bar{\mathbf{x}}, \tag{P1.44}$$

that achieves desired rates of convergence of solutions of (P1.43) to the origin.

Driving the states to the origin by thruster force would make the mooring system superfluous. The objective of the thruster is instead to assist the mooring system in the event that the center of turret moves so far away from the origin, (due to extreme environmental loads), that a risk of cable failure arises. The safety margin with respect to line failure can be quantified by means of the so-called reliability index, see e.g. Madsen et al. (1986). This index makes it possible to take all different types of statistical uncertainty into account, and a simplified version of it is defined as

$$\delta_j(t) = \frac{\left(T_{Br,mean} - T_j(t)\right)}{\sigma_{Break}}, \tag{P1.45}$$

where $T_{Br,mean}$ is the mean breaking strength, σ_{break} is the corresponding standard deviation, and $T_j(t)$ is the time-varying tension in line j. Clearly, from (P1.45) it is seen that a lower value of the delta index results in a higher probability of mooring line failure. With a given maximum allowed breaking probability P_{break}, the tension corresponding to this breaking probability can be read from the breaking probability distribution as defined by $T_{Br,mean}$ and σ_{break}, and inserted for $T_j(t)$ in (P1.45). The result is denoted

δ_{set}, and represents the minimum acceptable value for $\delta_j(t)$. The performance of the positioning system can be evaluated by computing $\delta_j(t)$ online, and comparing with δ_{set}. Based on in-field measurements (or in our case, open loop simulations using the "real world" simulator) r_{max} is defined to be the distance from the origin corresponding to $\delta = \delta_{set}$. The potential energy stored in the mooring system when $x_{lf}^2 + y_{lf}^2 = r_{\max}^2$ defines in turn the maximum total energy the system is allowed to have, that is $E_{\max} = \frac{1}{2}k_0 r_{\max}^2 + \int_0^{r_{\max}} k(r)\, r dr$. The total energy of the system is

$$E(\bar{\mathbf{x}}) = \frac{1}{2}m(\dot{x}_{lf}^2 + \dot{y}_{lf}^2) + \frac{1}{2}k_o^2\left(x_{lf}^2 + y_{lf}^2\right) + \int_0^{\sqrt{x_{lf}^2+y_{lf}^2}} k(r)\, r dr. \tag{P1.46}$$

Thus, applying the control (P1.44) whenever $E \geq E_{\max}$ makes the region defined by $E \leq E_{\max}$ exponentially attractive. In order to obtain a continuous (nonlinear) control, a lower energy threshold is defined as $E_t < E_{\max}$, at which point control is gradually activated according to

$$\mathbf{v} = f(E)\bar{\mathbf{K}}\bar{\mathbf{x}}, \tag{P1.47}$$

where

$$f(E) = \begin{cases} 0, & E \leq E_t \\ \frac{E^2}{\Delta E^2} - 2\frac{E_t}{\Delta E^2}E + \frac{E_t^2}{\Delta E^2}, & E_t < E < E_{\max} \\ 1, & E \geq E_{\max} \end{cases} \tag{P1.48}$$

$$\Delta E = E_{\max} - E_t. \tag{P1.49}$$

The selection of the lower and upper bounds for the function $f(E)$ becomes critical for the performance of the controller. Choosing a too narrow band may cause the controller to switch on and off rapidly, while choosing a too large band will result in an unnecessary high thruster usage.

Observer

The only likely measurement to be available is position, provided by a GPS receiver. Therefore, the controller suggested in the previous section cannot be implemented directly. An observer that provides an estimate of the states can be constructed by simply copying (P1.39) and adding an output injection term, giving

$$\dot{\hat{\mathbf{x}}} = \mathbf{A}\hat{\mathbf{x}} + \mathbf{B}\mathbf{u} + \mathbf{L}(\mathbf{y} - \mathbf{C}\hat{\mathbf{x}}), \tag{P1.50}$$

where $\mathbf{y} = [x_{lf}\ y_{lf}]^T$. In view of the fact that $(\mathbf{A}, \mathbf{C})$ is an observable pair, $\mathbf{L}$ can be designed to achieve any desired rate of convergence of the estimated state $\hat{\mathbf{x}}$, to the true state $\mathbf{x}$. The benefits of pole-placement techniques has been chosen to optimize the observer for this application.

Output feedback control law

In summary, the thruster assistance control system is a nonlinear dynamic output feedback controller, given by

$$\dot{\hat{\mathbf{x}}} = \tilde{\mathbf{A}}\left(\hat{E}\right)\hat{\mathbf{x}} + \mathbf{L}\mathbf{y}, \tag{P1.51}$$

$$\boldsymbol{\tau} = \mathbf{K}\left(\hat{E}\right)\hat{\mathbf{x}} + k(r)\,\mathbf{y}, \tag{P1.52}$$

where

$$\hat{E} = \frac{1}{2}m(\hat{x}_2^2 + \hat{x}_4^2) + \frac{1}{2}k_0\mathbf{y}^T\mathbf{y} + \int_0^{\sqrt{\mathbf{y}^T\mathbf{y}}} k(r)\,r dr, \tag{P1.53}$$

$$\mathbf{K}\left(\hat{E}\right) = \begin{bmatrix} f(\hat{E})\bar{\mathbf{K}} & 0 \\ 0 & -\mathbf{I} \end{bmatrix}, \tag{P1.54}$$

$$\tilde{\mathbf{A}}\left(\hat{E}\right) = \mathbf{A} + \mathbf{B}\mathbf{K}\left(\hat{E}\right) - \mathbf{L}\mathbf{C}. \tag{P1.55}$$

Exponential attractiveness of the region defined by $E \leq E_{\max}$ is claimed by the separation principle of linear time invariant systems. The importance of including nonlinear effects for the mooring system is evident when examining Figure P1.8. The figure displays the comparison between the real and the estimated environmental force. The result for the linear observer is in the upper graph of the figure, while the result for the nonlinear one is in the lower graph. Using a nonlinear function describing the stiffness properties of the mooring system has significantly improved the estimates of the environmental loads as compared to the observer proposed by Berntsen et al. (2003). There was no apparent improvement of the velocity estimates.

P1.5 Simulation study

Open loop simulations

After an initial transient due to initial conditions, the structure enters a periodic orbit driven by the tidal current, with a period of twelve hours. Figure P1.3 gives an impression of the instantaneous behavior of the interconnected structure during a 180 degree direction change of the current, while Figure P1.9 shows the low frequency orbits of the five surface modules.

The structure as a whole rotates counter clockwise. As expected, the chain of modules spends a large fraction of the time in almost a straight line, aligned with the strong current in the $x-$direction. This is an undesirable configuration, because modules towards the end of the chain lie in the wake

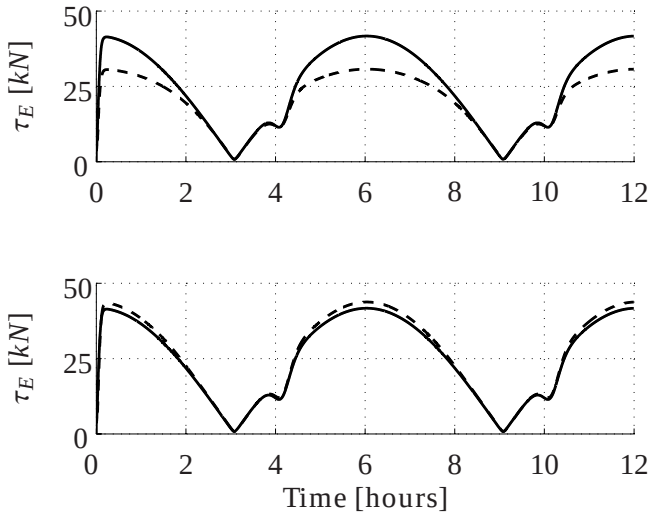

Figure P1.8: Comparison between the real (solid) and the estimated (dotted) results for the linear, upper graph, and the nonlinear, lower graph, observers.

of the foremost modules for long periods of time, resulting in poor environmental conditions for the fish. The high eccentricity of the tidal current also leads to an uneven loading of the mooring system.

The upper graph of Figure P1.10 shows the mooring forces in one of the mooring lines. The maximum tension is seen to be about 44 [kN]. For all the lines of the present mooring system the mean breaking strength is $T_{Br,mean}$ = 49 [kN], and the standard deviation of the breaking strength, σ_{Break}, is taken as 7.5 % of the mean value. With a design criteria of a failure probability of less than 10^{-3}, the corresponding lower bound on the delta index is δ_{set} = 3.1. Using these values in (P1.45), the resulting time variation of the delta index is shown in the lower graph of Figure P1.10. The minimum value of the index is seen to be about 1.5, which is well below δ_{set} = 3.1 and therefore represents an unacceptably high failure probability. Overload of the mooring system can be avoided by simply resizing it to withstand the most extreme conditions to be anticipated. However, by utilizing the possibility of introducing a motion control mechanism, the strength of the mooring system can be applied as criteria for activation of the control energy. The maximum offset permitted by the control system

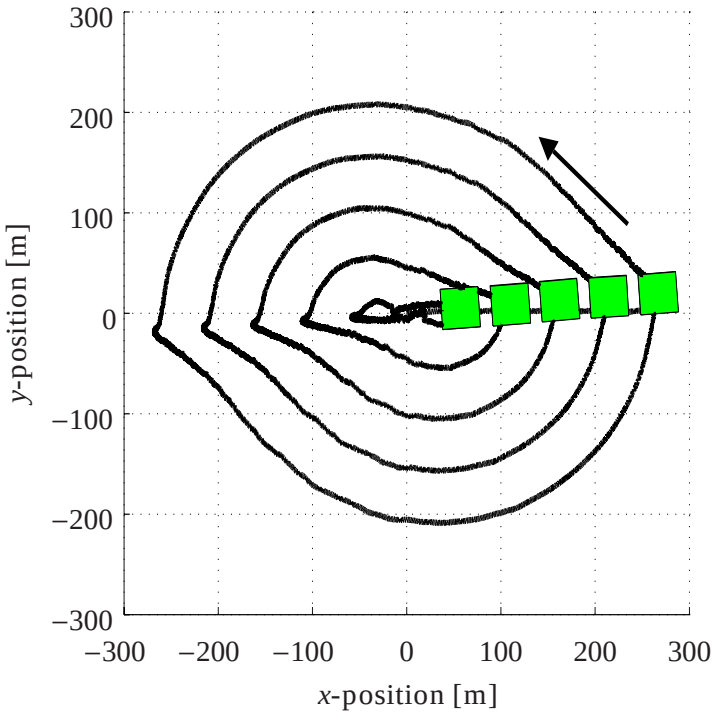

Figure P1.9: Position of surface vessels during one tidal cycle. Open loop.

will be decisive for the resulting probability of line failure.

Closed loop simulations

Following the procedure outlined in the previous chapter, the maximum allowed annual failure probability should be less than 10^{-3}, which corresponds to $\delta_{set} = 3.1$, resulting in $r_{\max} = 55$ [m]. The lower value, r_t, which defines E_t, is set to 52.3 [m].
The maximum value of r is approximately 53.5 [m], see Figure P1.11, which is below the preset limit of 55 [m]. The maximum r is hence reduced only slightly as compared to the open loop case. The corresponding tension and delta index of the most loaded mooring line, compared to the open loop results, are shown in the upper and middle graph of Figure P1.12. The maximum value for the critical line is now around 37 [kN], with the corresponding value of the delta index close to δ_{set}. This is achieved by

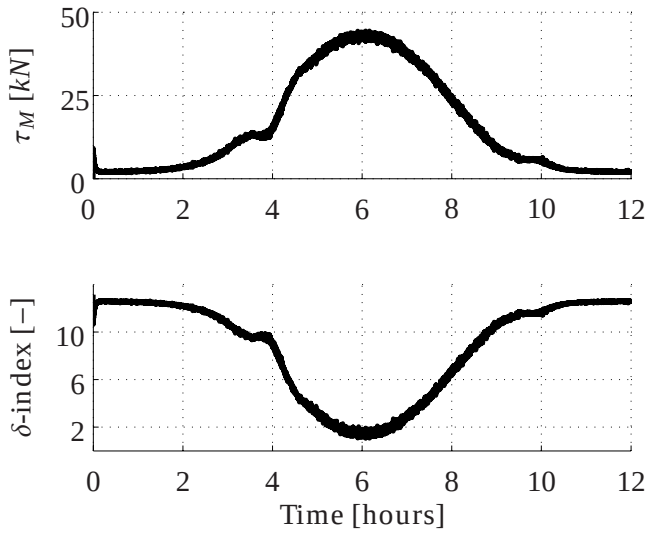

Figure P1.10: Tension, upper graph, and delta index, lower graph, for one of the four mooring lines. Open loop.

using the thruster approximately 35% of the time.

Positioning combining use of thruster and hydrofoil

A hydrofoil is used in combination with a thruster to position the modules favorably with respect to the incoming current. The modules are in this case exposed to steady current given by

$$V_c = \begin{bmatrix} v_x \\ v_y \end{bmatrix} = \begin{bmatrix} 0.3 \\ 0 \end{bmatrix}. \tag{P1.56}$$

The thruster will make sure that the energy contained by the system is limited, while the foils will place the structure transversely to the incoming current. In Figure P1.13 the effect a foil will have on the mooring system is seen. At first, only the thruster is active. Then, when the interconnected structure is at rest, after approximately 5 minutes, the hydrofoil is made active. A drag penalty in the $y-$direction is apparent. In Figure P1.14 the position and heading of the five vessels for stationary conditions are plotted. The foil successfully rotates the whole structure by approximately 10 degrees.

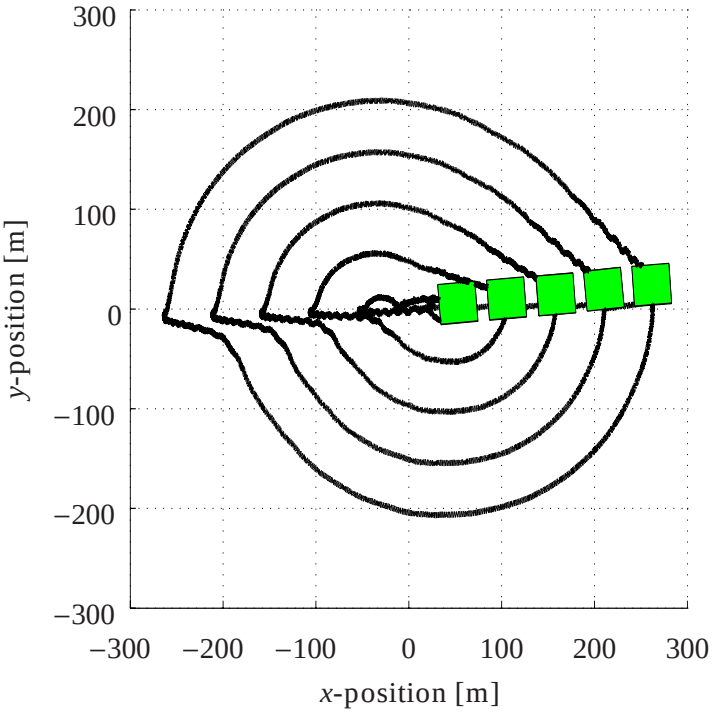

Figure P1.11: Position of surface vessels during one tidal cycle. Closed loop.

P1.6 Conclusions and future work

A model of a futuristic fish farming structure has been developed, and used for studying strategies for configuration control. For a chain of modules moored to the seabed a control system has been designed that: 1) Ensures limited loading of the mooring system in order to avoid cable breakage; 2) Keeps the chain of modules aligned transversely to the incoming current in order to ensure continuous supply of clean water to the fish, and; 3) Ensures positive strain in the connectors between modules in order to avoid buckling effects in turning currents, such as tidal currents with high eccentricity. Actuation was done by means of a thruster mounted on the first module, and a hydrofoil mounted on the last module. It was shown in simulations that a control system based on a very simple control plant model performs very well when applied to the much more complicated real

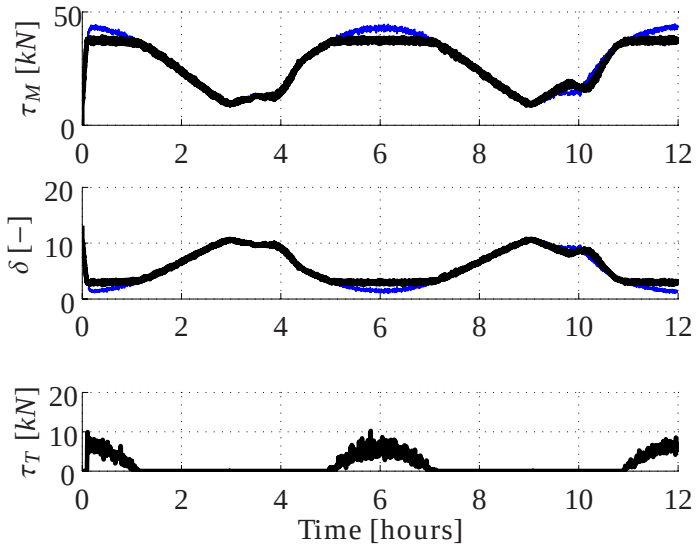

Figure P1.12: Tension in critical mooring line, upper graph, delta index for the critical mooring line, middle graph, and thruster output, lower graph.

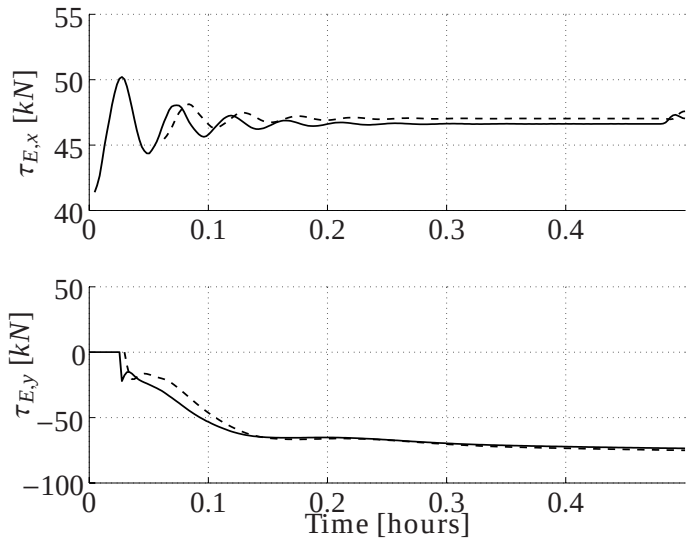

Figure P1.13: Comparison between the estimated (dotted) and the actual (solid) environmental load in $x-$ and $y-$direction.

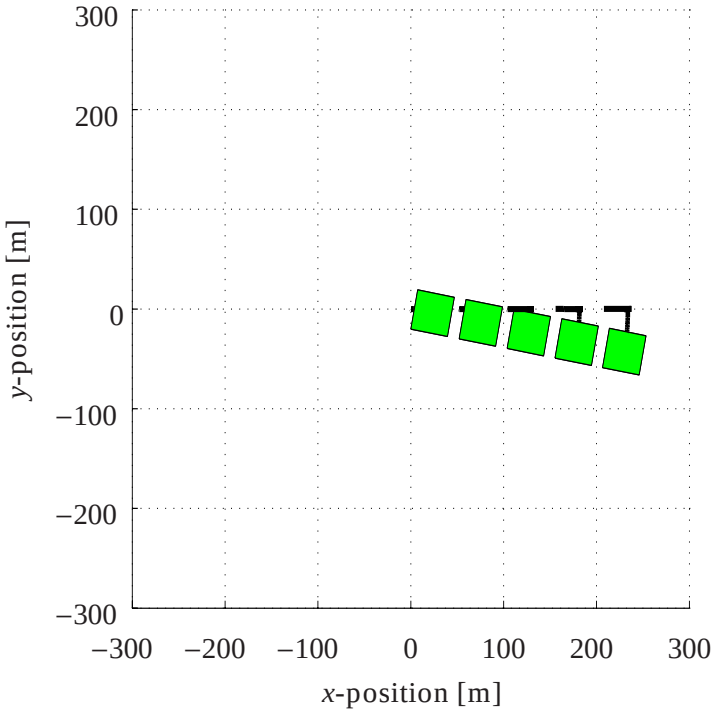

Figure P1.14: The position and heading of the five vessels with constant current, positioned by a thruster and a foil.

world simulator. Future work involves active connectors between surface modules for motion damping, and in particular damping of wave induced motions. Another possible development is the inclusion of the reliability index as an intrinsic part of the control law.

Acknowledgements

The authors wish to thank Arne Fredheim, Pål Lader, Jørgen Krokstad, and Leif Magne Sunde, of SINTEF Fisheries and Aquaculture, for valuable comments and suggestions.

Bibliography

Aamo, O. M., Fossen, T. I. (2001). Finite element modelling of moored vessels, *Mathematical and Computer Modelling of Dynamical Systems* **7(1)**:47–75.

Berntsen, P. I. B., Aamo, O. M., Sørensen, A. J. (2003). Modelling and control of single point moored interconnected structures, *Proceedings of the 6th Conference on Manoeuvring and Control of Marine Crafts, Girona, Spain*.

Fossen, T. I. (2002). *Marine Control Systems*. Marine Cybernetics, Trondheim, Norway.

Joshi, S. M. (1989). *Control of Large Flexible Space Structures*. Springer-Verlag New York Inc., New York, US.

Lin, J.-S., Kanellakopoulus, I. (1997). Nonlinear design of active suspensions. *IEEE Control Systems Magazine* **17(3)**:45–59.

Madsen, H., Krenk, S., Lind, N. (1986). *Methods of Structural Safety*. Prentice–Hall, New Jersey, US.

Newman, J. N. (1977). *Marine Hydrodynamics*. MIT Press, Cambridge, MA, US.

NS9415, (August, 2003). Marine fish farms. Requirements for design, dimensioning, production, installation and operation. *ICS 65.150; 67.260. 1. Edition, Oslo, Norway*.

Sørensen, A. J. (2004). *Marine Cybernetics - Modelling and Control*. Lecture notes, UK-2004-76, Department of Marine Technology, NTNU, Trondheim, Norway.

Sørensen, A. J., Lindegaard, K. P., Hansen, E. D. D. (2002). Locally multi objective H_2 and H_∞ control of large-scale interconnected marine structures, *Proceedings of the 41st IEEE Conference on Decision and Control, Las Vegas, NV, US* **2**:1705–1710.

Spong, M. W. (1990). The control of flexible joint robots: A Survey, *New Trends and Applications of Distributed Parameter Control Systems*. Lecture notes, Marcel Dekker Publishers, New York, US.

Paper II

Thruster Assisted Position Mooring Based on Structural Reliability

Per Ivar Barth Berntsen[a], Ole Morten Aamo[b], Bernt J. Leira[a]

[a]*Department of Marine Technology, Norwegian University of Science and Technology, N-7491 Trondheim, Norway*
[b]*Department of Engineering Cybernetics, Norwegian University of Science and Technology, N-7491 Trondheim, Norway*

Abstract

This paper addresses dynamic positioning of surface vessels moored to the seabed via a spread mooring system, referred to as position mooring. In normal weather conditions, the mooring system constrains the vessel and the controller applies thruster force for motion damping and heading control, only. When environmental loads due to wind, waves, and current increase, thruster assistance is required also for positioning in order to avoid damage to the mooring lines. While traditional position mooring systems apply thruster force based on constraining the vessel to lie within a predefined geographical region, the controller designed in this paper instead employs structural reliability measures for the mooring lines to restrict movement. These structural reliability measures become an intrinsic part of the controller, enabling it to automatically adjust the admissible region for the vessel in the presence of changing winds, currents, and waves.

Keywords: Marine Control, Reliability, Position Mooring, Backstepping.

P2.1 Introduction

Position mooring systems (PM) have been commercially available since the late 1980's, and have proved to be a cost-effective alternative to permanent platforms for offshore oil production. The current research on PM systems is based on the experience obtained from research on dynamic positioning (DP) systems since the 1970's. DP systems based on optimal control theory and Kalman-filtering were proposed in Balchen et al. (1976), and extended in Balchen et al. (1980), Balchen et al. (1981), Grimble et al. (1980), Grimble et al. (1983), Fung and Grimble (1983), Sælid et al. (1983) and Sørensen et al. (1996). More recently, nonlinear controllers have been developed for DP systems based on integrator backstepping techniques, see Fossen and Grøvlen (1998), Robertsson and Johansson (1998), Strand and Fossen (1999) and Aarset et al. (1998).

PM systems differ from DP systems in that thruster assistance is used mainly for damping the surge, sway and yaw motions and for keeping the desired heading, whereas the position is kept within an acceptable region by the mooring lines (Strand (1999)). Thus, fuel consumption is kept to a minimum in normal weather conditions. In rough weather conditions, thruster assistance may be needed for position keeping in order to avoid line tensions rising above safety limits. In Strand et al. (1997), a model for the mooring system based on line characteristics found by solving the catenary equations is presented and the optimal controller derived in Sørensen et al. (1996) is extended for this system. Common for existing PM systems, is that motion is restricted to lie within predefined safety regions, leading to considerable conservativeness with regards to exploiting the capacity of the mooring system. In Berntsen et al. (2008) we proposed a method for taking structural reliability measures of the mooring lines into account when designing PM systems. More precisely, we defined a reliability index for each mooring line and used them to estimate safety regions depending on the time varying weather conditions and seastate. The result was a controller that applies thruster assistance in accordance to environmental forces in order to keep the likelihood of mooring line failure at an acceptable level. In the present paper, we continue this work by designing a nonlinear controller that contains the reliability index as an intrinsic part rather than as a separate part for estimation of safety regions. In addition, the reliability controller is combined with heading regulation and motion damping. Stability properties are established using the backstepping technique.

This paper is organized as follows. In Section P2.2 we model the low-frequency motion of a 3 degrees-of-freedom surface vessel, and define the reliability index for the mooring lines. In Section P2.3 we develop the con-

troller, and in Section P2.4 we briefly describe the Marine Systems Simulator, and present simulation results. Conclusions are given in Section P2.5.

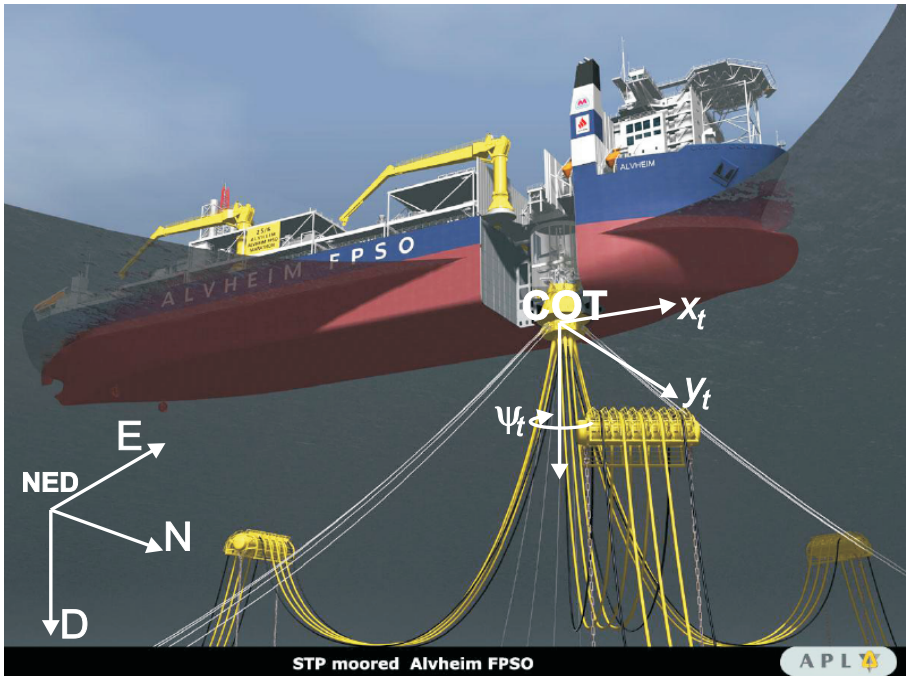

Figure P2.1: Illustration of a turret anchored FPSO. Courtesy of APL / Axis.

P2.2 Mathematical Modelling

We consider a surface vessel moored to the seabed via a spread mooring system with q cables. An example of the system is shown in Figure P2.1, along with the two reference frames used: the earth-fixed frame (*NED*), and; the vessel-fixed frame with origin located in the *center of turret* (COT). Mooring lines are usually composed of a mixture of chains, wire lines and synthetic fibers, depending on the sea depth. We will use a turret based mooring system, for which all mooring lines are connected to the same terminal point on the vessel (COT). The mooring lines introduce nonlinear stiffness to the system. The vessel is assumed to be fully actuated, and will be exposed to wind, waves and current for which the mooring system and the thrusters will need to compensate. Mathematical modelling of marine crafts can in general be divided into two regimes: i) Modelling for the pur-

pose of establishing a *process plant model* (PPM); ii) Modelling for establishing a *control plant model* (CPM). PPM serves the purpose of the real world in numerical simulations, and is usually a very complicated mathematical model, including both linear and nonlinear effects. CPM is a simplified model used for constructing and analyzing the controller. The simplifications can be several, both concerning hydrodynamic effects and degrees-of-freedom. For DP and PM problems, which consider a surface vessel at low speed, it is common to use only 3 degrees-of-freedom (3DOF) and assume linear hydrodynamics. We assume that the modelling of moored vessels is equivalent to established models for free-floating vessels with the restoring force from the mooring system as the only additional dynamic effect.

Vessel dynamics

The *low frequency, low speed CPM* model of a surface vessel in 3 DOF is given as

$$\mathbf{M}\dot{\boldsymbol{\nu}}+\mathbf{D}\boldsymbol{\nu}+\mathbf{g}(\boldsymbol{\eta}) = \boldsymbol{\tau} + \mathbf{J}^T(\psi)\,\mathbf{b}, \tag{P2.1}$$

$$\dot{\mathbf{p}} = \mathbf{J}_2(\psi)\,\mathbf{w}, \tag{P2.2}$$

$$\dot{\psi} = \rho, \tag{P2.3}$$

where $\boldsymbol{\eta} = \left[\mathbf{p}^T, \psi\right]^T = [x, y, \psi]^T$ is the position and heading vector in earth-fixed coordinates (NED), $\boldsymbol{\nu} = \left[\mathbf{w}^T, \rho\right]^T = [u, v, \rho]^T$ is the translational and rotational velocity vector in body-fixed coordinates (COT), $\mathbf{g}(\boldsymbol{\eta})$ consists of the mooring forces, $\boldsymbol{\tau} \in \mathbb{R}^3$ is the control vector, $\mathbf{b} \in \mathbb{R}^3$ is a slowly varying bias term representing external forces due to wind, currents, and waves, $\mathbf{M} \in \mathbb{R}^{3\times3}$ is the system inertia matrix, containing rigid body mass and added mass, $\mathbf{D} \in \mathbb{R}^{3\times3}$ is the hydrodynamic damping matrix and $\mathbf{J}(\psi)$ and $\mathbf{J}_2(\psi)$ are rotation matrices defined as

$$\mathbf{J}(\psi) = \begin{bmatrix} \mathbf{J}_2(\psi) & \mathbf{0} \\ \mathbf{0} & 1 \end{bmatrix} = \begin{bmatrix} \cos\psi & -\sin\psi & 0 \\ \sin\psi & \cos\psi & 0 \\ 0 & 0 & 1 \end{bmatrix}. \tag{P2.4}$$

The system inertia matrix $\mathbf{M}$ is symmetric positive definite. It is common to assume that $\bar{\mathbf{D}} = \left(\mathbf{D} + \mathbf{D}^T\right)/2$ is positive definite as well, but this is not necessary for our design. We refer the reader to Fossen (2002) for further details on modeling of marine vessels for control applications.

The mooring system is assumed to consist of q mooring lines, attached to a turret. The low frequency contact force of mooring line k, $k \in \{1, ..., q\}$, is

denoted $\mathbf{T}_k(\boldsymbol{\eta}) = [T_{x,k}, T_{y,k}, T_{z,k}]^T$, and the total mooring force acting on the vessel in COT is

$$\mathbf{g}(\boldsymbol{\eta}) = \begin{bmatrix} \sum_{k=1}^{q} T_{x,k} \\ \sum_{k=1}^{q} T_{y,k} \\ 0 \end{bmatrix}. \tag{P2.5}$$

The low frequency tension in mooring line k is given by

$$T_k\left(r_{k,lf}(t)\right) \triangleq \left\|\mathbf{T}_k(\boldsymbol{\eta})\right\|, \tag{P2.6}$$

where $r_{k,lf} = \|\mathbf{p} - \mathbf{p}_k\|$, $\mathbf{p}$ is the position of COT given in the NED frame, and $\mathbf{p}_k = [x_k, y_k]^T$ denotes the anchor point of mooring line k. The subscript lf emphasizes that it is only the low frequency variation that is considered. Note that the system, described by (P2.1)–(P2.3), is given with respect to the COT frame.

Usually, the computed system matrices from hydrodynamic software are given with respect to the software specific *data*-frame. The choice of using the COT frame as the basis for our control design is convenient because the yaw-component of (P2.5) becomes zero in this case. It is, however, not restrictive, since the system matrices may easily be transformed between different coordinate frames. Thus, the system matrices may be transformed to COT, in which frame the control law is derived, and then transformed to the frame utilized by the simulation tool.

Reliability index

The main objective of the controller design is to ensure that the mooring system is not overloaded under severe weather conditions. In order to reach that objective, we need to quantify mooring line load with respect to its expected endurance. This is done by defining a reliability index for each mooring line, as described by Madsen et al. (1986). The reliability index quantifies the probability of mooring line failure, and a somewhat simplified version is expressed in terms of the tension as

$$\delta_k(t) = \frac{T_{b,k} - \varkappa_k \sigma_k - T_k\left(r_{k,lf}(t)\right)}{\sigma_{b,k}}, \quad k = 1, \ldots, q, \tag{P2.7}$$

where $T_{b,k}$ is the mean breaking strength of mooring line k, σ_k is the standard deviation of the time varying tension (including high frequencies), $\varkappa_k$ is a scaling factor, $T_k\left(r_{k,lf}(t)\right)$ is the low frequency part of the mooring line tension, and $\sigma_{b,k}$ is the standard deviation of the mean breaking strength. In practice one would find $\sigma_{b,k}$ from tests, alternatively from data sheets

provided by the manufacturer. We, however, assume that $\sigma_{b,k} = 0.075 T_{b,k}$. We select a lower bound for δ_k, denoted δ_s (equal for all mooring lines), that defines the critical value of the reliability index. The condition $\delta_k < \delta_s$ represents a situation where the probability of line failure is intolerably high.

P2.3 Main Results

Controller design

In this section we develop a state feedback controller using the backstepping technique, under the condition that all states are available for feedback. Equation (P2.7) describes the reliability criterion for line k, based on $T(r_{k,lf})$. For simplicity of notation, we omit lf as a subscript, however the reader should keep in mind that only the low frequency part is considered, along with the standard deviation of the complete signal, σ_k. The controller will act based on the most critical reliability index, so we denote by j the subscript that represents the mooring line with the highest possibility of failure at any time. That is

$$\delta_j(t) = \min_{k \in \{1,\ldots,q\}} \delta_k(t). \tag{P2.8}$$

While the characteristics of the mooring lines are allowed to be nonlinear, we will nevertheless pose the following assumptions on the mooring system.

Assumption P2.1 *There exist constants ε_1 and ε_2 such that*

$$0 < \varepsilon_1 \leq T_j' \leq \varepsilon_2, \tag{P2.9}$$

for all $t \in \mathbb{R}_+$.

Assumption P2.2 *There exists a constant ϱ such that*

$$r_j \geq \varrho > 0, \tag{P2.10}$$

where r_j denotes the extension of mooring line j, for all $t \in \mathbb{R}_+$.

Assumption P2.1 says that the tension in a mooring line should increase as the surface vessel is moved further away from its anchor point, while Assumption P2.2 says that the anchor point of the most loaded anchor line will always be a horizontal distance away from the surface vessel. These assumptions always hold for a properly designed mooring system.

We will need the time derivative of δ_j, which is given by

$$\dot{\delta}_j(t) = -\frac{\dot{T}_j\left(r_j(t)\right)}{\sigma_{b,j}}, \tag{P2.11}$$

and since

$$\dot{T}_j\left(r_j(t)\right) = T_j'\dot{r}_j = \frac{T_j'}{r_j}\bar{\mathbf{p}}^T\dot{\mathbf{p}}, \tag{P2.12}$$

where $\bar{\mathbf{p}} = \left(\mathbf{p} - \mathbf{p}_j\right)$, we get

$$\dot{\delta}_j(t) = -\frac{T_j'}{\sigma_{b,j}r_j}\bar{\mathbf{p}}^T\mathbf{J}_2(\psi)\mathbf{w}. \tag{P2.13}$$

Formally, the controller should render the set

$$\mathcal{A} = \left\{(\boldsymbol{\eta}, \boldsymbol{\nu}) : \boldsymbol{\nu} = 0, \psi = \psi_s, \delta_j \geq \delta_s\right\}, \tag{P2.14}$$

asymptotically stable in some sense, where ψ_s is the desired heading. This objective, along with the structure of the model, makes backstepping a natural choice of control design method. By making the states of the system converge to $\mathcal{A}$, the velocity tends to zero, the heading to ψ_s, and $\delta_j < \delta_s$ is counteracted, respectively providing motion damping, heading regulation, and structural reliability. The following proposition presents our state feedback controller.

Proposition P2.1 *Let γ and κ be strictly positive constants, and $\boldsymbol{\Lambda}$ be a diagonal matrix such that $\boldsymbol{\Lambda} + \bar{\mathbf{D}}$ is positive definite. Then, the controller*

$$\boldsymbol{\tau} = \mathbf{M}\boldsymbol{\zeta} + \begin{bmatrix} \frac{T_j'}{\sigma_{b,j}}\bar{\delta}_j\boldsymbol{\vartheta} \\ -(\psi - \psi_s) \end{bmatrix} + (\mathbf{D} + \boldsymbol{\Lambda})\begin{bmatrix} \bar{\delta}_j\gamma\boldsymbol{\vartheta} \\ -\kappa(\psi - \psi_s) \end{bmatrix} - \boldsymbol{\Lambda}\boldsymbol{\nu} - \mathbf{J}^T(\psi)\mathbf{b} + \mathbf{g}(\boldsymbol{\eta}), \tag{P2.15}$$

where

$$\bar{\delta}_j = \min\left\{0, \delta_j - \delta_s\right\}, \tag{P2.16}$$

$$\boldsymbol{\zeta} = \begin{bmatrix} \gamma\left(\xi\mathbf{I} + \rho\bar{\delta}_j\mathbf{S}_2\right)\boldsymbol{\vartheta} + \frac{\gamma\bar{\delta}_j}{r_j}\left(\mathbf{I} - \boldsymbol{\vartheta}\boldsymbol{\vartheta}^T\right)\mathbf{w} \\ -\kappa\rho \end{bmatrix}, \tag{P2.17}$$

$$\boldsymbol{\vartheta} = \mathbf{J}_2^T(\psi)\frac{\left(\mathbf{p} - \mathbf{p}_j\right)}{r_j}, \tag{P2.18}$$

$$\xi = \begin{cases} 0, & \delta_j > \delta_s \\ -\frac{T_j'}{\sigma_{b,j}}\boldsymbol{\vartheta}^T\mathbf{w}, & \delta_j \leq \delta_s \end{cases}, \tag{P2.19}$$

$$\mathbf{S}_2 = \begin{bmatrix} 0 & 1 \\ -1 & 0 \end{bmatrix}, \tag{P2.20}$$

*renders the set $\mathcal{A}$ globally exponentially stable (*GES*). If* $\mathbf{b}$ *in (P2.15) is replaced by an estimate* $\hat{\mathbf{b}}$*, then the system is input-to-state stable (ISS) (with respect to* $\mathcal{A}$*), with input* $\tilde{\mathbf{b}} = \mathbf{b} - \hat{\mathbf{b}}$.

Proof. Consider the function

$$V_1 = \frac{1}{2}\overline{\delta}_j^2 + \frac{1}{2}(\psi - \psi_s)^2 . \tag{P2.21}$$

Its time derivative along solutions of (P2.1)–(P2.3) is

$$\dot{V}_1 = \overline{\delta}_j \dot{\delta}_j + (\psi - \psi_s)\dot{\psi}. \tag{P2.22}$$

Using (P2.13) and (P2.3), we obtain

$$\dot{V}_1 = -\overline{\delta}_j \frac{T_j'}{\sigma_{b,j}} \boldsymbol{\vartheta}^T \mathbf{w} + (\psi - \psi_s)\rho. \tag{P2.23}$$

Choosing $\mathbf{w}$ and ρ as virtual inputs, defining

$$\boldsymbol{\alpha}_w \triangleq \overline{\delta}_j \gamma \boldsymbol{\vartheta}, \tag{P2.24}$$

$$\alpha_\rho \triangleq -\kappa(\psi - \psi_s), \tag{P2.25}$$

and using Assumption P2.1 we get

$$\dot{V}_1 \leq -\frac{\gamma \varepsilon_1}{\sigma_{b,j}}\overline{\delta}_j^2 - \kappa(\psi - \psi_s)^2 - \overline{\delta}_j \frac{T_j'}{\sigma_{b,j}} \boldsymbol{\vartheta}^T (\mathbf{w} - \boldsymbol{\alpha}_w) + (\psi - \psi_s)\left(\rho - \alpha_\rho\right). \tag{P2.26}$$

Defining the change of variables

$$\mathbf{z} = \begin{bmatrix} \mathbf{z}_w \\ z_\rho \end{bmatrix} \triangleq \boldsymbol{\nu} - \boldsymbol{\alpha}, \tag{P2.27}$$

where $\boldsymbol{\alpha} = [\boldsymbol{\alpha}_w^T, \alpha_\rho]^T$, consider now the function

$$V_2 = V_1 + \frac{1}{2}\mathbf{z}^T \mathbf{M} \mathbf{z}. \tag{P2.28}$$

We get

$$\dot{V}_2 \leq -\frac{\gamma \varepsilon_1}{\sigma_{b,j}}\overline{\delta}_j^2 - \kappa(\psi - \psi_s)^2 + \mathbf{z}^T (\boldsymbol{\theta} - \mathbf{M}\dot{\boldsymbol{\alpha}}) + \frac{1}{2}\left(\dot{\boldsymbol{\nu}}^T \mathbf{M}\mathbf{z} + \mathbf{z}^T \mathbf{M}\dot{\boldsymbol{\nu}}\right), \tag{P2.29}$$

where

$$\boldsymbol{\theta} = \begin{bmatrix} -\overline{\delta}_j \frac{T_j'}{\sigma_{b,j}} \boldsymbol{\vartheta} \\ \psi - \psi_s \end{bmatrix}, \tag{P2.30}$$

and, using (P2.1), we obtain

$$\dot{V}_2 \leq -\frac{\gamma\varepsilon_1}{\sigma_{b,j}}\overline{\delta}_j^2 - \kappa(\psi-\psi_s)^2 - \mathbf{z}^T\overline{\mathbf{D}}\mathbf{z} + \mathbf{z}^T\left(\boldsymbol{\theta}+\boldsymbol{\tau}+\mathbf{J}^T(\psi)\,\mathbf{b} - \mathbf{D}\boldsymbol{\alpha} - \mathbf{g}(\boldsymbol{\eta}) - \mathbf{M}\dot{\boldsymbol{\alpha}}\right). \tag{P2.31}$$

From (P2.24)–(P2.25) we have that

$$\dot{\boldsymbol{\alpha}} = \begin{bmatrix} \gamma\left(\xi\mathbf{I}+\rho\overline{\delta}_j\mathbf{S}_2\right)\boldsymbol{\vartheta} + \frac{\gamma\overline{\delta}_j}{r_j}\left(\mathbf{I}-\boldsymbol{\vartheta}\boldsymbol{\vartheta}^T\right)\mathbf{w} \\ -\kappa\rho \end{bmatrix}. \tag{P2.32}$$

Substituting (P2.15) and (P2.32) into (P2.31) gives

$$\dot{V}_2 \leq -\frac{\gamma\varepsilon_1}{\sigma_{b,j}}\overline{\delta}_j^2 - \kappa(\psi-\psi_s)^2 + \mathbf{z}^T\left(-\left(\overline{\mathbf{D}}+\boldsymbol{\Lambda}\right)\mathbf{z} + \mathbf{J}^T(\psi)\,\tilde{\mathbf{b}}\right). \tag{P2.33}$$

Completing squares, we obtain

$$\dot{V}_2 \leq -\frac{\gamma\varepsilon_1}{\sigma_{b,j}}\overline{\delta}_j^2 - \kappa(\psi-\psi_s)^2 - \left|\left(\overline{\mathbf{D}}+\boldsymbol{\Lambda}\right)\mathbf{z} - \frac{1}{2}\mathbf{J}^T(\psi)\,\tilde{\mathbf{b}}\right|^2 + \frac{1}{4}\left|\mathbf{J}^T(\psi)\,\tilde{\mathbf{b}}\right|^2 \tag{P2.34}$$

$$\leq -\frac{\gamma\varepsilon_1}{\sigma_{b,j}}\overline{\delta}_j^2 - \kappa(\psi-\psi_s)^2 - \frac{1}{2}\mathbf{z}^T\left(\overline{\mathbf{D}}+\boldsymbol{\Lambda}\right)\mathbf{z} + \frac{1}{2\lambda_{\min}}\left|\tilde{\mathbf{b}}\right|^2, \tag{P2.35}$$

where $\lambda_{\min}$ is the smallest eigenvalue of the positive definite matrix $\left(\overline{\mathbf{D}}+\boldsymbol{\Lambda}\right)$. Defining the set,

$$\mathcal{B} = \left\{(\boldsymbol{\eta},\boldsymbol{\nu}) : \mathbf{z}=\mathbf{0}, \psi=\psi_s, \delta_j \geq \delta_s\right\}, \tag{P2.36}$$

and the generic norm

$$\left|(\boldsymbol{\eta},\boldsymbol{\nu})\right|_{\mathcal{B}} = \left(\overline{\delta}_j^2 + (\psi-\psi_s)^2 + \mathbf{z}^T\mathbf{M}\mathbf{z}\right)^{1/2}, \tag{P2.37}$$

we have that

$$V_2 = \frac{1}{2}\left|(\boldsymbol{\eta},\boldsymbol{\nu})\right|_{\mathcal{B}}^2, \tag{P2.38}$$

and

$$\dot{V}_2 < -c_1\left|(\boldsymbol{\eta},\boldsymbol{\nu})\right|_{\mathcal{B}}^2 + c_2^2|\tilde{\mathbf{b}}|^2, \tag{P2.39}$$

for some strictly positive constants c_1 and c_2. It follows that $\mathcal{B}$ is GES (Teel (2002)) when $\mathbf{b}$ is known ($\tilde{\mathbf{b}} \equiv \mathbf{0}$). Suppose $(\boldsymbol{\eta},\boldsymbol{\nu}) \in \mathcal{B}$. Then from (P2.24)–(P2.25), $\boldsymbol{\alpha} = 0$, so from (P2.27), $\boldsymbol{\nu} = 0$. Thus, $(\boldsymbol{\eta},\boldsymbol{\nu}) \in \mathcal{A}$, so $\mathcal{B} \subset \mathcal{A}$, and $\mathcal{A}$ is GES. For $\mathbf{b}$ unknown, the ISS part of the result follows from noticing that (P2.39) gives

$$\dot{V}_2 \leq -\frac{c_1}{2}\left|(\boldsymbol{\eta},\boldsymbol{\nu})\right|_{\mathcal{B}}^2 \;\forall\; \left|(\boldsymbol{\eta},\boldsymbol{\nu})\right|_{\mathcal{B}} \geq \left(\frac{2c_2}{c_1}\right)^{1/2}|\tilde{\mathbf{b}}|, \tag{P2.40}$$

and applying Theorem 4.19 in Khalil (2002).

Adaptation of unknown disturbances

We assume that both $\boldsymbol{\eta}$ and $\boldsymbol{\nu}$ are available via measurements. We implement the following identifier to estimate the unknown disturbance vector (Krstić et al. (1995)).

$$\dot{\hat{\boldsymbol{\nu}}} = -\mathbf{M}^{-1}\mathbf{D}\boldsymbol{\nu} - \mathbf{M}^{-1}\mathbf{g}(\boldsymbol{\eta}) + \mathbf{M}^{-1}\boldsymbol{\tau} + \mathbf{M}^{-1}\mathbf{J}^{T}(\psi)\hat{\mathbf{b}} - \mathbf{A}_m\tilde{\boldsymbol{\nu}}, \tag{P2.41}$$

where

$$\tilde{\boldsymbol{\nu}} = \boldsymbol{\nu} - \hat{\boldsymbol{\nu}}, \tag{P2.42}$$

and

$$\mathbf{A}_m = \mathbf{A}_0 - \lambda\mathbf{M}^{-T}\mathbf{M}^{-1}\mathbf{P}, \tag{P2.43}$$

where $\lambda > 0$ and $\mathbf{A}_0$ is a matrix satisfying

$$\mathbf{P}\mathbf{A}_0 + \mathbf{A}_0^{T}\mathbf{P} = -\mathbf{I}, \quad \mathbf{P} = \mathbf{P}^{T} > \mathbf{0}. \tag{P2.44}$$

The update law for $\hat{\mathbf{b}}$ is given by

$$\dot{\hat{\mathbf{b}}} = \boldsymbol{\Gamma}\mathbf{M}^{-1}\mathbf{P}\tilde{\boldsymbol{\nu}}, \tag{P2.45}$$

where $\boldsymbol{\Gamma} = \boldsymbol{\Gamma}^{T} > \mathbf{0}$. The error dynamics for the identifier becomes

$$\dot{\tilde{\boldsymbol{\nu}}} = \left(\mathbf{A}_0 - \lambda\mathbf{M}^{-T}\mathbf{M}^{-1}\mathbf{P}\right)\tilde{\boldsymbol{\nu}} + \mathbf{M}^{-T}\mathbf{J}^{T}\tilde{\mathbf{b}}, \tag{P2.46}$$

$$\dot{\tilde{\mathbf{b}}} = -\boldsymbol{\Gamma}\mathbf{M}^{-1}\mathbf{P}\tilde{\boldsymbol{\nu}}. \tag{P2.47}$$

For the identifier, we have the following result.

Proposition P2.2 *The origin of the identifier error dynamics (P2.46)–(P2.47) is globally asymptotically stable (GAS).*

Proof. Consider the Lyapunov function

$$V = \tilde{\mathbf{b}}^{T}\boldsymbol{\Gamma}^{-1}\tilde{\mathbf{b}} + \tilde{\boldsymbol{\nu}}^{T}\mathbf{P}\tilde{\boldsymbol{\nu}}. \tag{P2.48}$$

It's time derivative along solutions of (P2.46)–(P2.47) is

$$\dot{V} = -|\tilde{\boldsymbol{\nu}}|^2 - 2\lambda\left|\mathbf{M}^{-1}\tilde{\boldsymbol{\nu}}\right|^2. \tag{P2.49}$$

Since $\left(\tilde{\boldsymbol{\nu}}, \tilde{\mathbf{b}}\right) = \mathbf{0}$ is the only solution that can stay forever in the set $\left\{\left(\tilde{\boldsymbol{\nu}}, \tilde{\mathbf{b}}\right) : \tilde{\boldsymbol{\nu}} = \mathbf{0}\right\}$, the result now follows from LaSalle's invariance principle.

Adaptive controller

We are now ready to state the main result of the paper. Noticing that the identifier error dynamics (P2.46)–(P2.47) and the controlled surface vessel form a cascade, we can apply Lemma 4.7 in Khalil (2002) to obtain the following result.

Theorem P2.1 *The set*

$$\left\{\left(\boldsymbol{\eta}, \boldsymbol{\nu}, \tilde{\boldsymbol{\nu}}, \tilde{\mathbf{b}}\right) : \psi = \psi_s, \delta_j \geq \delta_s, \boldsymbol{\nu} = \tilde{\boldsymbol{\nu}} = \tilde{\mathbf{b}} = \mathbf{0}\right\} \tag{P2.50}$$

is GAS under the dynamics of the surface vessel (P2.1)–(P2.3) in closed loop with the controller (P2.15), with $\mathbf{b}$ *replaced by* $\hat{\mathbf{b}}$*, and the identifier (P2.41)–(P2.43).*

P2.4 Simulation Study

The performance of the controller is demonstrated in numerical simulations using a high fidelity ship simulator called the Marine Systems Simulator (MSS), developed at the Department of Marine Technology, NTNU (Perez et al., 2006). The Marine Systems Simulator serves the purpose of our PPM.

The Marine Systems Simulator

The Marine Systems Simulator constitutes a very realistic nonlinear ship simulator in 6DOF, and is ideal for testing the performance and robustness of control strategies. It employs the equations

$$\underbrace{\mathbf{M}_{RB}\dot{\boldsymbol{\nu}}+\mathbf{C}_{RB}(\boldsymbol{\nu})\boldsymbol{\nu}}_{\textit{rigid body effects}} + \underbrace{\mathbf{M}_A\dot{\boldsymbol{\nu}} + \mathbf{C}_A(\boldsymbol{\nu}_r)\boldsymbol{\nu}_r+\mathbf{D}(\boldsymbol{\nu}_r)\boldsymbol{\nu}_r + \mathbf{g}(\boldsymbol{\eta})}_{\textit{hydrodynamic effects}} = \boldsymbol{\tau}_{thr} + \boldsymbol{\tau}_{env}, \tag{P2.51}$$

$$\dot{\boldsymbol{\eta}} = \mathbf{J}(\boldsymbol{\eta})\nu, \tag{P2.52}$$

where $\boldsymbol{\eta} = [x, y, z, \phi, \theta, \psi]^T$ is the position and Euler angles vector, $\boldsymbol{\nu}_r = [u - u_c, v - v_c, w, p, q, \rho]^T$ is the translational and rotational velocity vector in body-fixed coordinates, where u_c and v_c are the slowly varying current velocities. $\boldsymbol{\tau}_{thr}$ is the control vector, and $\boldsymbol{\tau}_{env}$ contains environmental forces from wave drift and wind. We have split the equation into two terms, one containing effects from the rigid body, with subscript *RB*, and one containing hydrodynamic effects. $\mathbf{M}_{RB} \in \mathbb{R}^{6\times6}$ is the rigid body mass matrix, $\mathbf{C}_{RB}(\boldsymbol{\nu}) \in \mathbb{R}^{6\times6}$ is the rigid body Coriolis and Centripetal matrix, $\mathbf{g}(\boldsymbol{\eta}) \in \mathcal{R}^{6\times1}$ is the restoring matrix, $\mathbf{M}_A \in \mathbb{R}^{6\times6}$ is the added mass, $\mathbf{C}_A(\boldsymbol{\nu}_r) \in \mathbb{R}^{6\times6}$ is the hydrodynamic Coriolis and Centripetal matrix, and $\mathbf{D}(\boldsymbol{\nu}_r) \in \mathbb{R}^{6\times6}$ is the

damping matrix containing both linear and nonlinear effects. Note that only the hydrodynamic effects are dependent on $\boldsymbol{\nu}_r$. $\mathbf{J}(\boldsymbol{\eta})$ is the rotation matrix. For further details on surface ship modelling, see Fossen (2002). The mooring system consists of four mooring lines connected to a turret. The water depth is 200 meters and the four mooring lines are spread out, with approximately 1/3 of their total length of 400 meters laying on the sea bed. In the simulator, the mooring lines are represented by finite element models, each consisting of 30 elements. The mooring line model is described in detail in Aamo and Fossen (2001). The vessel is equipped with one bow thruster and three azimuth thrusters with fixed headings. The commanded thruster output is directed to each of the thrusters via a thruster allocation scheme as described by Sørensen et al. (1999).

Simulation results

The vessel is a 175 [m] long, 25 [m] wide ship, with a draught of 5.5 [m]. First, we will show some preliminary results, then we will present results from our two main scenarios.

Preliminary results

Exposing the vessel to an incoming current from the north with a magnitude of 0.5 [m/s], applying control, we see from Figure P2.2 that the controller allows the δ–index to converge to $\delta = 6$, while the minimum limit is set at $\delta_s = 4$. The thrust for this case is given in Figure P2.3, with the thrust in x– and y–direction in the upper and lower graph, respectively. The thrust varies around zero when δ has converged, implying that the controller only applies motion damping and heading regulation at this time, while the mooring forces balance the environmental forces on average. However, if the vessel is exposed to an incoming current with a magnitude of 0.9 [m/s], and the controller applies motion damping and heading regulation, only, we see from Figure P2.4 that the δ criterion is clearly violated, putting the mooring system in jeopardy.

Scenario 1

The vessel is exposed to an incoming current from the north, varying as shown in Figure P2.5. Figure P2.6 shows the time variation of δ and ψ as the current varies. In the upper graph we see that δ converges to δ_s, however, not before the actual environmental load exceeds what the mooring system safely can sustain. The lower graph shows that ψ regulates to ψ_s. Thus, we have achieved a reduction of the loading of the mooring lines

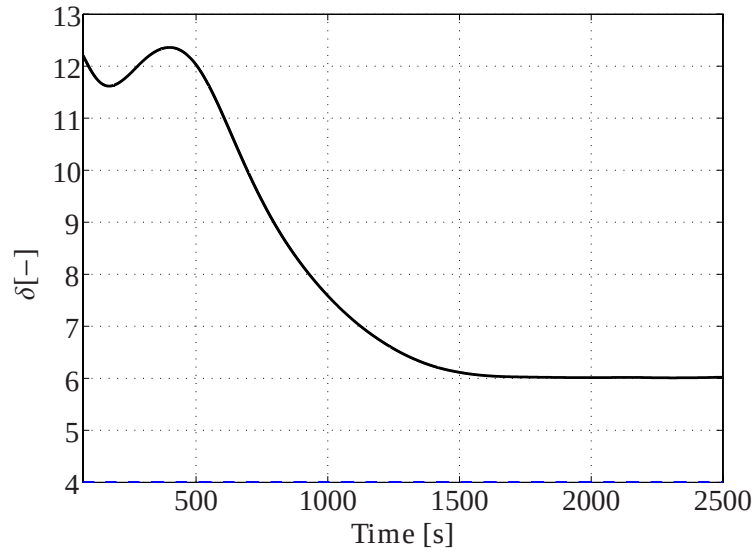

Figure P2.2: Time variation of δ for $\nu_c = 0.5[m/s]$.

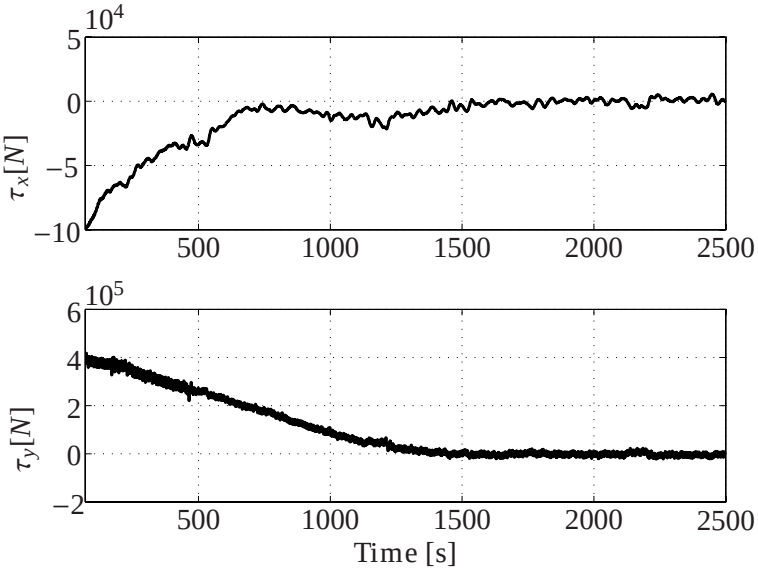

Figure P2.3: Time variation of thruster force for $\nu_c = 0.5[m/s]$.

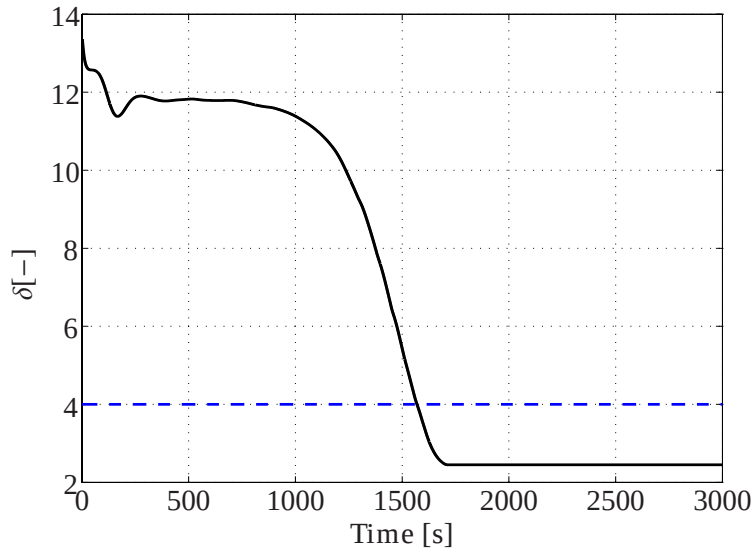

Figure P2.4: Time variation of δ for $v_c = 0.9[m/s]$, with motion damping and heading regulation, only.

when necessary, while maintaining the preset heading of $\psi_s = 30°$. We can see how the $\delta-$index is slightly influenced by the change in the heading. The position of the vessel in the $(x,y)-$plane is shown in Figure P2.7, with heading illustrated for $t = 1$ $[s]$, $t = 1000$ $[s]$, and $t = 10000$ $[s]$. Notice that the heading ψ has converged to ψ_s at $t = 1000$ $[s]$, while the vessel still moves around due to the varying environmental load. The thrust that achieves this is shown in Figure P2.8. After some initial transients, the thrust varies around zero as long as $\delta > \delta_s$, while thruster assistance for positioning is applied in the time interval $[2500, 7000]$ to maintain $\delta = \delta_s$. The controller utilizes estimated values of the environmental disturbances. The performance of the adaptation mechanism is shown in Figure P2.9. The estimated disturbances match the actual disturbances very well when the environmental load is constant, while they lag somewhat behind when the conditions are varying. It is possible to tune the adaptation mechanism so that the estimated values converge faster, however, it should be noted that the changes in environmental loading in the simulations are unrealistically rapid.

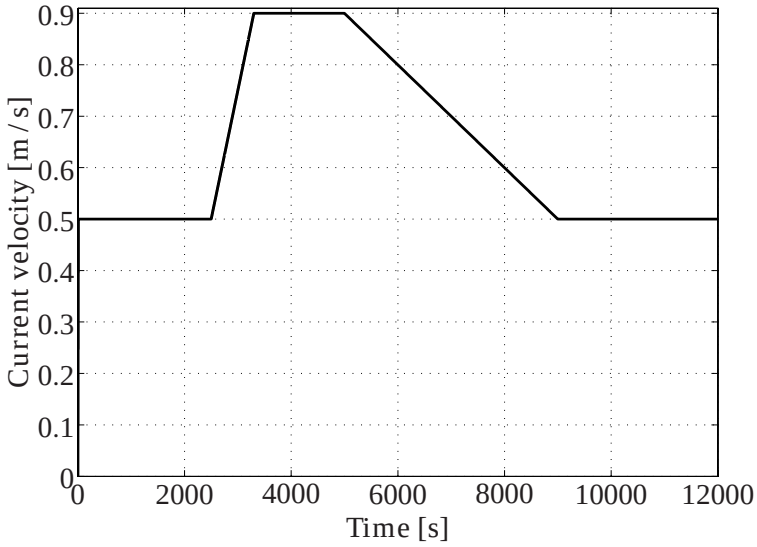

Figure P2.5: Current profile for scenario 1.

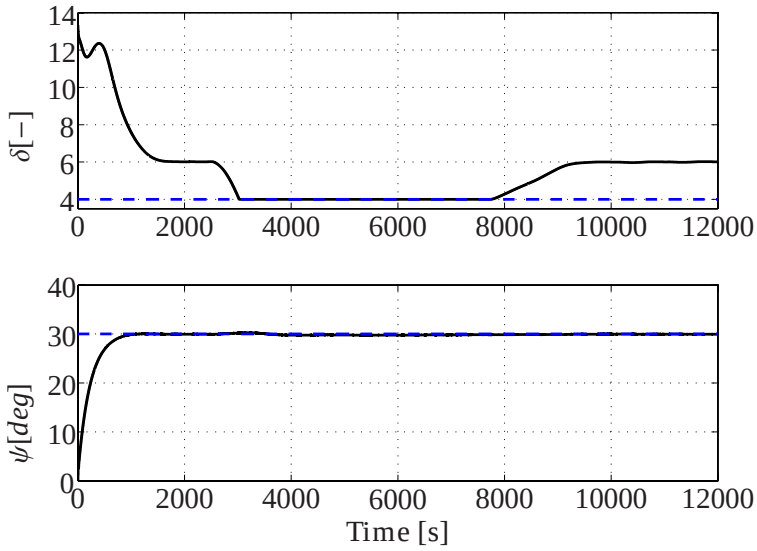

Figure P2.6: Time variation of δ and ψ for scenario 1.

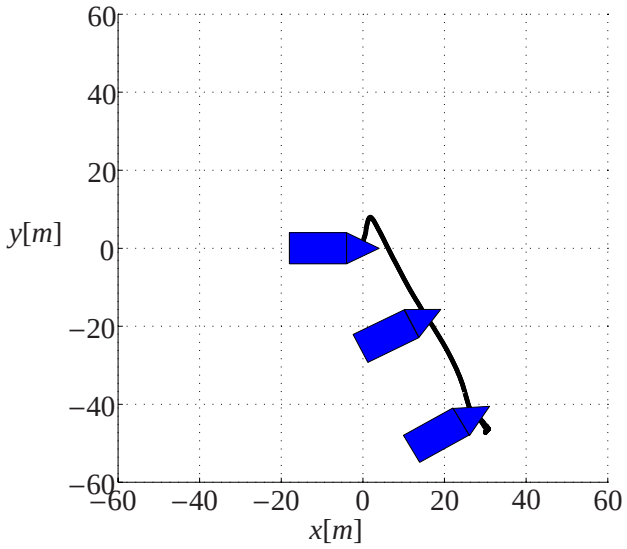

Figure P2.7: Position of the vessel for $t = 1[s]$, $t = 1000[s]$ and $t = 10000[s]$.

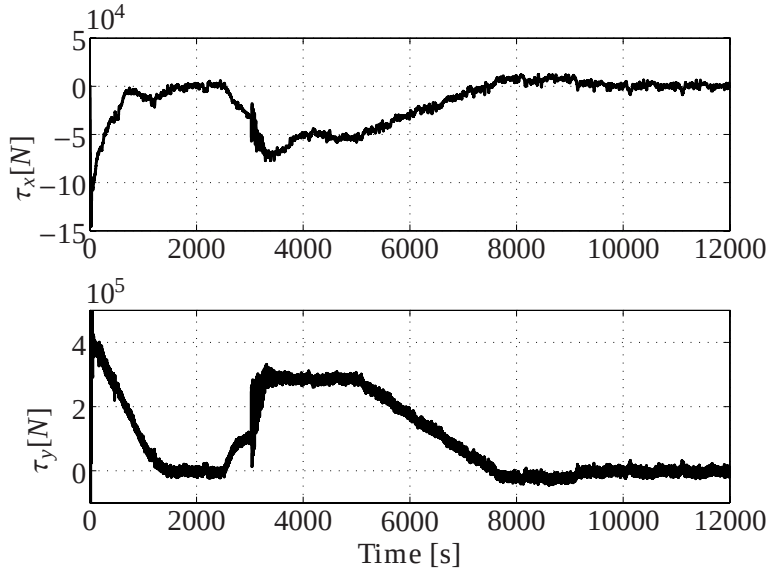

Figure P2.8: Time variation of the commanded thruster force for scenario 1.

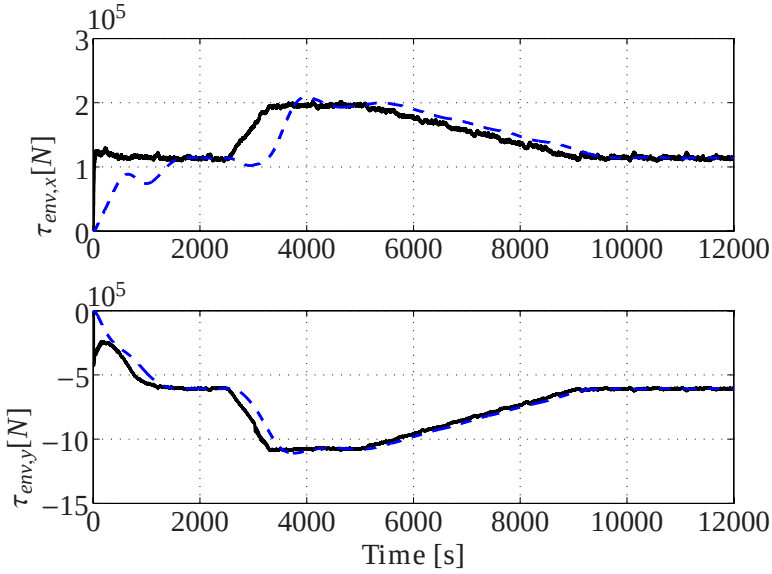

Figure P2.9: Time variation of the actual, solid line, and the estimated, dashed line, environmental force.

Scenario 2

In scenario 2 the current is constant, with a magnitude of 0.9 $[m/s]$ from the north, while the sea state increases from $H_s = 0.5$ $[m]$ to $H_s = 1.5$ $[m]$ between $t = 2000$ $[s]$ and $t = 4000$ $[s]$. This effect is captured by σ_j shown in Figure P2.10, which clearly reflects the increasing sea state. The increasing σ_j causes the thrusters to move the ship closer to the origin in order to keep δ at δ_s, as shown in the upper graph of Figure P2.11. The lower graph shows that δ remains at δ_s. The thrust for scenario 2 is shown in Figure P2.12, with the force in $x-$ and $y-$direction in the upper and lower graph, respectively. As expected, thruster assistance increases with increasing sea state as measured by σ_j.

P2.5 Conclusions

In this paper we have developed a controller for position mooring that takes into account structural reliability of the mooring lines and continuously performs heading regulation and motion damping. By making structural reliability an intrinsic part of the controller, the capacity of the moor-

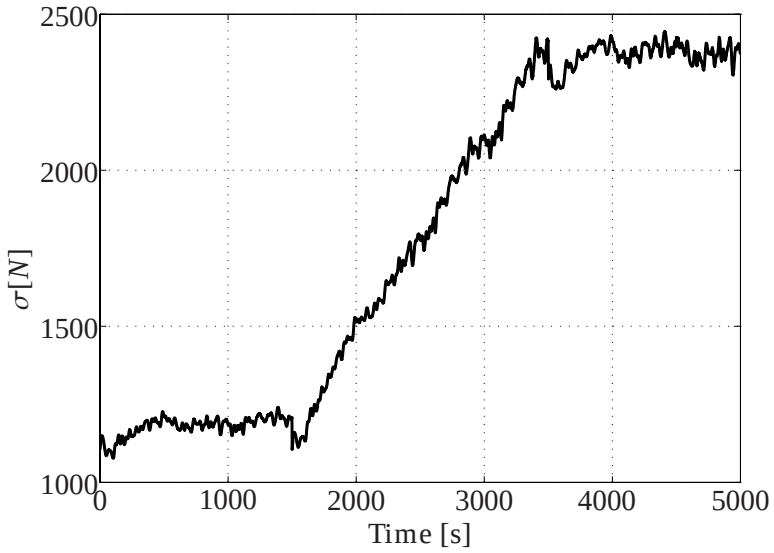

Figure P2.10: Time variation of σ_j.

ing system is utilized better while keeping the probability of mooring line breakage within acceptable limits. This is achieved by formulating a reliability criterion based on measurements of tension in each of the mooring lines. The performance of the controller is demonstrated in numerical simulations using a high fidelity ship simulator.

Acknowledgements

We gratefully acknowledge the support from the Norwegian Research Council.

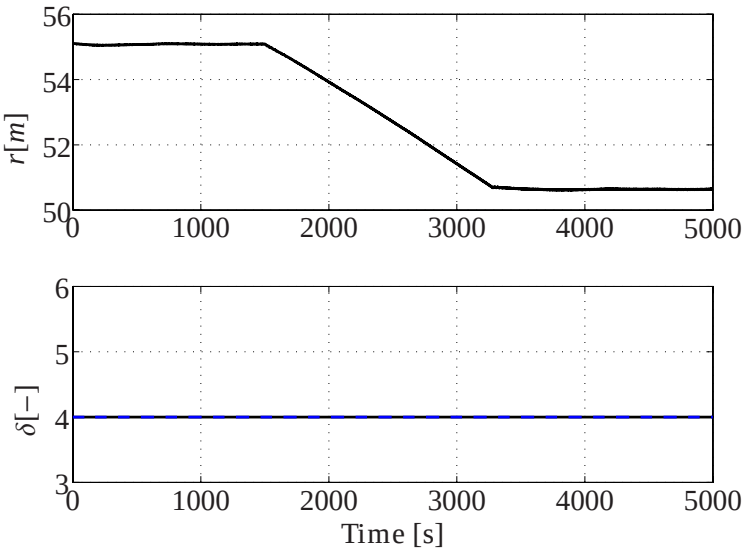

Figure P2.11: Time variation of the distance from origin (r), and δ for scenario 2.

Bibliography

Aamo, O.M., and Fossen, T.I. (2001). Finite Element Modelling of Moored Vessels, *Mathematical and Computer Modelling of Dynamical Systems* **7(1)**:47–75.

Aarset, M.F., Strand J.P. and Fossen, T.I. (1998). Nonlinear vectorial back–stepping with integral action and wave filtering for ships, *Proceedings of the IFAC Conference on Control Applications in Marine Systems, Fukuoka, Japan* pp. 83–89.

Balchen, J.G., Jenssen, N.A. and Sælid, S. (1981). Dynamic positioning of floating vessels based on Kalman filtering and optimal control, *Proceed–ings of the 19th IEEE Conference on Decision and Control, Albuquerque, New Mexico, US*, pp. 1–13.

Balchen, J.G., Jenssen, N.A., Mathisen E. and Sælid, S. (1980). A dynamic positioning system based on Kalman filtering and optimal control, *Mod–eling, Identification and Control* **1(3)**:135–163.

Balchen, J.G., Jenssen, N.A. and Sælid, S. (1976). Dynamic positioning us–

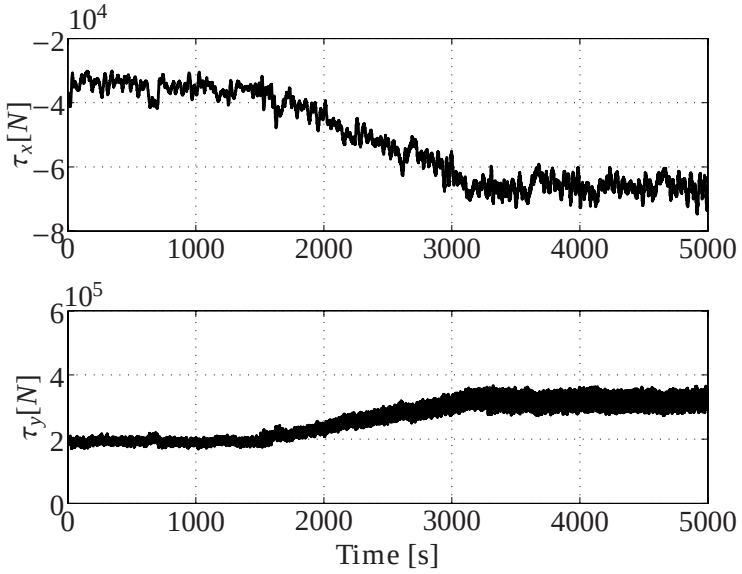

Figure P2.12: Time variation of the commanded thruster force for scenario 2.

ing filtering and optimal control theory, *Proceedings of the IFAC/IFIP Sym–posium, Amsterdam, The Netherlands* pp. 183–186.

Berntsen, P.I.B., Aamo, O.M. and Leira, B.J. (2007). Structural reliability–based control of moored interconnected structures, *Control Engineering Practice* **16(4):**495–504.

Fossen, T. I. (2002). *Marine Control Systems*. Marine Cybernetics, Trond–heim, Norway.

Fossen, T.I. and Grøvlen Å. (1998). Nonlinear output feedback control of dynamically positioned ships using vectorial observer backstepping, *IEEE Transactions on Control Systems Technology* **6(1)**:121–128.

Fung, P.T. and Grimble, M.J. (1983). Dynamic ship positioning using self–tuning Kalman filter, *IEEE Transactions on Automatic Control* **28(3)**:339–350.

Grimble, M.J., Patton, R.J. and Wise, D.A. (1980). The design of dynamic ship positioning control systems using stochastic optimal theory, *Opti–mal Control Applications and Methods*, **1:**167–202.

Grimble, M.J, Patton, R.J. and Wise, D. (1983). Use of Kalman filtering techniques in dynamic ship positioning systems, *IEEE Transactions on Automatic Control* **28(3)**:331–339.

Khalil, H.K. (2002). *Nonlinear Systems, 3rd ed.*, Prentice Hall, New Jersey, US.

Krstić, M., Kanellakopoulos, I. and Kokotović, P. (1995). *Nonlinear and Adaptive Control Design*, John Wiley and Sons, Inc, New York, US.

Madsen, H., Krenk, S., Lind, N.C. (1986). *Methods of Structural Safety*. Prentice Hall, New Jersey, US.

Perez, T., Smogeli, Ø.N., Fossen, T.I. and Sørensen, A.J. (2005). An overview of marine systems simulator (MSS): A Simulink toolbox for marine control systems, *Modelling, Identification and Control* **27(4):**259–275.

Robertsson, A. and Johansson, R. (1998). Comments on nonlinear output feedback control of dynamically positioned ships using vectorial observer backstepping, *IEEE Transactions on Control Systems Technology* **6(3)**: 439–441.

Sælid, S., Jenssen, N.A. and Balchen, J.G. (1983). Design and analysis of a dynamic positioning system based on Kalman filtering and optimal control, *IEEE Transactions on Automatic Control* **28(3)**:331–339.

Salvesen, N., Tuck, E.O. and Faltinsen, O. (1970), Ship motions and sea loads, *Transactions of the Society of Naval Architects and Marine Engineers* **78**:250–287.

Sørensen, A.J., Sagatun, S.I. and Fossen, T.I. (1996). Design of a dynamic positioning system using model-based control, *Control Engineering Practice* **4(3)**:359–368.

Strand, J.P. (1999). *Nonlinear Position Control Systems Design for Marine Vessels*. PhD thesis, Norwegian University of Science and Technology, Trondheim, Norway.

Strand, J.P. and Fossen, T.I. (1999). Passive nonlinear observer design for ships using Lyapunov methods: full-scale experiments with a supply vessel, *Automatica* **35(1)**:3–16.

Strand, J.P., Sørensen, A.J. and Fossen, T.I. (1997). Modelling and control of thruster assisted position mooring systems for ships, *Proceedings of the 4th Conference on Manouvering and Control of Marine Craft, Brijuni, Croa–*

tia, pp. 160–165.

Teel, A.R. (2002), *Notes on nonlinear control and analysis*, Lecture Notes, UCSB, Santa Barbara, California, US.

Paper III

Ensuring Mooring Line Integrity by Dynamic Positioning: Controller Design and Experimental Tests

Per Ivar Barth Berntsen[a], Ole Morten Aamo[b], Bernt J. Leira[a]
[a]*Department of Marine Technology, Norwegian University of Science and Technology, N-7491 Trondheim, Norway*
[b]*Department of Engineering Cybernetics, Norwegian University of Science and Technology, N-7491 Trondheim, Norway*

Abstract

This paper addresses dynamic positioning of surface vessels moored to the seabed via a turret based spread mooring system, an operation referred to as position mooring. While the mooring system keeps the surface vessel in place most of the time, thruster assistance is needed in severe weather conditions to avoid mooring line failure. Traditionally, this is done by keeping the vessel within a predefined geographical region. We present a conceptually new controller for position mooring operations. By using a structural reliability measure for the mooring lines, the new controller protects the mooring system whenever needed as a result of severe weather conditions and high environmental loads, by maintaining the probability of mooring line failure below a preset value. In particular, the excessive use of thrusters caused by conservatively defined safety regions in conventional PM systems is avoided, giving a fuel optimal operation. The feasibility of our controller is successfully verified in laboratory experiments.

P3.1 Introduction

The offshore structures used for drilling and production of oil and gas are exposed to some of the worlds most inhospitable environments, with temperatures often falling below the freezing point and winds reaching hurricane force. The reliability of the structure and it's subcomponents is crucial for keeping the crew safe and the operation up and running. Since the late 1980's, floating vessels moored to the seabed have proved to be a cost-effective alternative to permanent platforms for offshore oil production. While the mooring system holds the vessel in place in moderate weather conditions, thruster assistance may be needed during severe weather. A control system that provides thruster assistance for a moored vessel is referred to as a position mooring system (PM), as opposed to a dynamic positioning system (DP) which refers to the non-moored case. A PM system also uses thrusters constantly for damping the surge, sway and yaw motions and for keeping the desired heading Strand (1999).

The current research on PM systems is based on the experience obtained from research on DP systems since the 1970's (see Berntsen et al. (2008) and the references therein). Strand et al. (1997) present a model for the mooring system based on line characteristics, and extend the DP controller derived by Sørensen et al. (1996) for this system. Sørensen et al. (1999) reduced the number of tuning variables by introducing a nonlinear observer. A dynamic line tensioning controller was proposed by Aamo and Fossen (1999) in order to reduce the necessary thruster force. In order to expand the operational weather window for moored vessels, Nguyen et al. (2007) proposed a hybrid position mooring system which automatically switches between different controllers based on the actual weather condition. Nguyen and Sørensen (2007) implemented a setpoint chasing algorithm in order to reduce the possibility of mooring line breakage in extreme conditions.

Common for existing PM systems, is that motion is restricted to lie within predefined geographical safety regions, using linearization and gain-scheduling procedures to derive the controller. This leads to considerable conservativeness with regards to exploiting the capacity of the mooring system, and consequently excessive use of the thrusters. In order to deal with this problem, we proposed in Berntsen et al. (2004) a method for taking structural reliability measures of the mooring lines into account when designing PM systems. The controller acts to keep the probability of line failure below an acceptable level regardless of changing weather conditions. In this way, the conservativeness involved in defining a geographical region for traditional position mooring systems is removed, giving a controller that uses less fuel. The method is extended in Berntsen et al. (2006),

where the reliability measure becomes an intrinsic part of the controller. In this paper, we continue the development by implementing the controller using the reliability measure intrinsically on a scaled model vessel and conduct experimental tests to verify the performance of the controller under realistic conditions. The reliability measure behaves like a control objective, ensuring that the possibility of failure of the mooring system never exceeds a preset level.
The paper is organized as follows: In Sections P3.2 and P3.3 we review respectively the mathematical modelling of the moored vessel and the control design from Berntsen et al. (2006). Results from the laboratory experiments are reported in Section P3.4, and conclusions are offered in Section P3.5.

P3.2 Mathematical Modelling

We consider a surface vessel moored to the seabed via a turret based spread mooring system with q cables. Mooring lines are usually composed of a mixture of chains, wire lines and synthetic fibers, depending on the sea depth. We will use a turret based mooring system, for which all mooring lines are connected to the same terminal point on the vessel, referred to as *center o f turret* (COT), as indicated in Figure P3.1. The vessel is assumed to be fully actuated, and will be exposed to wind, waves and currents for which the mooring system and the thrusters will need to compensate. The control design employs a low frequency model based on the assumption that low frequency and wave frequency motions can be separated (Sørensen (2005)), and that the wave frequency part can be neglected. In this way, the excessive use of thrusters that would result from the controller trying to compensate for wave frequency motions is avoided. For vessels with sufficient metacentric height and waterplane area, such as ships, it is according to Strand (1999) sufficient to consider a three degrees-of-freedom model (3 DOF), incorporating surge, sway and yaw motions.

Vessel dynamics

The *low frequency* motion of a surface vessel in 3 degrees-of-freedom (3 DOF) can be modeled as (Fossen (2002))

$$\mathbf{M}\dot{\nu}+\mathbf{D}\nu+\mathbf{g}(\eta) = \tau + \mathbf{J}^T(\psi)\,\mathbf{b}, \tag{P3.1}$$

$$\dot{\mathbf{p}} = \mathbf{J}_2(\psi)\,\mathbf{w}, \tag{P3.2}$$

$$\dot{\psi} = \rho, \tag{P3.3}$$

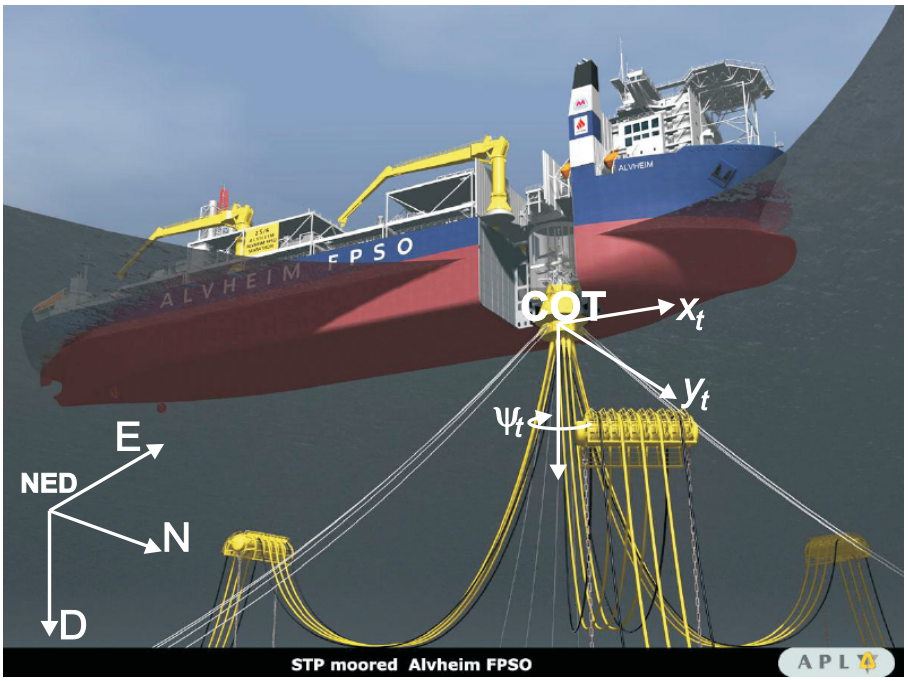

Figure P3.1: Illustration of a turret anchored FPSO. Courtesy of APL / Axis.

where $\boldsymbol{\eta} = \left[\mathbf{p}^T, \psi\right]^T = [x, y, \psi]^T$ is the position and heading in the NED frame (earth-fixed north-east-down coordinate system), $\boldsymbol{\nu} = \left[\mathbf{w}^T, \rho\right]^T = [u, v, \rho]^T$ is the translational and rotational velocities in body-fixed coordinates, $\mathbf{g}(\boldsymbol{\eta})$ constitutes the mooring forces and moment, $\boldsymbol{\tau} = \left[\tau_x, \tau_y, \tau_\psi\right]^T$ is the control input, $\mathbf{b}$ is a slowly varying bias term representing unmodelled environmental forces due to wind, currents, and waves, $\mathbf{M}$ is the system inertia matrix, $\mathbf{D}$ is the hydrodynamic damping matrix, including damping effects from the mooring system, and $\mathbf{J}(\psi)$ and $\mathbf{J}_2(\psi)$ are rotation matrices defined as

$$\mathbf{J}(\psi) = \begin{bmatrix} \mathbf{J}_2(\psi) & \mathbf{0} \\ \mathbf{0} & 1 \end{bmatrix}, \mathbf{J}_2(\psi) = \begin{bmatrix} \cos\psi & -\sin\psi \\ \sin\psi & \cos\psi \end{bmatrix}. \tag{P3.4}$$

While $\mathbf{g}(\boldsymbol{\eta})$ and $\boldsymbol{\tau}$ are given in body-fixed coordinates, $\mathbf{b}$ is given in the NED frame. The system inertia matrix $\mathbf{M}$ and $\bar{\mathbf{D}} = \left(\mathbf{D} + \mathbf{D}^T\right)/2$ are symmetric positive definite matrices. The system matrices are known, assuming that hullshape and loading condition is known. We refer the reader to Faltinsen (1990) and Fossen (2002) for further details on modelling of marine vessels.

The mooring system is assumed to consist of q mooring lines, attached to a turret. The contact force of mooring line k, $k \in \{1, ..., q\}$, is denoted $\mathbf{T}_k(\boldsymbol{\eta}) = [T_{x,k}, T_{y,k}, T_{z,k}]^T$. The 3 DOF mooring force acting on the vessel becomes

$$\mathbf{g}(\boldsymbol{\eta}) = \sum_{k=1}^{q} \begin{bmatrix} T_{x,k} & T_{y,k} & 0 \end{bmatrix}. \tag{P3.5}$$

The low frequency force of mooring line k is given by

$$T_k(r_k(t)) \triangleq \left\| \mathbf{T}_k(\boldsymbol{\eta}) \right\|, \tag{P3.6}$$

where $r_k = \left\| \mathbf{p}_{lf} - \mathbf{p}_k \right\|$ and $\mathbf{p}_k = [x_k, y_k]^T$ denotes the anchor point of mooring line k.

Structural integrity

The main idea behind the controller is to position the surface vessel by thruster assistance in such a way that the probability of mooring line failure is kept below a predefined acceptable level. The failure probability (corresponding to a given reference duration) for mooring line k is expressed in terms of the so-called δ-index as

$$p_{f,k} = \Phi(-\delta_k) \tag{P3.7}$$

where the index is defined in terms of the mooring line force as

$$\delta_k(t) = \frac{T_{b,k} - \varkappa_k \sigma_k - T_k(r_k(t))}{\sigma_{b,k}}, \quad k = 1, \ldots, q. \tag{P3.8}$$

where $T_{b,k}$ is the mean breaking strength, σ_k is the standard deviation of the time varying mooring line force (including high frequencies), $\varkappa_k$ is a scaling factor, $T_k(r_k(t))$ is the low frequency part of the mooring line force, and $\sigma_{b,k}$ is the standard deviation of the mean breaking strength. Notice that even though high frequencies of the force are included in the computation of σ_k, σ_k will be a slowly varying measure of the sea state, and will not excite wave frequency motion in the vessel. We select a lower bound for δ_k, denoted δ_s that defines the critical value of the reliability index. The condition $\delta_k < \delta_s$ thus represents a situation where the probability of line failure is intolerably high.

P3.3 Controller Design

The controller objectives are: 1) Ensure structural integrity of the mooring; 2) Regulate the heading to a preset desired heading, and; 3) Employ motion damping by limiting velocities in all three degrees of freedom.

In addition to measuring the mooring line forces, which enables computation of the reliability index, we assume that both $\boldsymbol{\eta}$ and $\boldsymbol{\nu}$ are measured. Thus, only the slowly varying bias term $\mathbf{b}$ in (P3.1) remains unknown. To compensate for these forces, an observer is constructed.

Observer

We implement the following observer to estimate the unknown disturbance vector $\mathbf{b}$, Krstić et al. (1995).

$$\dot{\hat{\boldsymbol{\nu}}} = -\mathbf{M}^{-1}\mathbf{D}\boldsymbol{\nu} - \mathbf{M}^{-1}\mathbf{g}(\boldsymbol{\eta}) + \mathbf{M}^{-1}\boldsymbol{\tau} + \mathbf{M}^{-1}\mathbf{J}^{T}(\psi)\hat{\mathbf{b}} - \mathbf{A}_m\tilde{\boldsymbol{\nu}}, \tag{P3.9}$$

where

$$\tilde{\boldsymbol{\nu}} = \boldsymbol{\nu} - \hat{\boldsymbol{\nu}}, \tag{P3.10}$$

and

$$\mathbf{A}_m = \mathbf{A}_0 - \lambda\mathbf{M}^{-T}\mathbf{M}^{-1}\mathbf{P}, \tag{P3.11}$$

where $\lambda > 0$ and $\mathbf{A}_0 \in \mathbb{R}^{3x3}$ is a Hurwitz matrix satisfying

$$\mathbf{P}\mathbf{A}_0 + \mathbf{A}_0^{T}\mathbf{P} = -\mathbf{I}, \quad \mathbf{P} = \mathbf{P}^{T} > \mathbf{0}. \tag{P3.12}$$

The update law for $\hat{\mathbf{b}}$ is given by

$$\dot{\hat{b}} = \boldsymbol{\Gamma}\mathbf{M}^{-1}\mathbf{P}\tilde{\boldsymbol{\nu}}, \tag{P3.13}$$

where $\boldsymbol{\Gamma} = \boldsymbol{\Gamma}^{T} > \mathbf{0}$. The error dynamics for the observer become

$$\dot{\tilde{\boldsymbol{\nu}}} = \left(\mathbf{A}_0 - \lambda\mathbf{M}^{-T}\mathbf{M}^{-1}\mathbf{P}\right)\tilde{\boldsymbol{\nu}} + \mathbf{M}^{-T}\mathbf{J}^{T}\tilde{\mathbf{b}}, \tag{P3.14}$$

$$\dot{\tilde{b}} = -\boldsymbol{\Gamma}\mathbf{M}^{-1}\mathbf{P}\tilde{\boldsymbol{\nu}}. \tag{P3.15}$$

The following holds for the observer.

Proposition P3.1 *The origin of the observer error dynamics (P3.14)–(P3.15) is globally asymptotically stable (GAS).*

Proof. Consider the Lyapunov function

$$V = \tilde{\mathbf{b}}^{T}\boldsymbol{\Gamma}^{-1}\tilde{\mathbf{b}} + \tilde{\boldsymbol{\nu}}^{T}\mathbf{P}\tilde{\boldsymbol{\nu}}. \tag{P3.16}$$

It's time derivative along solutions of (P3.14)–(P3.15) is

$$\dot{V} = -|\tilde{\boldsymbol{\nu}}|^2 - 2\lambda\left|\mathbf{M}^{-1}\tilde{\boldsymbol{\nu}}\right|^2. \tag{P3.17}$$

Since $\left(\tilde{\boldsymbol{\nu}}, \tilde{\mathbf{b}}\right) = \mathbf{0}$ is the only solution that can stay forever in the set $\left\{\left(\tilde{\boldsymbol{\nu}}, \tilde{\mathbf{b}}\right) : \tilde{\boldsymbol{\nu}} = \mathbf{0}\right\}$, the result now follows from LaSalle's invariance principle.

Adaptive controller

Formally, the controller should render the set

$$\mathcal{A} = \left\{\left(\boldsymbol{\eta}, \boldsymbol{\nu}, \tilde{\boldsymbol{\nu}}, \tilde{\mathbf{b}}\right) : \psi = \psi_s, \delta_j \geq \delta_s, \boldsymbol{\nu} = \tilde{\boldsymbol{\nu}} = \tilde{\mathbf{b}} = \mathbf{0}\right\} \tag{P3.18}$$

asymptotically stable in some sense, which implies heading regulation ($\psi = \psi_s$), mooring system integrity ($\delta_j \geq \delta_s$), and convergence of the estimates $\hat{\boldsymbol{\nu}}$ and $\hat{\mathbf{b}}$ to $\boldsymbol{\nu}$ and $\mathbf{b}$, respectively (j is the index of the most critically loaded mooring line). The following proposition presents our output feedback controller.

Proposition P3.2 *Let γ and κ be strictly positive constants, and $\boldsymbol{\Lambda}$ be a diagonal positive definite matrix. Then, the controller*

$$\boldsymbol{\tau} = \mathbf{M}\boldsymbol{\zeta} + \begin{bmatrix} \frac{T_j'}{\sigma_{b,j}}\bar{\delta}_j\boldsymbol{\vartheta} \\ -(\psi - \psi_s) \end{bmatrix} + (\mathbf{D} + \boldsymbol{\Lambda})\begin{bmatrix} \bar{\delta}_j\gamma\boldsymbol{\vartheta} \\ -\kappa(\psi - \psi_s) \end{bmatrix} - \boldsymbol{\Lambda}\boldsymbol{\nu} - \mathbf{J}^T(\psi)\hat{\mathbf{b}} + \mathbf{g}(\boldsymbol{\eta}), \tag{P3.19}$$

where

$$\bar{\delta}_j = \min\left\{0, \delta_j - \delta_s\right\}, \tag{P3.20}$$

$$\boldsymbol{\zeta} = \begin{bmatrix} \gamma\left(\xi\mathbf{I} + \rho\bar{\delta}_j\mathbf{S}_2\right)\boldsymbol{\vartheta} + \frac{\gamma\bar{\delta}_j}{r_j}\left(\mathbf{I} - \boldsymbol{\vartheta}\boldsymbol{\vartheta}^T\right)\mathbf{w} \\ -\kappa\rho \end{bmatrix}, \tag{P3.21}$$

$$\boldsymbol{\vartheta} = \mathbf{J}_2^T(\psi)\frac{\left(\mathbf{p} - \mathbf{p}_j\right)}{r_j}, \tag{P3.22}$$

$$\xi = \begin{cases} 0, & \delta_j > \delta_s \\ -\frac{T_j'}{\sigma_{b,j}}\boldsymbol{\vartheta}^T\mathbf{w}, & \delta_j \leq \delta_s \end{cases}, \tag{P3.23}$$

$$\mathbf{S}_2 = \begin{bmatrix} 0 & 1 \\ -1 & 0 \end{bmatrix}, \tag{P3.24}$$

*in closed loop with the system (P3.1)–(P3.3) and the observer (P3.9)–(P3.13) renders the set $\mathcal{A}$ globally asymptotically stable (*GAS*).*

Proof. Consider the function

$$V_1 = \frac{1}{2}\bar{\delta}_j^2 + \frac{1}{2}(\psi - \psi_s)^2. \tag{P3.25}$$

Its time derivative along solutions of (P3.1)–(P3.3) is

$$\dot{V}_1 = \bar{\delta}_j\dot{\delta}_j + (\psi - \psi_s)\dot{\psi}. \tag{P3.26}$$

Using (P3.3) and the time derivative of (P3.8), we obtain

$$\dot{V}_1 = -\bar{\delta}_j \frac{T_j'}{\sigma_{b,j}} \boldsymbol{\vartheta}^T \mathbf{w} + (\psi - \psi_s)\rho, \tag{P3.27}$$

where T_j' denotes the derivative of T_j with respect to r_j. Choosing $\mathbf{w}$ and ρ as virtual inputs, defining

$$\boldsymbol{\alpha}_w \triangleq \bar{\delta}_j \gamma \boldsymbol{\vartheta}, \tag{P3.28}$$

$$\alpha_\rho \triangleq -\kappa(\psi - \psi_s), \tag{P3.29}$$

and assuming that T_j' is bounded below by $\varepsilon > 0$, we get

$$\dot{V}_1 \leq -\frac{\gamma\varepsilon}{\sigma_{b,j}}\bar{\delta}_j^2 - \kappa(\psi - \psi_s)^2 - \bar{\delta}_j \frac{T_j'}{\sigma_{b,j}} \boldsymbol{\vartheta}^T (\mathbf{w} - \boldsymbol{\alpha}_w) + (\psi - \psi_s)\left(\rho - \alpha_\rho\right). \tag{P3.30}$$

Defining the change of variables

$$\mathbf{z} = \begin{bmatrix} \mathbf{z}_w \\ z_\rho \end{bmatrix} \triangleq \boldsymbol{\nu} - \boldsymbol{\alpha}, \tag{P3.31}$$

where $\boldsymbol{\alpha} = [\boldsymbol{\alpha}_w^T, \alpha_\rho]^T$, consider now the function

$$V_2 = V_1 + \frac{1}{2}\mathbf{z}^T \mathbf{M} \mathbf{z}. \tag{P3.32}$$

By using (P3.1), we obtain

$$\dot{V}_2 \leq -\frac{\gamma\varepsilon}{\sigma_{b,j}}\bar{\delta}_j^2 - \kappa(\psi - \psi_s)^2 - \mathbf{z}^T \bar{\mathbf{D}} \mathbf{z} + \mathbf{z}^T \left(\boldsymbol{\theta} + \boldsymbol{\tau} + \mathbf{J}^T(\psi)\,\mathbf{b} - \mathbf{D}\boldsymbol{\alpha} - \mathbf{g}(\boldsymbol{\eta}) - \mathbf{M}\dot{\boldsymbol{\alpha}}\right). \tag{P3.33}$$

where

$$\boldsymbol{\theta} = \begin{bmatrix} -\bar{\delta}_j \frac{T_j'}{\sigma_{b,j}} \boldsymbol{\vartheta} \\ \psi - \psi_s \end{bmatrix}. \tag{P3.34}$$

Substituting (P3.19) and the time derivatives of (P3.28)–(P3.29) into (P3.33) gives

$$\dot{V}_2 \leq -\frac{\gamma\varepsilon}{\sigma_{b,j}}\bar{\delta}_j^2 - \kappa(\psi - \psi_s)^2 + \mathbf{z}^T \left(-\left(\bar{\mathbf{D}} + \boldsymbol{\Lambda}\right)\mathbf{z} + \mathbf{J}^T(\psi)\,\tilde{\mathbf{b}}\right). \tag{P3.35}$$

Completing squares, we obtain

$$\dot{V}_2 \leq -\frac{\gamma\varepsilon}{\sigma_{b,j}}\bar{\delta}_j^2 - \kappa(\psi - \psi_s)^2 - \frac{1}{2}\mathbf{z}^T \left(\bar{\mathbf{D}} + \boldsymbol{\Lambda}\right)\mathbf{z} + \frac{1}{2\lambda_{\min}}\left|\tilde{\mathbf{b}}\right|^2, \tag{P3.36}$$

where $\lambda_{\min}$ is the smallest eigenvalue of the positive definite matrix $\left(\bar{\mathbf{D}} + \mathbf{\Lambda}\right)$. Defining the set,

$$\mathcal{B} = \left\{(\boldsymbol{\eta}, \boldsymbol{\nu}) : \mathbf{z} = \mathbf{0}, \psi = \psi_s, \delta_j \geq \delta_s\right\}, \tag{P3.37}$$

and the generic norm

$$\left|(\boldsymbol{\eta}, \boldsymbol{\nu})\right|_{\mathcal{B}} = \left(\bar{\delta}_j^2 + (\psi - \psi_s)^2 + \mathbf{z}^T \mathbf{M} \mathbf{z}\right)^{1/2}, \tag{P3.38}$$

we have that

$$V_2 = \frac{1}{2} \left|(\boldsymbol{\eta}, \boldsymbol{\nu})\right|_{\mathcal{B}}^2, \tag{P3.39}$$

and

$$\dot{V}_2 < -c_1 \left|(\boldsymbol{\eta}, \boldsymbol{\nu})\right|_{\mathcal{B}}^2 + c_2^2 |\tilde{\mathbf{b}}|^2, \tag{P3.40}$$

for some strictly positive constants c_1 and c_2. It follows that $\mathcal{B}$ is GES (Teel (2002)) when $\mathbf{b}$ is known ($\tilde{\mathbf{b}} \equiv \mathbf{0}$). Suppose $(\boldsymbol{\eta}, \boldsymbol{\nu}) \in \mathcal{B}$. Then from (P3.28)–(P3.29), $\boldsymbol{\alpha} = 0$, so from (P3.31), $\boldsymbol{\nu} = 0$. Thus, $(\boldsymbol{\eta}, \boldsymbol{\nu}) \in \mathcal{A}$, so $\mathcal{B} \subset \mathcal{A}$, and $\mathcal{A}$ is GES. For $\mathbf{b}$ unknown, (P3.40) gives

$$\dot{V}_2 \leq -\frac{c_1}{2} \left|(\boldsymbol{\eta}, \boldsymbol{\nu})\right|_{\mathcal{B}}^2 \ \forall \ \left|(\boldsymbol{\eta}, \boldsymbol{\nu})\right|_{\mathcal{B}} \geq \left(\frac{2c_2}{c_1}\right)^{1/2} |\tilde{\mathbf{b}}|, \tag{P3.41}$$

so by Theorem 4.19 in Khalil (2002) the dynamics of the controlled surface vessel is input-to-state stable (with respect to $\mathcal{A}$), with input $\tilde{b}$. Since the ISS dynamics of the controlled surface vessel and the observer error dynamics, which origin is GAS by Proposition 1, form a cascade, the result follows from Lemma 4.7 in Khalil (2002).

P3.4 Experimental Tests

The experimental tests were performed in the Marine Cybernetics Laboratory (MCLab) at NTNU. MCLab is a 6.45 by 40 meter test basin specifically designed for testing control strategies for marine vessels. It contains a wave generator and a movable control bridge. The vessel used is the *CyberShip III (CS3)*, shown in Figure P3.2. CS3 is a scale model of an offshore supply vessel, and is equipped with 4 thrusters. The main characteristics of the CS3, along with those of the full scale supply vessel, are shown in Table P3.1. The vessel is equipped with five illuminated balls. The lightballs are detected by four cameras and the information is processed to yield position and velocity measurements for the vessel.

In the experimental setup, we moored CS3 from the bow to the basin with one mooring cable. In order to simulate the slowly varying environmental

forces, we tied a cord to the aft of the vessel and used weights to drag it backwards. The increase in the weights were introduced instantly, representing a step in the environmental loads. Although this does not represent a realistic transition between two environmental loading conditions, but rather an extreme case, it provides information about the performance of the controller.

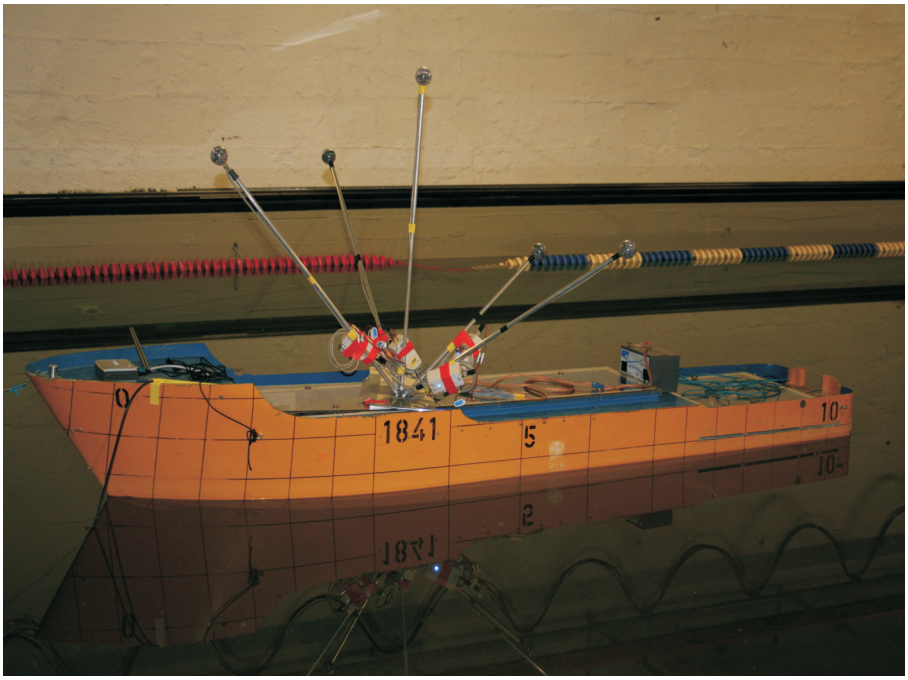

Figure P3.2: Cybership III (CS3).

Experimental results

Two different scenarios were tested in order to evaluate the controller. For the the scenarios, we applied the same weight to the aft of the vessel, and the controller parameters were not changed. The varying parameter was the significant wave height, H_s, with $H_s = 0$ [m] for scenario 1 and $H_s = 0.06$ [m] for scenario 2. The scaling factor between model waves and full scale waves is 30, so the model waves corresponds to $H_s = 0$ [m] and 1.8[m] for the full scale vessel. The initial heading was about 0 [deg].

Table P3.1: Main characteristics of CS3.

	Model	Full Scale
Length over all	2.275 $[m]$	68.28 $[m]$
Length between particulars	1.971 $[m]$	59.13 $[m]$
Breadth	0.437 $[m]$	13.11 $[m]$
Draught	0.153 $[m]$	4.59 $[m]$
Weight	74.2 $[kg]$	$2.3 * 10^6$ $[kg]$
Azimuth thrusters(3)	27 $[W]$	1200 $[kW]$
Tunnel thruster	27 $[W]$	410 $[kW]$

Scenario 1

Scenario 1 is the basic one, with no waves, and the environmental load applied at $t = 2.3$ $[min]$. The controller was turned on at $t = 0$ $[min]$. As seen from Figure P3.3, where the desired and measured levels are shown in dashed lines and solid lines, respectively, the heading quickly regulates to the setpoint $\psi_s = 10$ $[deg]$ when the controller is turned on. The δ-index is slightly affected by the change of heading. When the environmental load is applied, the δ-index starts decreasing, indicating that the vessel is moving. The movement initiates motion damping, as shown by the increase in thruster usage in Figure P3.4. The figures clearly show that the controller acts to prevent the δ-index from going below the critical level $\delta_s = 4$. At $t = 4.3$ $[min]$, the environmental load is removed, and the δ-index increases while the thruster usage decreases.

Scenario 2

The controller is turned on at $t = 0$ $[min]$ in this case, while the environmental load is applied at $t = 1.8$ $[min]$. The drop in δ-index, see Figure P3.5 within the first minute is partly due to vessel movement as a result of heading regulation, but also caused by the fact that the ship was not at rest when at the beginning of the experiment, due to the incoming waves. The thruster usage, shown in Figure P3.6 has more variations than for scenario 1, due to the increased sea state. The main features of the controller remains evident in higher sea states, as heading regulates to the desired heading, and the δ-index stays above its critical value.

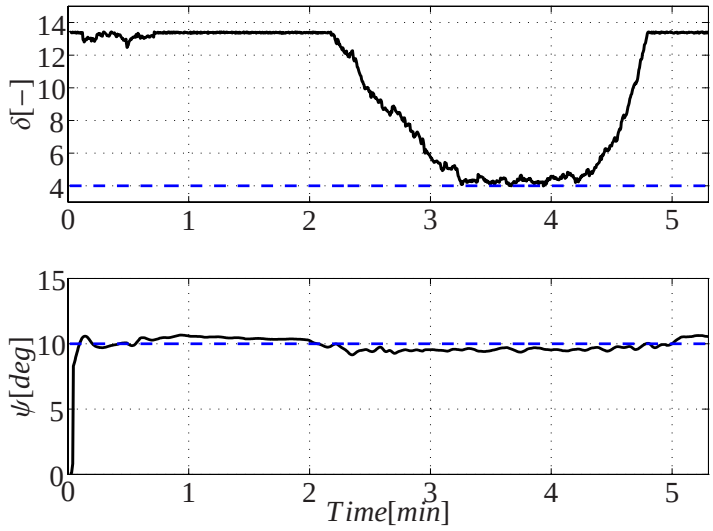

Figure P3.3: Time variation of δ and ψ for scenario 1.

P3.5 Conclusions

We have presented a conceptually new controller for thruster assisted positioning of moored vessels. By using a structural reliability measure for the mooring lines, the controller protects the mooring system whenever needed as a result of severe weather conditions and high environmental loads. In particular, we avoid the excessive use of thrusters caused by conservatively defined safety regions in conventional PM systems, giving a more fuel optimal operation. The feasibility of our controller has been successfully verified in laboratory experiments. Further work includes automatic heading control in order to minimize drag (the current solution applies heading regulation to a fixed setpoint), and adaptation of potentially unknown vessel parameters.

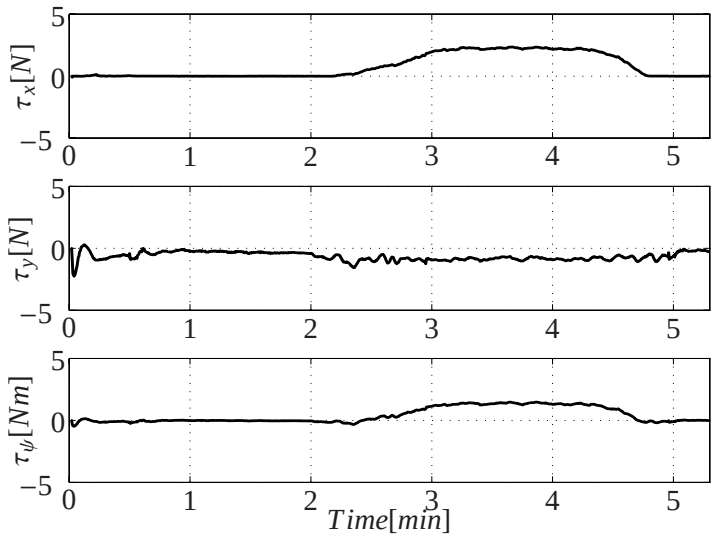

Figure P3.4: Time variation of thruster force for scenario 1.

Bibliography

Aamo, O. M. and Fossen, T. I. (1999). Controlling line tension in thruster assisted mooring systems, *Proceedings of the IEEE International Conference on Control Applications, Hawaii, US*. **2:**1104–1009

Berntsen, P., Aamo, O. and Leira, B. (2006). Position mooring based on structural reliability, *Proceedings of the 7th Conference on Manoeuvring and Control of Marine Craft Lisbon, Portugal*.

Berntsen, P.I.B., Aamo, O.M. and Leira, B.J. (2007). Structural reliability–based control of moored interconnected structures, *Control Engineering Practice* **16(4):**495–504.

Berntsen, P., Aamo, O. and Leira, B. (2004). Structural reliability criteria for control of large-scale interconnected marine structures, *Proceedings of the 23rd International Conference on Offshore Mechanics and Arctic Engi–neering, Vancouver, Canada*.

Faltinsen, O. (1990). *Sea Loads on Ships and Offshore Structures*. Cambridge University Press, Cambridge, UK.

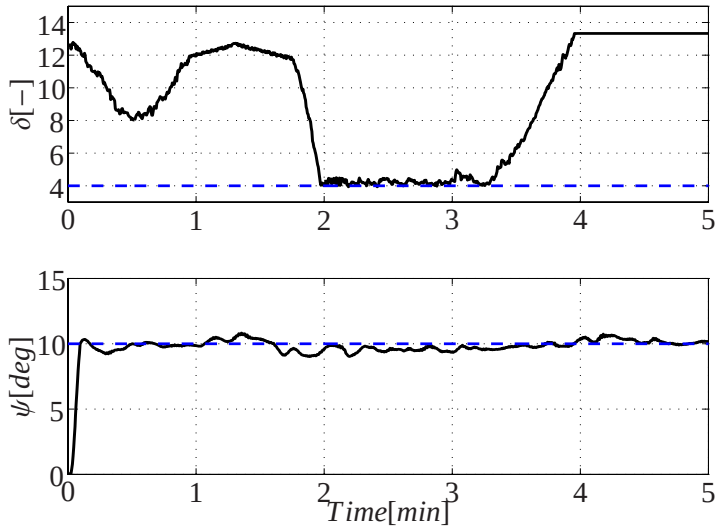

Figure P3.5: Time variation of δ and ψ for scenario 2.

Fossen, T. I. (2002). *Marine Control Systems*. Marine Cybernetics, Trond–heim, Norway.

Fossen, T. and Grøvlen Å. (1998). Nonlinear output feedback control of dynamically positioned ships using vectorial observer backstepping, *IEEE Transactions on Control Systems Technology* **6(1)**:121–128.

Khalil, H. K. (2002). Nonlinear Systems, 3rd ed., *Prentice Hall, New Jersey, US*.

Krstić, M., Kanellakopoulos, I. and Kokotović, P. (1995). *Nonlinear and Adaptive Control Design*, John Wiley and Sons, Inc, New York, US.

Nguyen, T. D. and Sørensen, A. J. (2007). Setpoint chasing for thruster-assisted position mooring, *Proceedings of the 26th International Conference on Offshore Mechanics and Arctic Engineering, San Diego, California, US*.

Nguyen, T. D., Sørensen, A. J. and Quek, S. T. (2007). Design of hybrid controller for dynamic positioning from calm to extreme sea conditions, *Automatica* **43:**768–785.

Sørensen, A. J. (2005). Structural issues in the design and operation of

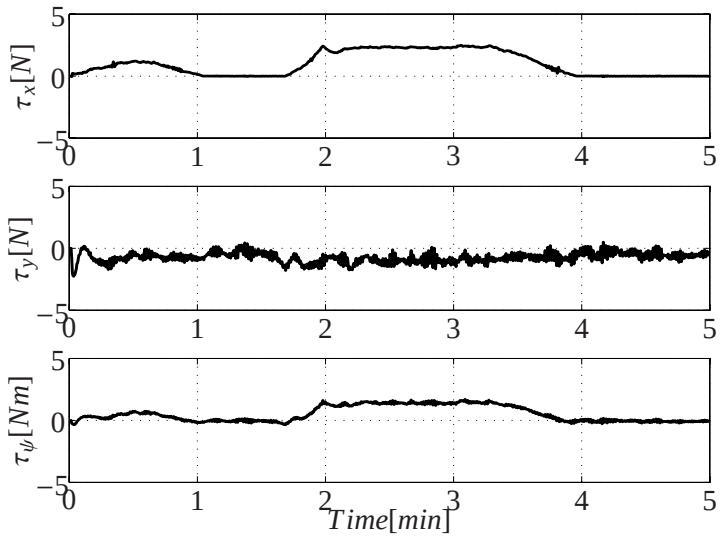

Figure P3.6: Time variation of thruster force for scenario 2.

marine control systems, *Annual Reviews in Control* **29:**125–149.

Sørensen, A., Sagatun, S. and Fossen, T. (1996). Design of a dynamic po–sitioning system using model-based control, *Control Engineering Practice* **4(3)**:359–368.

Strand, J. (1999). *Nonlinear Position Control Systems Design for Marine Ves–sels*.PhD thesis, Norwegian University of Science and Technology, Trond–heim, Norway.

Strand, J. and Fossen, T. (1999). Passive nonlinear observer design for ships using Lyapunov methods: full-scale experiments with a supply vessel, *Automatica* **35(1)**:3–16.

Strand, J., Sørensen, A. and Fossen, T. (1997). Modelling and control of thruster assisted position mooring systems for ships, *Proceedings of the 4th Conference on Manouvering and Control of Marine Craft, Brijuni, Croa–tia*, pp. 160–165.

Teel, A.R. (2002), *Notes on nonlinear control and analysis*, Lecture Notes, UCSB, Santa Barbara, California, US.

R A P P O R T E R
UTGITT VED
INSTITUTT FOR MARIN TEKNIKK
(tidligere: FAKULTET FOR MARIN TEKNIKK)
NORGES TEKNISK-NATURVITENSKAPELIGE UNIVERSITET

UR-79-01 Brigt Hatlestad, MK:	The finite element method used in a fatigue evaluation of fixed offshore platforms. (Dr.Ing. Thesis)
UR-79-02 Erik Pettersen, MK:	Analysis and design of cellular structures. (Dr.Ing. Thesis)
UR-79-03 Sverre Valsgård, MK:	Finite difference and finite element methods applied to nonlinear analysis of plated structures. (Dr.Ing. Thesis)
UR-79-04 Nils T. Nordsve, MK:	Finite element collapse analysis of structural members considering imperfections and stresses due to fabrication. (Dr.Ing. Thesis)
UR-79-05 Ivar J. Fylling, MK:	Analysis of towline forces in ocean towing systems. (Dr.Ing. Thesis)
UR-80-06 Nils Sandsmark, MM:	Analysis of Stationary and Transient Heat Conduction by the Use of the Finite Element Method. (Dr.Ing. Thesis)
UR-80-09 Sverre Haver, MK:	Analysis of uncertainties related to the stochastic modelling of ocean waves. (Dr.Ing. Thesis)
UR-85-46 Alf G. Engseth, MK:	Finite element collapse analysis of tubular steel offshore structures. (Dr.Ing. Thesis)
UR-86-47 Dengody Sheshappa, MP:	A Computer Design Model for Optimizing Fishing Vessel Designs Based on Techno-Economic Analysis. (Dr.Ing. Thesis)
UR-86-48 Vidar Aanesland, MH:	A Theoretical and Numerical Study of Ship Wave Resistance. (Dr.Ing. Thesis)
UR-86-49 Heinz-Joachim Wessel, MK:	Fracture Mechanics Analysis of Crack Growth in Plate Girders. (Dr.Ing. Thesis)
UR-86-50 Jon Taby, MK:	Ultimate and Post-ultimate Strength of Dented Tubular Members. (Dr.Ing. Thesis)
UR-86-51 Walter Lian, MH:	A Numerical Study of Two-Dimensional Separated Flow Past Bluff Bodies at Moderate KC-Numbers. (Dr.Ing. Thesis)
UR-86-52 Bjørn Sortland, MH:	Force Measurements in Oscillating Flow on Ship Sections and Circular Cylinders in a U-Tube Water Tank. (Dr.Ing. Thesis)
UR-86-53 Kurt Strand, MM:	A System Dynamic Approach to One-dimensional Fluid Flow. (Dr.Ing. Thesis)

UR-86-54 Arne Edvin Løken, MH: Three Dimensional Second Order Hydrodynamic Effects on Ocean Structures in Waves. (Dr.Ing. Thesis)

UR-86-55 Sigurd Falch, MH: A Numerical Study of Slamming of Two-Dimensional Bodies. (Dr.Ing. Thesis)

UR-87-56 Arne Braathen, MH: Application of a Vortex Tracking Method to the Prediction of Roll Damping of a Two-Dimension Floating Body. (Dr.Ing. Thesis)

UR-87-57 Bernt Leira, MR: Gaussian Vector Processes for Reliability Analysis involving Wave-Induced Load Effects. (Dr.Ing. Thesis)

UR-87-58 Magnus Småvik, MM: Thermal Load and Process Characteristics in a Two-Stroke Diesel Engine with Thermal Barriers (in Norwegian). (Dr.Ing. Thesis)

MTA-88-59 Bernt Arild Bremdal, MP: An Investigation of Marine Installation Processes - A Knowledge - Based Planning Approach. (Dr.Ing. Thesis)

MTA-88-60 Xu Jun, MK: Non-linear Dynamic Analysis of Space-framed Offshore Structures. (Dr.Ing. Thesis)

MTA-89-61 Gang Miao, MH: Hydrodynamic Forces and Dynamic Responses of Circular Cylinders in Wave Zones. (Dr.Ing. Thesis)

MTA-89-62 Martin Greenhow, MH: Linear and Non-Linear Studies of Waves and Floating Bodies. Part I and Part II. (Dr.Techn. Thesis)

MTA-89-63 Chang Li, MH: Force Coefficients of Spheres and Cubes in Oscillatory Flow with and without Current. (Dr.Ing. Thesis)

MTA-89-64 Hu Ying, MP: A Study of Marketing and Design in Development of Marine Transport Systems. (Dr.Ing. Thesis)

MTA-89-65 Arild Jæger, MH: Seakeeping, Dynamic Stability and Performance of a Wedge Shaped Planing Hull. (Dr.Ing. Thesis)

MTA-89-66 Chan Siu Hung, MM: The dynamic characteristics of tilting-pad bearings.

MTA-89-67 Kim Wikstrøm, MP: Analysis av projekteringen for ett offshore projekt. (Licenciat-avhandling)

MTA-89-68 Jiao Guoyang, MR: Reliability Analysis of Crack Growth under Random Loading, considering Model Updating. (Dr.Ing. Thesis)

MTA-89-69 Arnt Olufsen, MK: Uncertainty and Reliability Analysis of Fixed Offshore Structures. (Dr.Ing. Thesis)

MTA-89-70 Wu Yu-Lin, MR: System Reliability Analyses of Offshore Structures using improved Truss and Beam Models. (Dr.Ing. Thesis)

MTA-90-71 Jan Roger Hoff, MH: Three-dimensional Green function of a vessel with forward speed in waves. (Dr.Ing. Thesis)

MTA-90-72 Rong Zhao, MH: Slow-Drift Motions of a Moored Two-Dimensional Body in Irregular Waves. (Dr.Ing. Thesis)

MTA-90-73 Atle Minsaas, MP: Economical Risk Analysis. (Dr.Ing. Thesis)

MTA-90-74 Knut-Aril Farnes, MK: Long-term Statistics of Response in Non-linear Marine Structures. (Dr.Ing. Thesis)

MTA-90-75 Torbjørn Sotberg, MK: Application of Reliability Methods for Safety Assessment of Submarine Pipelines. (Dr.Ing. Thesis)

MTA-90-76 Zeuthen, Steffen, MP: SEAMAID. A computational model of the design process in a constraint-based logic programming environment. An example from the offshore domain. (Dr.Ing. Thesis)

MTA-91-77 Haagensen, Sven, MM: Fuel Dependant Cyclic Variability in a Spark Ignition Engine - An Optical Approach. (Dr.Ing. Thesis)

MTA-91-78 Løland, Geir, MH: Current forces on and flow through fish farms. (Dr.Ing. Thesis)

MTA-91-79 Hoen, Christopher, MK: System Identification of Structures Excited by Stochastic Load Processes. (Dr.Ing. Thesis)

MTA-91-80 Haugen, Stein, MK: Probabilistic Evaluation of Frequency of Collision between Ships and Offshore Platforms. (Dr.Ing. Thesis)

MTA-91-81 Sødahl, Nils, MK: Methods for Design and Analysis of Flexible Risers. (Dr.Ing. Thesis)

MTA-91-82 Ormberg, Harald, MK: Non-linear Response Analysis of Floating Fish Farm Systems. (Dr.Ing. Thesis)

MTA-91-83 Marley, Mark J., MK: Time Variant Reliability under Fatigue Degradation. (Dr.Ing. Thesis)

MTA-91-84 Krokstad, Jørgen R., MH: Second-order Loads in Multidirectional Seas. (Dr.Ing. Thesis)

MTA-91-85 Molteberg, Gunnar A., MM: The Application of System Identification Techniques to Performance Monitoring of Four Stroke Turbocharged Diesel Engines. (Dr.Ing. Thesis)

MTA-92-86 Mørch, Hans Jørgen Bjelke, MH: Aspects of Hydrofoil Design: with Emphasis on Hydrofoil Interaction in Calm Water. (Dr.Ing. Thesis)

MTA-92-87 Chan Siu Hung, MM: Nonlinear Analysis of Rotordynamic Instabilities in High-speed Turbomachinery. (Dr.Ing. Thesis)

MTA-92-88 Bessason, Bjarni, MK: Assessment of Earthquake Loading and Response of Seismically Isolated Bridges. (Dr.Ing. Thesis)

MTA-92-89 Langli, Geir, MP: Improving Operational Safety through exploitation of Design Knowledge - an investigation of offshore platform safety. (Dr.Ing. Thesis)

MTA-92-90 Sævik, Svein, MK: On Stresses and Fatigue in Flexible Pipes. (Dr.Ing. Thesis)

MTA-92-91 Ask, Tor Ø., MM: Ignition and Flame Growth in Lean Gas-Air Mixtures. An Experimental Study with a Schlieren System. (Dr.Ing. Thesis)

MTA-86-92 Hessen, Gunnar, MK: Fracture Mechanics Analysis of Stiffened Tubular Members. (Dr.Ing. Thesis)

MTA-93-93 Steinebach, Christian, MM: Knowledge Based Systems for Diagnosis of Rotating Machinery. (Dr.Ing. Thesis)

MTA-93-94 Dalane, Jan Inge, MK: System Reliability in Design and Maintenance of Fixed Offshore Structures. (Dr.Ing. Thesis)

MTA-93-95 Steen, Sverre, MH: Cobblestone Effect on SES. (Dr.Ing. Thesis)

MTA-93-96 Karunakaran, Daniel, MK: Nonlinear Dynamic Response and Reliability Analysis of Drag-dominated Offshore Platforms. (Dr.Ing. Thesis)

MTA-93-97 Hagen, Arnulf, MP: The Framework of a Design Process Language. (Dr.Ing. Thesis)

MTA-93-98 Nordrik, Rune, MM: Investigation of Spark Ignition and Autoignition in Methane and Air Using Computational Fluid Dynamics and Chemical Reaction Kinetics. A Numerical Study of Ignition Processes in Internal Combustion Engines. (Dr.Ing. Thesis)

MTA-94-99 Passano, Elizabeth, MK: Efficient Analysis of Nonlinear Slender Marine Structures. (Dr.Ing. Thesis)

MTA-94-100 Kvålsvold, Jan, MH: Hydroelastic Modelling of Wetdeck Slamming on Multihull Vessels. (Dr.Ing. Thesis)

MTA-94-102 Bech, Sidsel M., MK: Experimental and Numerical Determination of Stiffness and Strength of GRP/PVC Sandwich Structures. (Dr.Ing. Thesis)

MTA-95-103 Paulsen, Hallvard, MM: A Study of Transient Jet and Spray using a Schlieren Method and Digital Image Processing. (Dr.Ing. Thesis)

MTA-95-104 Hovde, Geir Olav, MK: Fatigue and Overload Reliability of Offshore Structural Systems, Considering the Effect of Inspection and Repair. (Dr.Ing. Thesis)

MTA-95-105 Wang, Xiaozhi, MK: Reliability Analysis of Production Ships with Emphasis on Load Combination and Ultimate Strength. (Dr.Ing. Thesis)

MTA-95-106 Ulstein, Tore, MH: Nonlinear Effects of a Flexible Stern Seal Bag on Cobblestone Oscillations of an SES. (Dr.Ing. Thesis)

MTA-95-107 Solaas, Frøydis, MH: Analytical and Numerical Studies of Sloshing in Tanks. (Dr.Ing. Thesis)

MTA-95-108 Hellan, øyvind, MK: Nonlinear Pushover and Cyclic Analyses in Ultimate Limit State Design and Reassessment of Tubular Steel Offshore Structures. (Dr.Ing. Thesis)

MTA-95-109 Hermundstad, Ole A., MK: Theoretical and Experimental Hydroelastic Analysis of High Speed Vessels. (Dr.Ing. Thesis)

MTA-96-110 Bratland, Anne K., MH: Wave-Current Interaction Effects on Large-Volume Bodies in Water of Finite Depth. (Dr.Ing. Thesis)

MTA-96-111 Herfjord, Kjell, MH: A Study of Two-dimensional Separated Flow by a Combination of the Finite Element Method and Navier-Stokes Equations. (Dr.Ing. Thesis)

MTA-96-112 Æsøy, Vilmar, MM: Hot Surface Assisted Compression Ignition in a Direct Injection Natural Gas Engine. (Dr.Ing. Thesis)

MTA-96-113 Eknes, Monika L., MK: Escalation Scenarios Initiated by Gas Explosions on Offshore Installations. (Dr.Ing. Thesis)

MTA-96-114 Erikstad, Stein O., MP: A Decision Support Model for Preliminary Ship Design. (Dr.Ing. Thesis)

MTA-96-115 Pedersen, Egil, MH: A Nautical Study of Towed Marine Seismic Streamer Cable Configurations. (Dr.Ing. Thesis)

MTA-97-116 Moksnes, Paul O., MM: Modelling Two-Phase Thermo-Fluid Systems Using Bond Graphs. (Dr.Ing. Thesis)

MTA-97-117 Halse, Karl H., MK: On Vortex Shedding and Prediction of Vortex-Induced Vibrations of Circular Cylinders. (Dr.Ing. Thesis)

MTA-97-118 Igland, Ragnar T., MK: Reliability Analysis of Pipelines during Laying, considering Ultimate Strength under Combined Loads. (Dr.Ing. Thesis)

MTA-97-119 Pedersen, Hans-P., MP: Levendefiskteknologi for fiskefartøy. (Dr.Ing. Thesis)

MTA-98-120 Vikestad, Kyrre, MK: Multi-Frequency Response of a Cylinder Subjected to Vortex Shedding and Support Motions. (Dr.Ing. Thesis)

MTA-98-121 Azadi, Mohammad R. E., MK: Analysis of Static and Dynamic Pile-Soil-Jacket Behaviour. (Dr.Ing. Thesis)

MTA-98-122 Ulltang, Terje, MP: A Communication Model for Product Information. (Dr.Ing. Thesis)

MTA-98-123 Torbergsen, Erik, MM: Impeller/Diffuser Interaction Forces in Centrifugal Pumps. (Dr.Ing. Thesis)

MTA-98-124 Hansen, Edmond, MH: A Discrete Element Model to Study Marginal Ice Zone Dynamics and the Behaviour of Vessels Moored in Broken Ice. (Dr.Ing. Thesis)

MTA-98-125 Videiro, Paulo M., MK: Reliability Based Design of Marine Structures. (Dr.Ing. Thesis)

MTA-99-126 Mainçon, Philippe, MK: Fatigue Reliability of Long Welds Application to Titanium Risers. (Dr.Ing. Thesis)

MTA-99-127 Haugen, Elin M., MH: Hydroelastic Analysis of Slamming on Stiffened Plates with Application to Catamaran Wetdecks. (Dr.Ing. Thesis)

MTA-99-128 Langhelle, Nina K., MK: Experimental Validation and Calibration of Nonlinear Finite Element Models for Use in Design of Aluminium Structures Exposed to Fire. (Dr.Ing. Thesis)

MTA-99-129 Berstad, Are J., MK: Calculation of Fatigue Damage in Ship Structures. (Dr.Ing. Thesis)

MTA-99-130 Andersen, Trond M., MM: Short Term Maintenance Planning. (Dr.Ing. Thesis)

MTA-99-131 Tveiten, Bård Wathne, MK: Fatigue Assessment of Welded Aluminium Ship Details. (Dr.Ing. Thesis)

MTA-99-132 Søreide, Fredrik, MP: Applications of underwater technology in deep water archaeology. Principles and practice. (Dr.Ing. Thesis)

MTA-99-133 Tønnessen, Rune, MH: A Finite Element Method Applied to Unsteady Viscous Flow Around 2D Blunt Bodies With Sharp Corners. (Dr.Ing. Thesis)

MTA-99-134 Elvekrok, Dag R., MP: Engineering Integration in Field Development Projects in the Norwegian Oil and Gas Industry. The Supplier Management of Norne. (Dr.Ing. Thesis)

MTA-99-135 Fagerholt, Kjetil, MP: Optimeringsbaserte Metoder for Ruteplanlegging innen skipsfart. (Dr.Ing. Thesis)

MTA-99-136 Bysveen, Marie, MM: Visualization in Two Directions on a Dynamic Combustion Rig for Studies of Fuel Quality. (Dr.Ing. Thesis)

MTA-2000-137 Storteig, Eskild, MM: Dynamic characteristics and leakage performance of liquid annular seals in centrifugal pumps. (Dr.Ing. Thesis)

MTA-2000-138 Sagli, Gro, MK: Model uncertainty and simplified estimates of long term extremes of hull girder loads in ships. (Dr.Ing. Thesis)

MTA-2000-139 Tronstad, Harald, MK: Nonlinear analysis and design of cable net structures like fishing gear based on the finite element method. (Dr.Ing. Thesis)

MTA-2000-140 Kroneberg, André, MP: Innovation in shipping by using scenarios. (Dr.Ing. Thesis)

MTA-2000-141 Haslum, Herbjørn Alf, MH: Simplified methods applied to nonlinear motion of spar platforms. (Dr.Ing. Thesis)

MTA-2001-142 Samdal, Ole Johan, MM: Modelling of Degradation Mechanisms and Stressor Interaction on Static Mechanical Equipment Residual Lifetime. (Dr.Ing. Thesis)

MTA-2001-143 Baarholm, Rolf Jarle, MH: Theoretical and experimental studies of wave impact underneath decks of offshore platforms. (Dr.Ing. Thesis)

MTA-2001-144 Wang, Lihua, MK: Probabilistic Analysis of Nonlinear Wave-induced Loads on Ships. (Dr.Ing. Thesis)

MTA-2001-145 Kristensen, Odd H. Holt, MK: Ultimate Capacity of Aluminium Plates under Multiple Loads, Considering HAZ Properties. (Dr.Ing. Thesis)

MTA-2001-146 Greco, Marilena, MH: A Two-Dimensional Study of Green-Water Loading. (Dr.Ing. Thesis)

MTA-2001-147 Heggelund, Svein E., MK: Calculation of Global Design Loads and Load Effects in Large High Speed Catamarans. (Dr.Ing. Thesis)

MTA-2001-148 Babalola, Olusegun T., MK: Fatigue Strength of Titanium Risers - Defect Sensitivity. (Dr.Ing. Thesis)

MTA-2001-149 Mohammed, Abuu K., MK: Nonlinear Shell Finite Elements for Ultimate Strength and Collapse Analysis of Ship Structures. (Dr.Ing. Thesis)

MTA-2002-150 Holmedal, Lars E., MH: Wave-current interactions in the vicinity of the sea bed. (Dr.Ing. Thesis)

MTA-2002-151 Rognebakke, Olav F., MH: Sloshing in rectangular tanks and interaction with ship motions. (Dr.Ing. Thesis)

MTA-2002-152 Lader, Pål Furset, MH: Geometry and Kinematics of Breaking Waves. (Dr.Ing. Thesis)

MTA-2002-153 Yang, Qinzheng, MH: Wash and wave resistance of ships in finite water depth. (Dr.Ing. Thesis)

MTA-2002-154 Melhus, Øyvin, MM: Utilization of VOC in Diesel Engines. Ignition and combustion of VOC released by crude oil tankers. (Dr.Ing. Thesis)

MTA-2002-155 Ronæss, Marit, MH: Wave Induced Motions of Two Ships Advancing on Parallel Course. (Dr.Ing. Thesis)

MTA-2002-156 Økland, Ole D., MK: Numerical and experimental investigation of whipping in twin hull vessels exposed to severe wet deck slamming. (Dr.Ing. Thesis)

MTA-2002-157 Ge, Chunhua, MK: Global Hydroelastic Response of Catamarans due to Wet Deck Slamming. (Dr.Ing. Thesis)

MTA-2002-158 Byklum, Eirik, MK: Nonlinear Shell Finite Elements for Ultimate Strength and Collapse Analysis of Ship Structures. (Dr.Ing. Thesis)

IMT-2003-1 Chen, Haibo, MK: Probabilistic Evaluation of FPSO-Tanker Collision in Tandem Offloading Operation. (Dr.Ing. Thesis)

IMT-2003-2 Skaugset, Kjetil Bjørn, MK: On the Suppression of Vortex Induced Vibrations of Circular Cylinders by Radial Water Jets. (Dr.Ing. Thesis)

IMT-2003-3 Chezhian, Muthu Three-Dimensional Analysis of Slamming. (Dr.Ing. Thesis)

IMT-2003-4 Buhaug, Øyvind Deposit Formation on Cylinder Liner Surfaces in Medium Speed Engines. (Dr.Ing. Thesis)

IMT-2003-5 Tregde, Vidar	Aspects of Ship Design: Optimization of Aft Hull with Inverse Geometry Design. (Dr.Ing. Thesis)
IMT-2003-6 Wist, Hanne Therese	Statistical Properties of Successive Ocean Wave Parameters. (Dr.Ing. Thesis)
IMT-2004-7 Ransau, Samuel	Numerical Methods for Flows with Evolving Interfaces. (Dr.Ing. Thesis)
IMT-2004-8 Soma, Torkel	Blue-Chip or Sub-Standard. A data interrogation approach of identity safety characteristics of shipping organization. (Dr.Ing. Thesis)
IMT-2004-9 Ersdal, Svein	An experimental study of hydrodynamic forces on cylinders and cables in near axial flow. (Dr.Ing. Thesis)
IMT-2005-10 Brodtkorb, Per Andreas	The Probability of Occurrence of Dangerous Wave Situations at Sea. (Dr.Ing. Thesis)
IMT-2005-11 Yttervik, Rune	Ocean current variability in relation to offshore engineering. (Dr.Ing. Thesis)
IMT-2005-12 Fredheim, Arne	Current Forces on Net-Structures. (Dr.Ing. Thesis)
IMT-2005-13 Heggernes, Kjetil	Flow around marine structures. (Dr.Ing. Thesis)
IMT-2005-14 Fouques, Sebastien	Lagrangian Modelling of Ocean Surface Waves and Synthetic Aperture Radar Wave Measurements. (Dr.Ing. Thesis)
IMT-2006-15 Holm, Håvard	Numerical calculation of viscous free surface flow around marine structures. (Dr.Ing. Thesis)
IMT-2006-16 Bjørheim, Lars G.	Failure Assessment of Long Through Thickness Fatigue Cracks in Ship Hulls. (Dr.Ing. Thesis)
IMT-2006-17 Hansson, Lisbeth	Safety Management for Prevention of Occupational Accidents. (Dr.Ing. Thesis)
IMT-2006-18 Zhu, Xinying	Application of the CIP Method to Strongly Nonlinear Wave-Body Interaction Problems. (Dr.Ing. Thesis)
IMT-2006-19 Reite, Karl Johan	Modelling and Control of Trawl Systems. (Dr.Ing. Thesis)
IMT-2006-20 Smogeli, Øyvind Notland	Control of Marine Propellers. From Normal to Extreme Conditions. (Dr.Ing. Thesis)
IMT-2007-21 Storhaug, Gaute	Experimental Investigation of Wave Induced Vibrations and Their Effect on the Fatigue Loading of Ships. (Dr.Ing. Thesis)
IMT-2007-22 Sun, Hui	A Boundary Element Method Applied to Strongly Nonlinear Wave-Body Interaction Problems. (PhD Thesis, CeSOS)
IMT-2007-23 Rustad, Anne Marthine	Modelling and Control of Top Tensioned Risers. (PhD Thesis, CeSOS)

IMT-2007-24 Johansen, Vegar — Modelling flexible slender system for real-time simulations and control applications.

IMT-2007-25 Wroldsen, Anders Sunde — Modelling and control of tensegrity structures. (PhD Thesis, CeSOS)

IMT-2007-26 Aronsen, Kristoffer Høye — An experimental investigation of in-line and combined in-line and cross flow vortex induced vibrations. (Dr.avhandling, IMT)

IMT-2007-27 Zhen, Gao — Stochastic response analysis of mooring systems with emphasis on frequency-domain analysis of fatgue due to wide-band processes. (PhD-thesis CeSOS).

IMT-2007-28 Thorstensen, Tom Anders — Lifetime Profit Modelling of Ageing Systems Utilizing Information about Technical Condition. Dr.ing. thesis, IMT.

IMT-2007-29 Ye, Naiquan — Fatigues Assessment of Aluminium Welded Box stiffener Joints in ships. Dr.ing.-Thesis, IMT.

IMT-2007-30 Pákozdi, Csaba — A Smoothed Particle Hydrodynamics Study of Two-dimensional Nonlinear Sloshing in Rectangular Tanks. Dr.ing.thesis, IMT.

IMT-2007-31 Thorhus, Runar — Alliances in Development of Short-sea Transport systems. Dr.ing.thesis, IMT.

IMT-2008-32 Norum, Viggo L. — Analysis of Ignituin and Combustion in Otto Lean-Burn Engines with Prechambers. Dr.ing. thesis, IMT.